GEOLOGICA ULTRAIECTINA

Mededelingen van het
Instituut voor Aardwetenschappen
der Rijksuniversiteit Utrecht

No. 25

FLUID INCLUSIONS IN HIGH-GRADE METAMORPHIC ROCKS FROM S.W. NORWAY

H.E.C. SWANENBERG

STELLINGEN

1

Indien homogenisatie van de CO_2-rijke fase in H_2O-CO_2 insluitsels plaatsvindt beneden de dissociatietemperatuur van het CO_2-hydraat dient bij opgave van de homogenisatietemperatuur de aan- of afwezigheid van dit hydraat te worden vermeld.

2

Het optreden van retrograde condensatie in isochore binaire systemen is niet erg waarschijnlijk.

Ypma, P.J.M. (1963) Proefschrift, Leiden.

3

De zogeheten "Burruss inconsistency test" berust op een foutieve interpretatie van de fasenrelaties in het systeem CO_2-CH_4.

Hollister, L.S. & Burruss, R.C. (1976) Geochim.Cosmochim. Acta 40, 163-175.

Konnerup-Madsen, J. (1977) Am.J.Sci. 277, 673-696.

4

De aanname door Kelly en Rye dat in H_2O-CO_2 insluitsels uit Panasqueira het CO_2 in de waterrijke fase kan worden verwaarloosd is niet juist en leidt dan ook tot grote afwijkingen in de schattingen van de druk.

Kelly, W.C. & Rye, R.O. (1979) - Ec. Geol. 74, 1721-1822.

Malinin, S.D. & Kurovskaya, N.A. (1975) Geochem. Int. 12, 199-201.

5

Lekkage in "ductiele deformatie insluitsels" zoals beschreven door Wilkins & Barkas lijkt eerder het gevolg van *post*-tektonische dan van *syn*-tektonische processen te zijn.

Wilkins, R.W.T. & Barkas, J.P. (1978) Contrib. Mineral. Petrol. 65, 293-299.

6

De door Field en Råheim gepostuleerde resetting van Rb-Sr total rock isochronen bij 1060 Ma als gevolg van laaggradige metamorfose is niet erg aannemelijk.

Field, D. & Råheim, A. (1979) - Earth & Plan. Science Letters 45, 32-44.

7

De deflectie van pigeoniet-lamellen in augiet in pyroxeen-monzonieten van de leukonoritische fase van de Bjerkreim-Sokndal lopoliet kan het gevolg zijn van tussentijdse opwarming bij afkoeling.

8

De door Rice gevolgde methodiek bij het vaststellen van temperatuurverdelingen in een contact-aureool, door middel van calciet-dolomiet thermometrie, is verwerpelijk.

Rice, J.M. (1977) - Contrib. Mineral. Petrol. 59, 237-259.

9

De gemeten magnetische anomaliëen bij de Walvisrug sluiten een (eventueel gedeeltelijk) continentale oorsprong van deze rug niet uit.

Van der Linden, W.J.M. In prep.

10

Het model van ontgassing op Venus, zoals toegepast door Walker, is niet goed bruikbaar als argument voor een relatief snelle ontgassing in het vroegste Archeïcum op Aarde.

Walker, J.C.G. (1977) - In: Ponnamperuma, C. (Ed.) Chemical evolution of the early Precambrian.

Kerr, R.A. (1980) - Science 207, 289-293.

11

De invoering van wetenschappelijke databanken verdient krachtige stimulering.

12

Deeltijdarbeid binnen het basisonderwijs heeft de laatste jaren zijn bestaansrecht bewezen.

13

Door bij de bereiding van gekookte eieren het gas voortijdig uit te draaien kan in ons land jaarlijks circa 1,5 miljoen gulden worden bespaard. Bij zachtgekookte eieren bijvoorbeeld (3 stuks) dient men deze, nadat het water 1 minuut heeft gekookt, nog 3 minuten in het hete water te houden.

14

Grote boodschappen van honden dienen thuis te worden bezorgd.

Utrecht, 21 april 1980.
H.E.C. Swanenberg

Stellingen behorende bij het proefschrift: "Fluid inclusions in high-grade metamorphic rocks from S.W. Norway".

GEOLOGICA ULTRAIECTINA

Mededelingen van het
Instituut voor Aardwetenschappen
der Rijksuniversiteit Utrecht

No. 25

FLUID INCLUSIONS IN HIGH-GRADE METAMORPHIC ROCKS FROM S.W. NORWAY

KRIPS REPRO MEPPEL
1980

FLUID INCLUSIONS IN HIGH-GRADE METAMORPHIC ROCKS FROM S.W. NORWAY

PROEFSCHRIFT

ter verkrijging van de graad van doctor in de wiskunde en natuurwetenschappen aan de Rijksuniversiteit te Utrecht, op gezag van de Rector Magnificus Prof. Dr. A. Verhoeff, volgens besluit van het College van Decanen in het openbaar te verdedigen op maandag 21 april 1980 des namiddags te 4.15 uur

door

Hugo Edmond Charles Swanenberg

geboren op 26 juni 1950 te Tiel

PROMOTORES : Prof. Dr. R.D. Schuiling
Dr. A.C. Tobi

DIT PROEFSCHRIFT KWAM TOT STAND MEDE
ONDER LEIDING VAN DR. R. KREULEN

aan Eliletje
Jeroen en Sjoerd

ter nagedachtenis aan mijn moeder

VOORWOORD

Bij de afsluiting van mijn academische opleiding wil ik graag allen bedanken die aan de totstandkoming van dit proefschrift hebben meegewerkt. In het bijzonder wil ik hierbij noemen:

Mijn vrouw Elletje, zonder wie dit werkstuk nooit tot stand zou zijn gekomen. Door haar bereidheid om vele avonden in eenzaamheid door te brengen heeft zij de grootste bijdrage geleverd.

Mijn promotoren, Prof. Schuiling en Dr. Tobi, onder wier supervisie het vloeistofinsluitsel-onderzoek stond en die op directe of indirecte wijze hebben bijgedragen aan mijn wetenschappelijke vorming. In hen bedank ik tevens de Rijksuniversiteit Utrecht die mij voortdurend de gelegenheid en de faciliteiten heeft geboden om dit promotie-onderzoek te verrichten.

Mijn co-referent, Rob Kreulen, die voortdurend als inspirerende discussiepartner bij het onderzoek betrokken is geweest en die waardevolle suggesties heeft gedaan voor een reductie van het manuscript.

Prof. Jacques Touret, thans verbonden aan de Vrije Universiteit te Amsterdam, die door zijn enthousiasme voor de studie van vloeistofinsluitsels ook op dit onderzoek stimulerend heeft gewerkt.

Erkentelijk ben ik ook Dr. Harry Oonk van de vakgroep Chemische Thermodynamica, voor zijn suggestie om isochoren te berekenen met behulp van de "gemodificeerde Redlich-Kwong vergelijking".

De stafleden Dr. Cees Maijer en Ir. Gé Hermans van de afdeling Petrologie, alsmede mijn kamergenoten Frans Rietmeijer en Paul Sauter bedank ik voor de vele Rogaland-discussies, die aan de gedachtevorming in dit proefschrift hebben bijgedragen.

Jan de Groot, chef afdeling Gesteentebewerking, en zijn medewerkers Hans Bliek en Inge Nüssgen brachten met grote bekwaamheid de gesteenten letterlijk "aan het licht".

Frans Henzen, chef afdeling Foto- en Tekenkamer en zijn medewerkers besteedden veel aandacht aan de copyproofs en waren ook altijd bereid er nog even "snel iets tussendoor" te doen.

Jan Meesterburrie voerde met grote nauwgezetheid de stabiele-isotopen analysen uit en was tevens behulpzaam bij activiteiten langs de (vacuum)lijn.

Aad Engelhart-Bruin, Marieke Draaisma- v.d. Houten, Jeannie Ingen- v.Vliet en Marcel Stelling, medewerkers van de Bibliotheek, waren voortdurend behulpzaam bij het zoeken naar boeken en publicaties. Tevens bedank ik hen voor de clementie als een werkje toch onder handbereik bleek te liggen.

Voor hun bijdrage in een deel van het manuscript ("typescript") bedank ik Weia Reynders-Smid, Ineke Kalt en Ava Feldman.

Jeg takker befolkningen fra Moi, i saerdeleshet Magnus og Borgny Gürsli, for oppriktig hjelp i feltarbeidet som ble utfort sommeren 1975 og 1976.

Ten slotte wil ik bedanken de Stichting Molengraaff-Fonds te Delft voor financiële steun bij het veldwerk, alsmede de Niels Stensen Stichting te Amsterdam voor het verlenen van een stipendium.

ABSTRACT

In part one of this thesis, isochoric sections, based on a modified Redlich-Kwong equation, are presented for the systems CO_2, CO_2-N_2, N_2-CH_4 and H_2O-CO_2. This allows the P-T interpretation of fluid inclusion freezing data in terms of the above-mentioned reference systems.

Part two deals with fluid inclusions in quartz of high-grade metamorphic rocks from S.W. Norway. This region is essentially a plutonic complex of anorthosite masses and a layered lopolithic intrusion (in the southwest) surrounded by HT-LP granulite-facies rocks and by high-grade amphibolite-facies rocks (prevailing in the northeastern part).

The major types of fluid inclusions are: 1. H_2O-rich, 2. CO_2-rich, 3. H_2O-CO_2 and 4. N_2-rich. On a regional scale, CO_2-rich inclusions seem to predominate in the granulite-facies rocks. Abundant CO_2-rich inclusions (with low densities) have been found close to a dolerite dike. In general, the variability in properties of types 1-3 at the scale of a handspecimen is not clearly related to the high-grade mineralogy. N_2-rich inclusions have been found in quartz-rich rocks in the vicinity of mafic rocks (preferably with amphibole or clinopyroxene) and in a number of pegmatites.

Most fluid inclusions are arranged along trails. Transposition of trails indicates that the inclusions are able to migrate, possibly as the result of stress. Not uncommonly, trails that (in part) consist of carbonic inclusions are oriented subbasally.

Temperatures of liquid phase homogenization of type 2 (essentially CO_2 with some N_2) display a wide range in individual samples, particularly in strongly retromorphic or deformed rocks. In general, however, the values are rather low, compared with most other granulite-facies terranes. In terms of CO_2-equivalent density, the freezing data of type 2 reflect a range of 0.70 to 1.23 g/cc. Type 4 yields 0.45-0.75 g/cc N_2. There is a striking incompatibility between the occurrence of extremely dense inclusions and the HT-LP conditions of granulite-facies metamorphism.

It is suggested that pre-existing inclusions are able to re-equilibrate towards higher densities when, during an initial isobaric cooling, the retrograde P-T path of the rock complex intersects isochores of increasing density. Extremely high densities, mainly found in intensily deformed or retromorphosed rocks, possibly result from tectonic overpressures (Caledonian influence?) which may amount up to 3.5 kbars at relatively low tempe-

ratures. Interaction of H_2O-rich fluids, possibly introduced during a late-stage uplift, and (pre-existing) CO_2 at about 300°C and 1-2 kbars (hydrostatic pressure) could effectively explain a number of thermo-optical properties of mixed H_2O-CO_2 inclusions.

SAMENVATTING

VLOEISTOFINSLUITSELS IN HOOGGRADIG METAMORFE GESTEENTEN UIT Z.W.NOORWEGEN

In het eerste deel van dit proefschrift worden isochore doorsneden, gebaseerd op een gemodificeerde Redlich-Kwong vergelijking, gegeven voor de systemen CO_2, CO_2-N_2, N_2-CH_4 en H_2O-CO_2. Dit maakt de geologische P-T interpretatie mogelijk van homogenizatie-temperaturen van vloeistofinsluitsels in bovengenoemde referentie-systemen.

Deel twee betreft de studie van vloeistofinsluitsels in kwarts in hooggradig metamorfe gesteenten uit Z.W. Noorwegen. Dit gebied bestaat in hoofdzaak uit een magmatisch complex met anorthosieten en een gelaagde lopoliet (in het zuidwesten), omgeven door granulietfacies (type HT-LP) gesteenten en door hooggradige amfiboliet-facies gesteenten meer naar het noordoosten.

De belangrijkste typen insluitsels zijn: 1. H_2O-rijk, 2. CO_2-rijk, 3. H_2O-CO_2 en 4. N_2-rijk. Op regionale schaal lijken de CO_2-rijke insluitsels het meest voor te komen in het granuliet-facies gebied. Grote hoeveelheden van type 2 zijn aangetroffen nabij een doleriet. In het algemeen is de variabiliteit in de insluitsel-eigenschappen niet duidelijk gerelateerd aan de hooggradige mineralogie. N_2-rijke insluitsels worden gevonden in kwarts-rijke gesteenten nabij mafische gesteenten (bij voorkeur met amfibool of clinopyroxeen) en in een aantal pegmatieten.

De meeste vloeistofinsluitsels zijn gebonden aan zg. "trails" (insluitelvlakken). Transpositie van deze "trails" geeft aan dat insluitsels in staat zijn te migreren, mogelijk als gevolg van stress. Trails met CO_2-rijke insluitsels vertonen niet zelden een subbasale orientatie.

Homogenizatietemperaturen (vloeistoffase) van type 2 insluitsels (in hoofdzaak CO_2 met een weinig N_2) vertonen een grote spreiding in individuele monsters, in het bijzonder wanneer het gastheer gesteente sterk gedeformeerd of retrograad-metamorf is. In termen van CO_2-equivalent dichtheid leveren de homogenizatie- en smelttemperaturen van type 2 een dichtheids-

variatie op van 0.70 tot 1.23 g/cc. Type 4 heeft een dichtheid van 0.45-0.75 g/cc N_2. In het algemeen echter, zijn de dichtheden betrekkelijk hoog in vergelijking met andere granuliet-facies gebieden. Met name de extreem hoge dichtheden zijn onverenigbaar met de hoge-temperatuur, lage-druk condities bij de granuliet-facies metamorfose in zuidwest Noorwegen.

Het is waarschijnlijk dat bestaande (bij voorbeeld synmetamorfe) insluitsels kunnen re-equilibreren naar een hogere dichtheid, wanneer bij een isobare afkoeling (direct volgend op de hoofdfase van metamorfose) het retrograde P-T pad van het gesteentecomplex isochoren doorsnijdt van toenemende dichtheid. De extreem hoge dichtheden, die voornamelijk gevonden zijn in sterk gedeformeerde of retrograad-metamorfe gesteenten, zijn mogelijk ontstaan als gevolg van "tectonic overpressure" (invloed van de Caledonieden?), die bij lage temperatuur tot 3.5 kbar zou bedragen.
Interactie van een H_2O-rijke vloeistoffase, mogelijk binnengedrongen tijdens een late opheffing van het gesteentecomplex, en (bestaand) CO_2 bij ongeveer 300°C en 1-2 kbar (hydrostatische druk) heeft waarschijnlijk ten grondslag gelegen aan de vorming van H_2O-CO_2 insluitsels.

ABSTRAKT

VAESKE INNESLUTTNINGER I HØYGRAD METAMORFE BERGARTER FRA SØR-VEST NORGE

I første del av disse doktoravhandling ble behandlet konstruksjonen av isovolumetriske gjennomsnitter i systemer CO_2, CO_2-N_2, N_2-CH_4 og H_2O-CO_2. Dette sette i stand å fortolke mikrothermometriske data i geologisk betydningsfulle temperaturer og trykker.

I annet del finnes beskrivelse og fortolking av vaeske innesluttninger i kvarts fra metasedimenter, migmatitter, pegmatitter og kvartsganger. Den flytende fase er H_2O (og saltholdig oppløsning), CO_2, N_2 , CH_4 eller blandinger.

I alminnelighet finnes det CO_2(CO_2-N_2) og H_2O (sannsynligvis med forholdsvis store mengder Ca-Mg joner) i varierende mengder og forhold. Kvarts i naerheten av en doleritgang (*Rusdalsvatnet*) inneholder en saerlig stor mengde CO_2-innesluttninger. Nitrogen innesluttninger ble funnet i kvarts i naerheten av noen mafiske bergarter og pegmatitter. CH_4 er sjelden (*Mydland, Kvitingen*).

Primäre innesluttninger finnes kun sjelden: kvartsganger i marmor (*Seldal, Stølsfjellet*) inneholder primär CO_2 og CO_2-H_2O mens kvarts, krystallisert i en retrogradert grunnskiferfacies metamorfose, inneholder primäre innesluttninger med saltholdig vann (*Stølsfjellet*). Sannsynligvis ble de fleste innesluttninger dannet etter krystallisationen av vertsmineralet og er derfor sekundär.

Tettheten av CO_2 og N_2 innesluttninger er forholdsvis stor: ekvivalent-CO_2 tettheten varierer mellom 0.70 og 1.23 g/kc (gjennomsnittlig 0.95 g/kc; høyeste verdie finnes i en metasedimentäre kvartsitt (*Asheim området*). For N_2, tettheten er bestemmt til 0.45-0.75 g/kc).

Slike tettheter viser at innesluttninger kan ikke ble dannet i likevekt med høy-temperatur og lave-trykk betingelser i granulitfacies metamorfose i Rogaland. Innesluttninger (fortrinnsvis med CO_2) med meget stor tetthet er påvist i bergarter som viser retrogradering eller plastisk deformasjon. Det antydes at store tettheter kan ble framkalt i CO_2 og N_2 innesluttninger ved isobar sekning av temperaturen (med forholdsvis høy trykk).

Ved samtidig tilførsel av H_2O (temperaturen 200-400^{o}C) ble både H_2O og H_2O-CO_2 innesluttninger dannet ved forholdsvis lave trykk (1-2 kbar). CO_2 innesluttninger ved dolerit ble også dannet ved lave trykk.

INDEX

Part I
ISOCHORIC SECTIONS OF NON-IONIC SYSTEMS

Part II
FLUID INCLUSION STUDY

8 tables
76 figures

GENERAL INTRODUCTION

The occurrence of carbonic (CO_2-rich) inclusions in rocks that originated in deep-seated environments has been known since the early sixties from work by Deicha and Roedder. The systematic investigation of fluid inclusions in high-grade metamorphic rocks, however, has been initiated by Touret in the early seventies. He showed the predominance of carbonic inclusions over aqueous inclusions in quartz from granulite-facies rocks and the inverse relation in amphibolite-facies rocks (Bamble region, southern Norway). Such a characteristic occurrence of carbonic inclusions has been confirmed by later studies (Bilal, 1976; Berglund & Touret, 1976; Konnerup-Madsen, 1977, 1979; Klatt, 1979).

Touret's results have been the incentive to start a fluid inclusion study on high grade metamorphic and related rocks from S.W. Norway. This region has been metamorphosed under granulite-facies conditions in the west (mainly Rogaland) and in high-grade amphibolite-facies in the East (mainly Vest-Agder). The present study, however, did not primarily focuse on regional trends in fluid inclusion properties but merely aimed at answering the following (vital) questions:

- does any type of fluid inclusion represent a synmetamorphic fluid phase in terms of composition and density?
- does a relation exist between inclusion properties and specific local geologic conditions?
- do fluid inclusions remain stable systems during the post-metamorphic history of the host rock or may certain properties (composition, density) be modified according to varying conditions of pressure and temperature?

Such approach requires the determination of distribution, size, shape, number, composition, and density of the inclusions. The last-mentioned property can be derived from melting and homogenization temperatures (microthermometry), measured on a heating-freezing stage. Unfortunately, however, the available experimental data of the systems involved (CO_2, CH_4, N_2, H_2O, and their mixtures) are usually insufficient to permit an accurate interpretation of the heating-freezing data. Additional theoretical work (presented in Pt.I) was, therefore, required in order to obtain isochores of relevant unary and binary systems in P-T regions of interest.

Part I

ISOCHORIC SECTIONS OF NON-IONIC SYSTEMS

I.1 INTRODUCTION

Fluid inclusions in metamorphic and related rocks mainly consisting of neutral species have been reported by several investigators (Touret, 1971, 1974 ab; Bilal, 1976; Hollister & Burruss, 1976; Murck *et al.*, 1978; Konnerup-Madsen, 1979; Kreulen, 1980).

The interpretation of phase changes observed when heating or cooling such inclusions requires knowledge of the phase relations and P-V-T properties of a number of chemical systems.

In the following sections the systems CO_2, N_2, CH_4, N_2-CH_4, CO_2-CH_4, CO_2-N_2 and H_2O-CO_2 will be discussed. The unary system H_2O will not be dealt with because its P-V-T properties are sufficiently well-known over a large range of geologically interesting temperatures and pressures (Burnham *et al.*, 1969), and have already been graphically portrayed by Fisher (1976).

In general, two regions of interest are distinguished:

1. A 'low-temperature' region where melting and homogenization temperatures are measured and interpreted in terms of composition and density.
2. A 'high-temperature' region, which encompasses geologically relevant temperatures and pressures. In this region the P-T conditions of formation of inclusions that did not originate on a two-phase boundary curve can be estimated from isochores, known from experimental work or derived from an equation of state.

For the unary systems, P-V-T data in both regions of interest are at present available. P-V-T-X data of binary systems in the low-temperature region can only be obtained if experimentally determined phase boundaries are known. Commonly, however, the experimental work does not cover the complete range of compositions and involves only a limited range of bulk densities. In the high-temperature region, the experimental data are almost exclusively reported for low-density fluids and are thus of limited value for direct application to fluid inclusion studies.

If not known from experiments, binary isochores (and to a certain extent also unary isochores at elevated densities) can be constructed using an equation of state in which the parameters, combined in appropriate mixing rules, are calculated from P-V-T data of the pure components. In the present study, a modified Redlich-Kwong equation (henceforth designated as MRK) has been used as a basis for the calculation of volumetric properties of various systems:

$$P_{MRK} = \frac{RT}{V-b} - \frac{a(T)}{V(V+b).T^{\frac{1}{2}}} \qquad (1)$$

where P_{MRK} is the pressure (bars), R is the gas constant (0.08314 liter bar/°K mole), T is the temperature (°K), and V is the molar volume of the fluid (liter/mole).

The parameter b (liter/mole) is related to a molecular distance parameter σ, associated with short-range repulsive forces. The parameter a (bar liter^2 K$^{\frac{1}{2}}$/mole^2) reflects an energy parameter ε, associated with long-range attractive forces.

Unless stated otherwise in the specific sections, the following mixing rules have been employed for the parameters a and b in binary mixtures:

$$a_{mix} = X_1^2 a_1 + X_2^2 a_2 + 2X_1 X_2 a_{12} \qquad (2)$$

$$a_{12} = (a_1^o a_2)^{\frac{1}{2}} \qquad (3)$$

$$b_{mix} = X_1^2 b_1 + X_2^2 b_2 + 2X_1 X_2 \frac{(b_1 + b_2)}{2} \qquad (4)$$

where X_1 and X_2 are molar fractions of components 1 and 2 respectively. Parameter a_1^o is a constant for H_2O or CO_2 and a_2 is a temperature dependent parameter of a non-polar component (de Santis *et al.*, 1974). The mixing rule for b is the so-called Lorentz combination rule (Hirschfelder *et al.*, 1964).

The MRK (1) has been proposed by de Santis *et al.* (1974) to obtain volumetric properties of aqueous gas mixtures, mainly for engineering purposes. In the field of petrology it has been introduced by Holloway (1977) and has since - with minor corrections - become a popular equation of state among fluid inclusion workers (Stecher, 1977; Swanenberg, 1979; Touret & Bottinga, 1979).

The original MRK has been designed for application at rather low pressures (up to 1500 bars). At low to intermediate densities of the fluid, the variable V in the denominator of the first term of Eq. (1) is large with respect to b and hence a slightly erroneous value of b will not have a dramatic effect on the final results (P_{MRK}).

At higher densities, however, V becomes relatively small and therefore, the parameter b needs to be carefully defined. In particular at high

temperatures the first term of Eq. (1) is the determining part and consequently the definition of a(T) becomes less critical. From molecular dynamics theory it follows that at elevated densities (small intermolecular distances) the magnitude of the repulsive term in the so-called '6-12 Lennard Jones' potential energy function is appreciable. As a consequence the parameter b (reflecting repulsive forces) becomes a function of pressure and temperature. For CO_2, e.g., Stecher (1977) showed that at given a(T) the parameter b can no longer be considered a constant, such as proposed by de Santis *et al.* (1974). Unfortunately, however, short-range forces cannot be described physically in the same rigorous manner as the attractive forces (e.g. London dispersion forces). This implies that at elevated densities there is no firm theoretical justification for the definition of b^{MRK} and the mixing rules for b^{MRK}_{mix}. Mixing rule (4) is based on:

$$\sigma_{12} = (\sigma_1 + \sigma_2)/2 \tag{5}$$

Physical models of molecular interaction at short distances (discussed by Pesuit, 1978) take into account the energy of deformation of the electron clouds. For this case Eq. (5) becomes:

$$\sigma_{12} = F.\ (\sigma_1 + \sigma_2)/2 \tag{6}$$

where F is a complex function of σ and ε. F can be calculated for various systems and provides a check on the validity of Eq. (5).

Parameters a^{MRK} and b^{MRK} can be extracted from two, experimentally determined P-V relations at the same temperature (Stecher, 1977):

$$b^3(P_1V_1-P_2V_2) + b^2(RT(V_1-V_2) + V_1V_2(P_2-P_1)) +$$
$$b(P_2V_2^3-P_1V_1^3-RT(V_2^2-V_1^2)) + V_1V_2(RT(V_2-V_1) - P_2V_2^2+P_1V_1^2) = 0 \tag{7}$$

Substituting b in Eq. (1) yields:

$$a(T) = T^{\frac{1}{2}}((RT/V-b)-P_{MRK})(V^2 + Vb) \tag{8}$$

Values of a^{MRK} and b^{MRK} thus obtained, may serve as a basis for (re-)constructing isochores in unary or binary systems, both at low and high

temperatures.

1.2 THE SYSTEM CO_2

1.2.1 THE LOW-TEMPERATURE REGION

Volumetric data of CO_2 close to, and on the boiling curve at temperatures down to the triple point (-56.6°C) are given by Vagarftik (1972). These data have been graphically reproduced by Touret & Bottinga (1979). Volumetric data obtained by Kennedy & Holser (1966) and Arai *et al.* (1971) have lower-temperature limits of 0° and -20°C respectively. The CO_2 end-

Reference	Temperature (°C)	Pressure (bars)	Density (g/cc)	Molar volume (l/mole)	b^{MRK} (l/mole)	a^{MRK} ($bar_2 l^2 K^{\frac{1}{2}}$/ $mole^2$)
Vagarftik (1972)	-50	13.5	1.158	0.0380	0.02891	76.98
	-50	87.8	1.173	0.0375		
	-40	43.9	1.128	0.0390	0.02885	75.32
	-40	106.2	1.143	0.0385		
	-30	35.8	1.086	0.0405	0.02867	73.00
	-30	79.4	1.100	0.0400		
	-20	46.4	1.047	0.0420	0.02840	70.53
	-20	111.5	1.073	0.0410		
	-10	50.7	1.000	0.0440	0.02886	72.49
	-10	100.0	1.023	0.0430		
	0	70.7	0.956	0.0460	0.02882	71.10
	0	106.7	0.977	0.0450	0.02812	67.27
Kennedy & Holser (1966)	0	50.0	0.947	0.0465	0.0296	75.75
	0	75.0	0.954	0.0461		
Arai et al (1971)	0	49.0	0.976	0.0451	0.0270	64.80
	0	75.0	0.996	0.0442	0.0280	70.00
	0	90.6	1.005	0.0438	0.0266	62.72
	0	113.9	1.021	0.0431	0.0212	42.28
	0	121.6	1.036	0.0425	0.0271	66.15
	0	145.1	1.048	0.0420		

TABLE 1 Volumetric data and MRK-parameters a and b of CO_2 between -50° and 0°C.

member data by Arai *et al.* (1971) are important because they provide a reference for the (scanty) volumetric data of the binary systems CO_2-CH_4 and CO_2-N_2.

Table 1 comprises volumetric data close to the boiling curve as well as calculated values for a^{MRK} and b^{MRK}. A good MRK approach of CO_2 between -50^{o} and $0^{o}C$ at pressures between 10 and 150 bars can be obtained using $b = 0.02822$ and the function $a(T) = 71.22-0.97T$ (T in ^{o}C).

1.2.2 METASTABLE HOMOGENIZATION OF EXTREMELY DENSE INCLUSIONS

In some fluid inclusions gross undercooling results in the nucleation of a vapor bubble in a liquid at temperatures where a solid-vapor equilibrium would be the stable configuration. Provided the density is sufficiently high, subsequent heating may bring about homogenization in the liquid phase at temperatures lower than the triple point ($-56.6^{o}C$). The phase behavior of such a high-density inclusion has been portrayed in figure 1. After

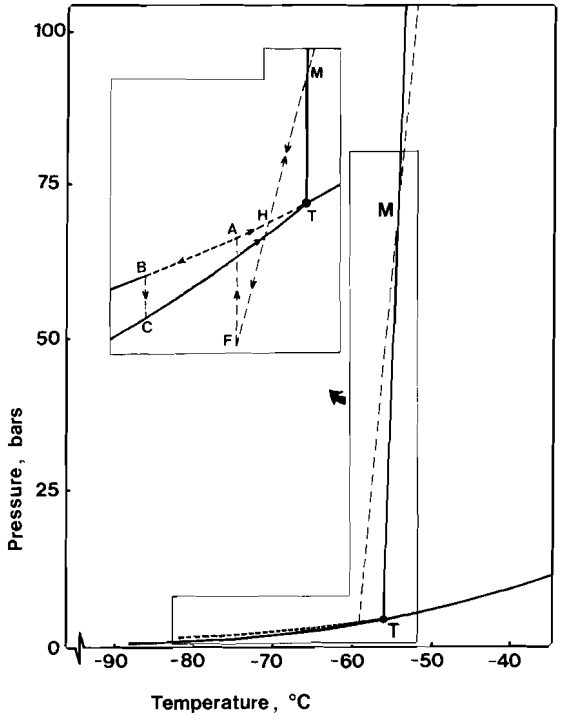

FIG. 1 Phase equilibria of CO_2 in the vicinity of the triple point. Heavy, broken line is the metastable extension of the liquid-vapor curve. Light, broken line is a high-density isochore (1.18 g/cc). Inset (not to scale) shows phenomenon of metastable homogenization in the liquid phase at high density of CO_2. See text for further discussion. In part after Touret & Bottinga (1979).

supercooling along MF (inset figure 1) a vapor bubble is generated on FA, where A is located on the metastable extension of the liquid-vapor equilibrium curve. Upon subsequent heating, the system follows a P-T path along AT where at H the fluid homogenizes in the liquid phase and proceeds along HM at higher temperatures. If at A the system were further cooled, solidification would result on BC. After subsequent heating, the vapor pressure migrates along CT until melting starts at T. After homogenization of the liquid and vapor phases has been completed at T, melting proceeds along TM until at M the system is completely liquid again.

Theoretically, melting of CO_2 in the absence of a vapor phase only takes place above the triple point temperature. In practice, however, such a deviation from the triple point value will be difficult to detect owing to the small size of the inclusions involved.

1.2.3 THE HIGH-TEMPERATURE REGION

A compilation of the volumetric data of CO_2 in the monophase fluid region up to 1000°C and 10 kbars is given by Swanenberg (1979). For convenience, the isochore diagram is reproduced in figure 2.

Touret & Bottinga (1979) have used the MRK with adjustable parameters a and b to construct isochores up to 1200°C and 20 kbars, with a maximum density of 1.58 g/cc. A remarkable difference exists between the essentially curved isochores determined by Shmonov & Shmulovich (1974) and the straight isochores calculated by Touret & Bottinga (1979). For instance, at 1000°C and 10 kbars the difference in pressure is about 25%.

If CO_2 molecules do di- or polymerize, a process envisaged by Touret & Bottinga (1979), one would expect high-density isochores that are curved concave towards the temperature axis. Such effect, however, is not observed in the isochores calculated by Touret & Bottinga (1979).

The curvature in the high-density isochores of CO_2 already follows from experimental data by Jůza *et al.* (1965). In addition to this, the high-density isochores of N_2 , a system that is comparable, to some extent, with CO_2 , are also curved (fig. 6).

The curved "Shmonov-Shmulovich isochores" imply that pressure estimates based on extrapolated data by Kennedy & Holser (1966) are too high. For instance (assuming pure CO_2 inclusions), pressure estimates by Klatt (1979) on the basis of the 1.02 g/cc isochore are 25% higher; pressure estimates by Bilal & Touret (1976) on the basis of the 1.075 g/cc isochore are 34% higher.

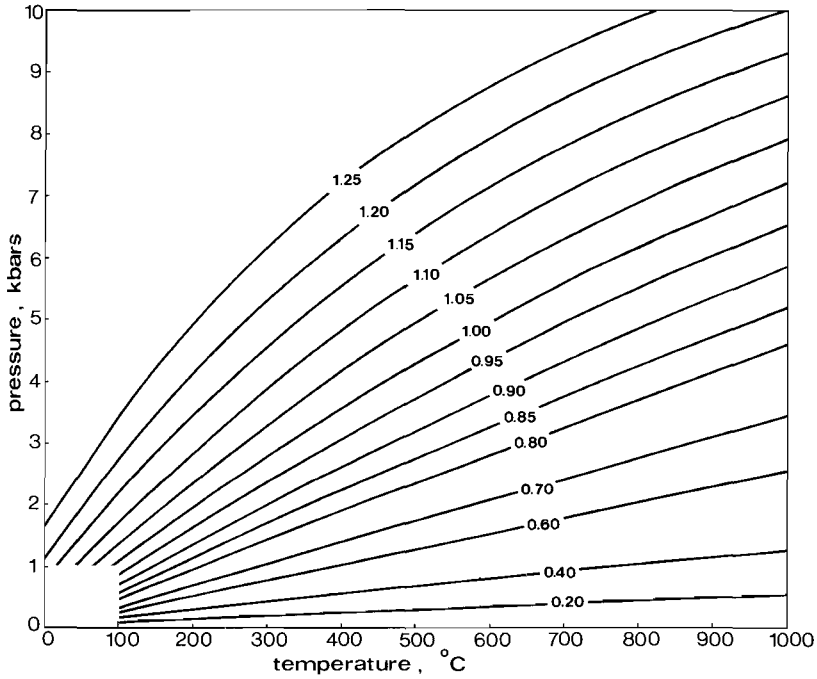

FIG. 2 Isochores of CO_2 (density range 0.20-1.25 g/cc). Compiled from Jůza *et al.* (1965), Kennedy & Holser (1966), and Shmonov & Shmulovich (1974).

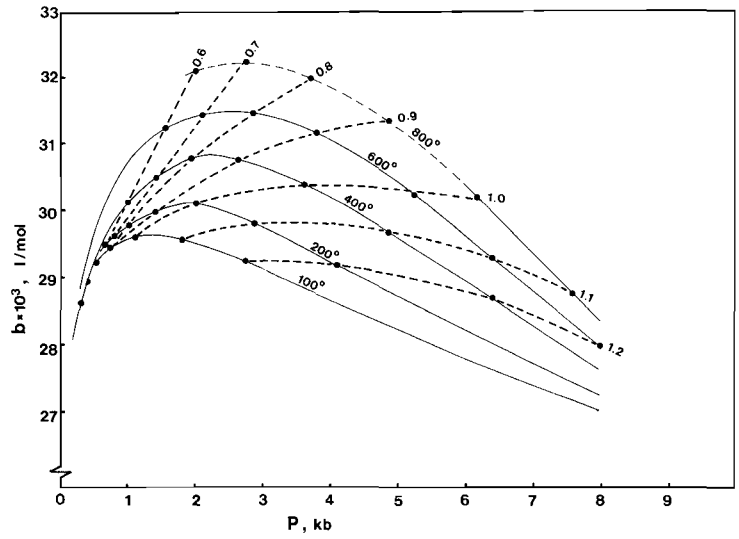

FIG. 3

FIG. 3 MRK-parameter b_{CO_2} as a function of temperature and pressure (Stecher, 1977). Broken lines are isochores (density range 0.6-1.2 g/cc), which have been superposed to show the variation of b_{CO_2} with density.

Values of b^{MRK}, at given a(T) according to Holloway (1977), have been calculated by Stecher (1977)(figure 3). It is evident that, depending on temperature and pressure, the parameter b^{MRK} needs a proper adjustment. As will be shown in the sections dealing with binary systems it is convenient to know the b^{MRK} as a function of the density. A number of isochores have, therefore, been superimposed on figure 3, thus providing a basis for the calculation of isochores in CO_2-bearing systems using the MRK.

1.3 THE SYSTEM CH_4

1.3.1 THE LOW-TEMPERATURE REGION

Because CH_4 is a constituent of many types of fluid inclusions, its P-V-T properties at low temperatures must be known if volumetric data in, or in the vicinity of the two-phase region of CH_4-bearing mixtures are approached theoretically. A number of such observations (Zagoruchenko & Zhuravlev, 1969) and the corresponding values for a^{MRK} and b^{MRK} are presented in table 2. If all values for b are reset to 0.03044, the parameter a(T) appears to be essentially constant (35.6 ± 1.2) at temperatures between -113 and -78°C and pressures ranging from 34 to 510 bars. Applying these values for a and b, maximum deviations between observed and calculated MRK pressures are in the order of plus or minus 14 bars. Although this error is appreciable, the reconstruction of liquid densities by intersecting the boiling curves with the isochores, gives quite satisfactory results (see also section 1.5.1 and figure 10).

Reference	Temperature (°C)	Pressure (bars)	Density (g/cc)	Molar volume (l/mole)	b^{MRK} (l/mole)	a^{MRK} ($bar_2 l^2 K^{\frac{1}{2}}/mole^2$)
Zagoruchenko & Zhuravlev (1969)	-113.15	159.0	0.400	0.0400	0.02530	24.61
	-108.15	452.0	0.400	0.0400	0.03065	36.70
	-103.15	510.0	0.400	0.0400	0.03064	36.72
	- 98.15	168.0	0.350	0.0458	0.03001	34.67
	- 88.15	245.5	0.350	0.0458	0.03027	35.36
	- 88.15	82.9	0.300	0.0534	0.02803	30.96
	- 78.15	330.0	0.350	0.0458	0.03066	36.33
	- 78.15	133.7	0.300	0.0534	0.02903	32.68
	+300.00	319.6	0.100	0.1601	0.03669	50.10
	+300.00	422.1	0.125	0.1281	0.03351	40.45
	+300.00	678.7	0.175	0.0915	0.03013	26.02
	+300.00	831.0	0.200	0.0801	0.03204	34.62
	+300.00	1020.8	0.225	0.0712	0.03169	32.61
	+300.00	1250.2	0.250	0.0641	0.03271	40.06

TABLE 2 Volumetric data and MRK-parameters a and b of CH_4 between -113.15° and -78.15°C, and at 300°C.

I.3.2 THE HIGH-TEMPERATURE REGION

A number of P-V-T observations at 300°C are included in Table 2. At

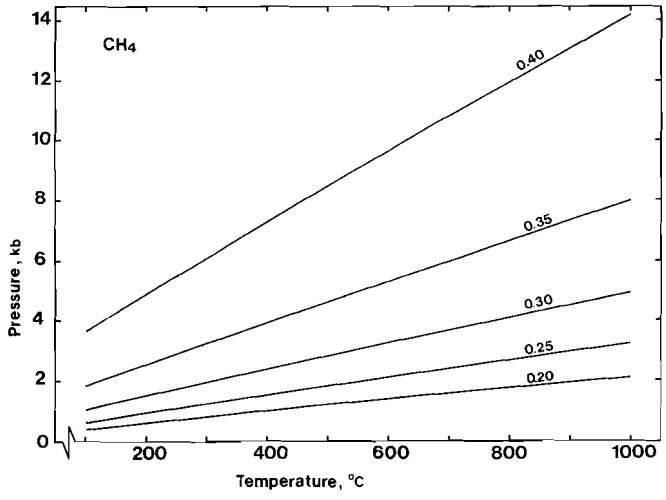

FIG. 4 Isochores of CH_4, calculated with MRK.

densities above 0.175 g/cc there seems to be a tendency for a^{MRK} to increase with increasing pressure but the available data do not permit an estimate for values above 0.25. If the values 0.03271 and 40.06 (corresponding to the isochore d = 0.25 g/cc) are used for parameters b^{MRK} and a^{MRK} the deviations between real and calculated MRK-pressures do not exceed 1.5% (at 300°C). By using constant values for a and b, a tentative isochore diagram for CH_4 at high temperatures and pressures has been constructed (figure 4).

I.4 THE SYSTEM N_2

I.4.1 THE LOW-TEMPERATURE REGION

Densities of the liquid and vapor phases on the boiling curve are given by Vagarftik (1972). These data are graphically represented in figure 5. Specific volume data by Vagarftik (1972) in the region between -183 and +27°C and pressures ranging from 40 to 150 bars allow the extraction of a^{MRK} and b^{MRK} (tables 3-4), both to be used in binary mixtures of N_2-bearing fluids.

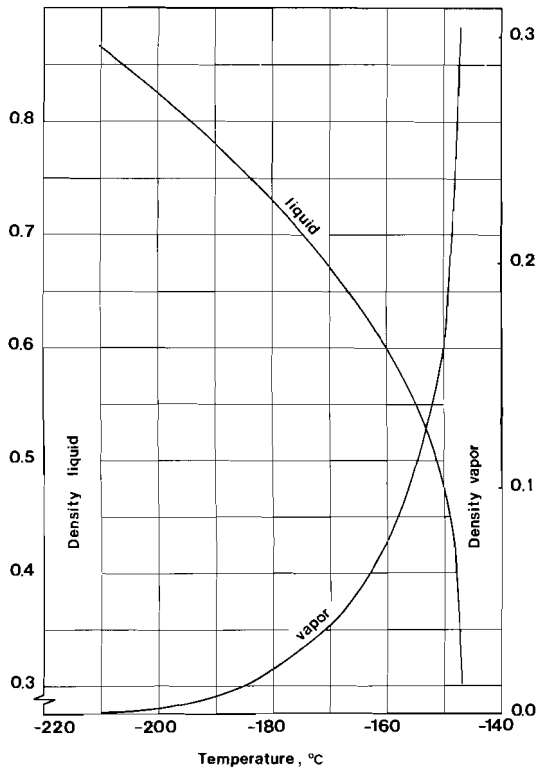

FIG. 5 Densities (g/cc) of liquid and gaseous N_2 along the boiling curve. After Vagarftik (1972).

For practical purposes, however, values of b^{MRK} are normalized to a constant value and a^{MRK} is recalculated accordingly. Thus, between -183 and -93°C, at given constant b = 0.02677 (mean value at -143°C), the values of a range from 15.0 to 16.4, depending on temperature

Reference	Temperature (°C)	Pressure (bars)	Density (g/cc)	Molar volume (l/mole)	b^{MRK} (l/mole)	a^{MRK} (bar $l^2K^{\frac{1}{2}}$/ $mole^2$)
Vagarftik (1972)	-183.15	40	0.75832	0.0369	0.02813	18.45
	-183.15	60	0.76452	0.0366	0.02803	18.18
	-183.15	80	0.77042	0.0364	0.02812	18.41
	-173.15	40	0.70746	0.0396	0.02834	18.79
	-173.15	60	0.71633	0.0391	0.02818	18.44
	-173.15	80	0.72464	0.0387	0.02850	19.17
	-163.15	40	0.64838	0.0432	0.02830	18.58
	-163.15	60	0.66225	0.0423	0.02847	18.87
	-163.15	80	0.67385	0.0416	0.02834	18.63
	-153.15	40	0.56867	0.0493	0.02735	17.17
	-153.15	60	0.59701	0.0469	0.02790	17.86
	-153.15	80	0.61690	0.0454	0.02818	18.27
	-143.15	60	0.50150	0.0559	0.02629	15.98
	-143.15	80	0.54615	0.0513	0.02725	16.97
	-133.15	40	0.15099	0.1855	0.02543	15.14
	-133.15	60	0.33967	0.0825	0.02510	15.05
	-133.15	80	0.45005	0.0623	0.02594	15.63
	-123.15	40	0.12134	0.2309	0.02412	14.66
	-123.15	60	0.22743	0.1232	0.02523	15.09
	-123.15	80	0.34270	0.0818	0.02544	15.18
	-113.15	40	0.10489	0.2671	0.02344	14.33
	-113.15	60	0.18005	0.1556	0.02468	14.76
	-113.15	80	0.26724	0.1048	0.02546	15.13
	-103.15	40	0.09363	0.2992	0.02287	14.00
	-103.15	60	0.15389	0.1821	0.02408	14.42
	-103.15	80	0.22168	0.1264	0.02517	14.89
	- 93.15	40	0.08525	0.3286	0.02289	13.87
	- 93.15	60	0.13652	0.2052	0.02381	14.19
	- 93.15	80	0.19238	0.1456	0.02477	14.59
Vagarftik (1972)	-183.15	40-100	normalized values:		0.02809	18.33
	-173.15	"	"		0.02834	18.78
	-163.15	"	"		0.02837	18.69
	-153.15	"	"		0.02781	17.71
	-143.15	"	"		0.02677	16.42
	-133.15	"	"		0.02549	15.22
	-123.15	"	"		0.02499	14.91
	-133.15	"	"		0.02454	14.65
	-103.15	"	"		0.02404	14.36
	- 93.15	"	"		0.02382	14.17

3

Reference	Temperature (°C)	Pressure (bars)	Density (g/cc)	Molar volume (l/mole)	b^{MRK} (l/mole)	a^{MRK} (bar $l^2 K^{\frac{1}{2}}$/ $mole^2$)	
Vagarftik (1972)	- 83.15	80	0.17182	0.1631	0.02457	14.37	
	- 83.15	100	0.22041	0.1271	0.02593	15.05	
	- 83.15	150	0.32658	0.0858	0.02697	15.81	
	- 73.15	80	0.15632	0.1792	0.02447	14.17	
	- 73.15	100	0.19924	0.1406	0.02582	14.84	
	- 63.15	80	0.14409	0.1944	0.02450	14.03	
	- 63.15	100	0.18268	0.1534	0.02575	14.66	
	- 63.15	150	0.27241	0.1028	0.02701	15.53	
	- 53.15	80	0.13410	0.2089	0.02466	13.95	
	- 53.15	100	0.16929	0.1655	0.02571	14.48	
	- 53.15	150	0.25221	0.1111	0.02704	15.39	
	- 43.15	80	0.12571	0.2229	0.02473	13.82	
	- 43.15	100	0.15818	0.1771	0.02581	14.38	
	- 43.15	150	0.23518	0.1191	0.02701	15.20	
	- 33.15	80	0.11851	0.2364	0.02485	13.70	
	- 33.15	100	0.14872	0.1884	0.02591	14.27	
	- 33.15	150	0.22065	0.1270	0.02698	15.01	
	- 23.15	80	0.11226	0.2496	0.02522	13.71	
	- 23.15	100	0.14055	0.1993	0.02594	14.11	
	- 23.15	150	0.20816	0.1346	0.02703	14.87	
	- 13.15	80	0.10675	0.2624	0.02557	13.72	
	- 13.15	100	0.13340	0.2100	0.02599	13.96	
	- 13.15	150	0.19724	0.1420	0.02708	14.73	
	- 3.15	80	0.10184	0.2751	0.02572	13.62	
	- 3.15	100	0.12708	0.2205	0.02616	13.88	
	- 3.15	150	0.18758	0.1494	0.02708	14.54	
	+ 6.85	80	0.09747	0.2874	0.02691	14.15	
	+ 6.85	100	0.12143	0.2307	0.02630	13.77	
	+ 6.85	150	0.17899	0.1565	0.02720	14.44	
	+ 16.85	80	0.09346	0.2998	0.02639	13.65	
	+ 16.85	100	0.11635	0.2408	0.02648	13.70	
	+ 16.86	150	0.17129	0.1636	0.02734	14.36	
	+ 26.85	80	0.08985	0.3118	0.02740	14.10	
	+ 26.85	100	0.11173	0.2507	0.02665	13.61	
	+ 26.85	150	0.16431	0.1705	0.02736	14.17	[4]

TABLES 3-4 Volumetric data and MRK-parameters a and b of N_2 between -183.15° and +26.85°C.

and pressure. Analogous to CH_4, volumetric data, obtained by using the MRK, can be reproduced with satisfaction (figure 10). At temperatures between -83^{o} and $+27^{o}C$ - a field of interest to the system CO_2-N_2 - a reasonable MRK approach of the isochores is obtained using $b_{N_2} = 0.02645$ and $a_{N_2} = 14.1 - 0.0165T$ (T in ^{o}C).

I.4.2 THE HIGH-TEMPERATURE REGION

Volumetric data by Benedict (1937), Robertson & Babb (1969), and Malbrunot & Vodar (1973) permit the construction of isochores up to $800^{o}C$ and 6000 bars (figure 6). Parameters a^{MRK} and b^{MRK}, extracted from the experimental data, clearly depend on temperature and pressure. Figure 7 shows that in a large part of the P-T field a^{MRK} has a negative value; this will raise problems if the mixing rule (3) is applied to binary N_2-bearing fluids. Therefore, all values of a^{MRK} were reset to 0, reducing

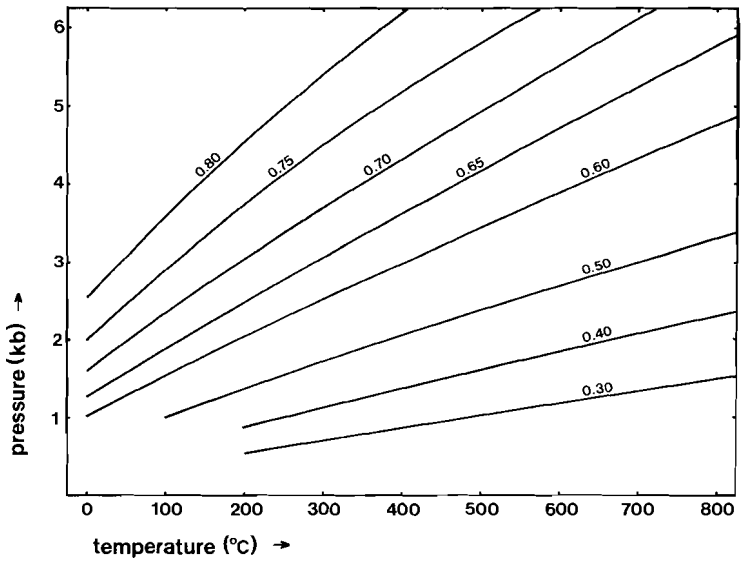

FIG. 6 Isochores of N_2. Compiled from Benedict (1937), Tsiklis & Polyakov (1968), Robertson & Babb (1969), and Malbrunot & Vodar (1973).

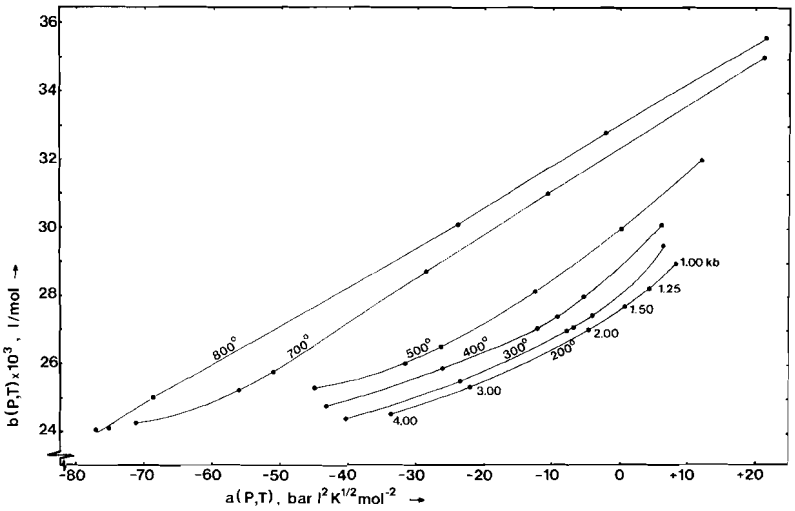

FIG. 7 MRK parameters a_{N_2} and b_{N_2} as a function of temperature and pressure. The 600° isotherm has been omitted because of erroneous data presentation by Malbrunot & Vodar (1973).

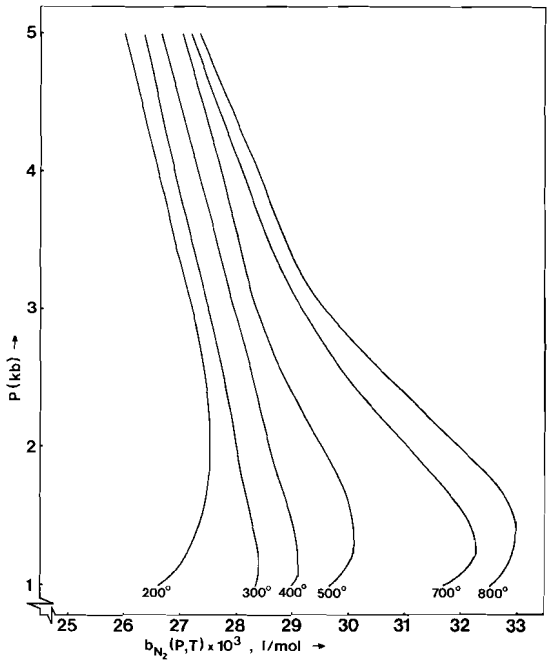

FIG. 8 Values of b_{N_2} fitting the experimental data to P=RT/(V-b).

equation (1) to:

$$P_{MRK} = \frac{RT}{V-b}$$

The adjusted values of the corresponding b_{N_2} are presented in figure 8. If experimentally determined isochores are superimposed in figure 8, it can be demonstrated that, owing to the convergence of the isotherms at high pressures, a reasonable approach of the isochores at high temperatures and pressures should be possible (figure 9). For instance, the calculated isochores of very dense N_2 at 400°C deviate up to 70 bars (about 1%) from the experimentally determined ischores of Tsiklis & Polyakov (1968)

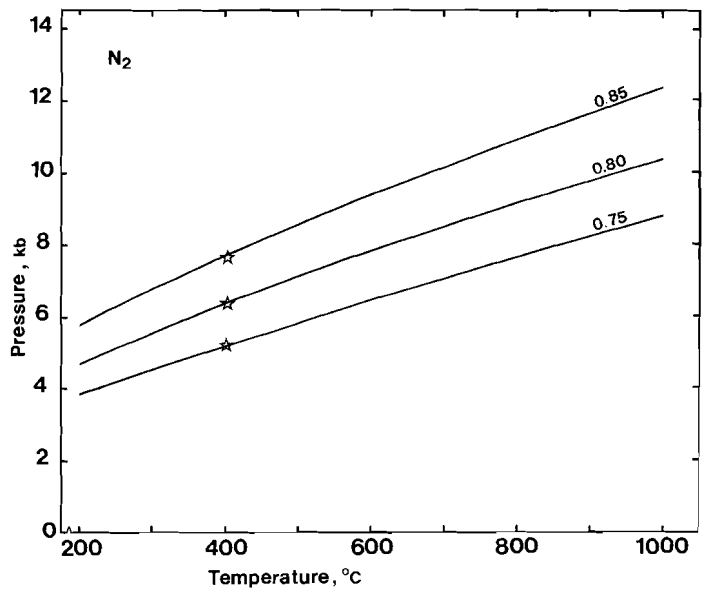

FIG. 9 High-density isochores of N_2, calculated with MRK. Stars represent experimental data by Tsiklis & Polyakov (1968).

I.5 THE SYSTEM N_2-CH_4

I.5.1 THE LOW-TEMPERATURE REGION

The boundary curves of the system N_2-CH_4, defining the regions of liquid-gas unmixing (fig. 10) have been graphically interpolated using the Landolt-Börnstein tables (1960). Densities of the liquid phases along the bubble-point curves, have been determined by linear intersection of isochores with the appropriate bubble-point curves. These binary isochores have been calculated by applying the MRK within the restricted field of pressures between 10 and 200 bars, thus allowing the use of constant values for a_{CH_4}, b_{CH_4}, b_{N_2}, and relatively simple expressions for a_{N_2} as a function of P and T. The use of constant values of a_{CH_4} and b_{CH_4} between -180 and -78°C has already been discussed in section I.3.1.

It is evident that a pressure-dependent a_{N_2} necessitates an iteration procedure whereby the parameter a_{N_2} is being adjusted according to the total pressure P_{MRK}.

For the cross-parameter a_{12} the following mixing rule has been employed:

$$a_{12} = \left[a_{N_2}(P_{MRK}).a_{CH_4}\right]^{\frac{1}{2}} \quad \text{(after de Santis } et\ al.\text{, 1974)}$$

A three-step iteration procedure was needed to produce the volumetric data presented in figure 10. Unfortunately, the validity of the method cannot be checked for binary compositions because volumetric data of the system N_2-CH_4 at low temperatures are not available at present. Concerning the pure end members CH_4 and N_2 it appears that high densities along the boiling curves can be reproduced with satisfaction (plus or minus 0.002 g/cc). Moderate densities of the liquid phase, however, show larger deviations, up to plus or minus 0.03 g/cc. Such departures are not surprising because isochores in the vicinity of the critical point are curved rather than rectilinear. In addition, the slope of the boiling curve is steep, and, therefore, a relatively small error in the pressure of the isochores will have a rather dramatic effect on the position of the intersection point.

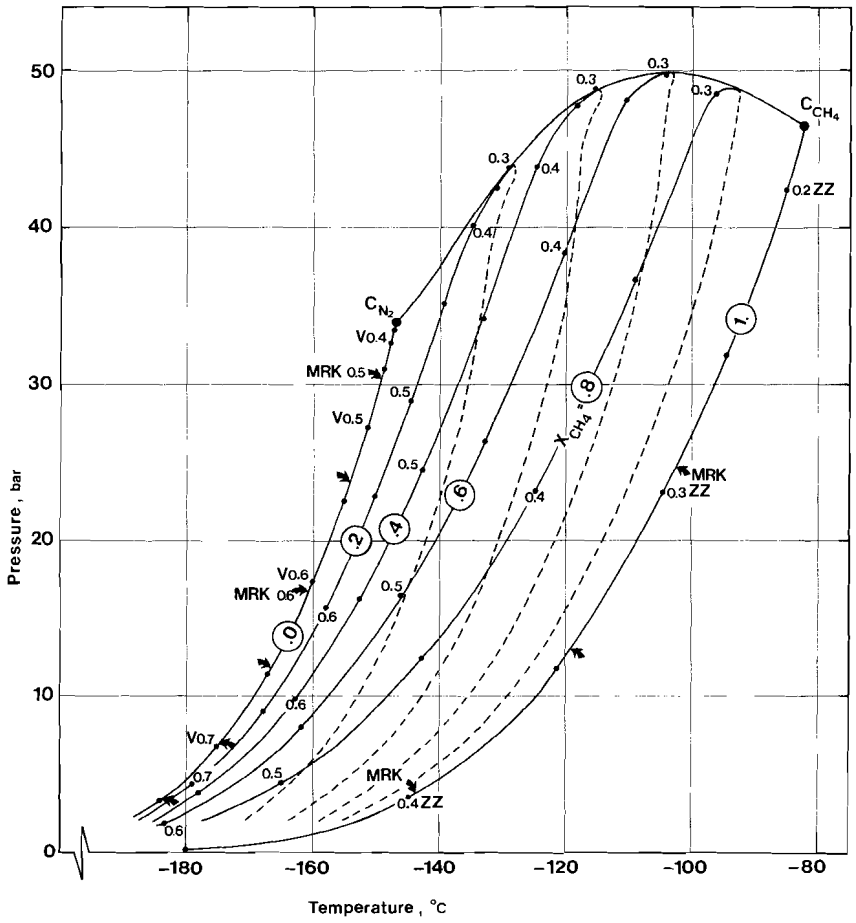

FIG. 10 Isocompositional sections and volumetry of the system N_2-CH_4 at low temperatures. Data for pure N_2 are derived from Vagarftik (1972) and for pure CH_4 from Zagoruchenko & Zhuravlev (1969). Bubble- and dew-point curves are given for X_{CH_4} ranging from 0.2 to 0.8 (Landolt-Börnstein tables, 1960). Densities along bubble-point curves are calculated with MRK (see text). Arrows indicate the position of MRK-derived densities on the boiling curve of the pure end members.

1.5.2 THE HIGH-TEMPERATURE REGION

Values of a and b of the pure end-members, given in Sections 1.3.2 and 1.4.2 together with the mixing rules defined in Sections 1.1 and 1.5.1, allow the MRK calculation of binary isochores at given composition and bulk

density. The results for molar fractions X_{CH_4} =0.2, 0.4, 0.6, and 0.8 are depicted in figures 11, 12, 13, and 14 respectively.

FIGS 11-14 MRK-derived isochores of the system N_2-CH_4. Numbers along isochores denote bulk densities (g/cc) corresponding to those given in fig. 10.

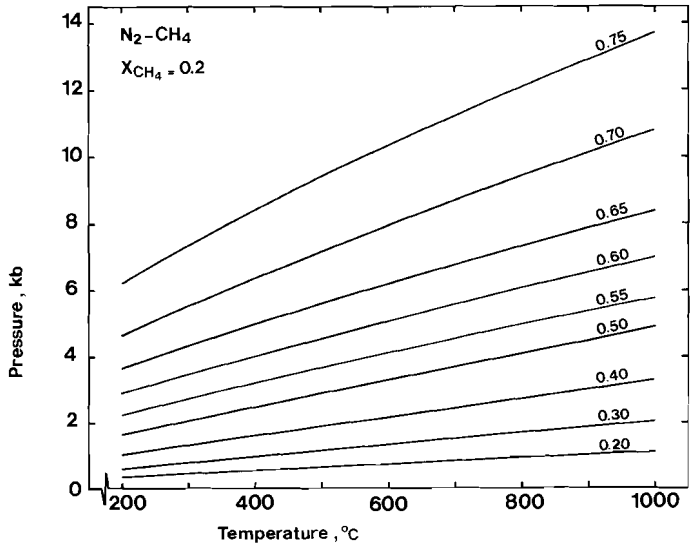

11

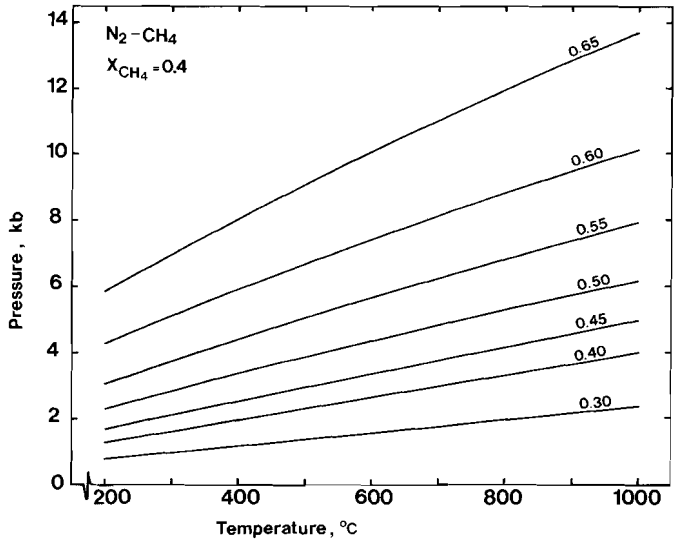

12

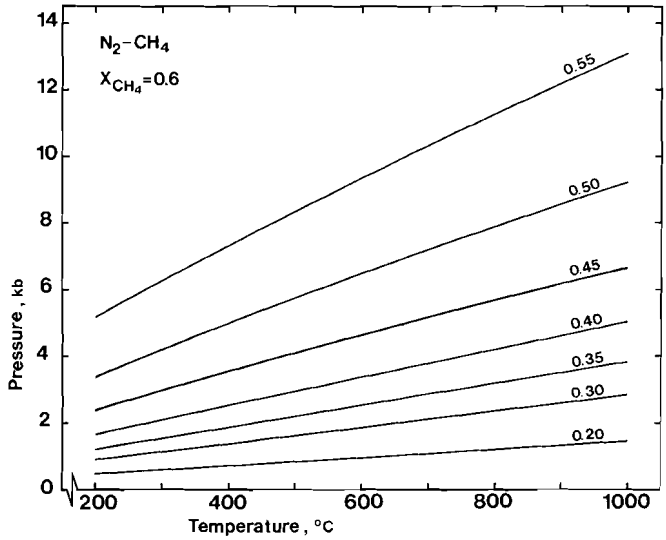

13

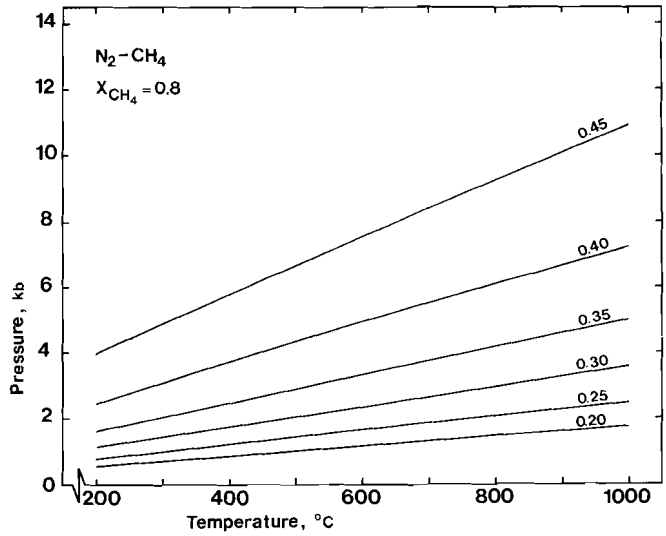

14

I.6 THE SYSTEM CO_2-CH_4

The system CO_2-CH_4 has been described extensively by Swanenberg (1979). From his work it follows that a fluid inclusion is completely defined in terms of composition (CO_2-CH_4) and bulk density if the final melting

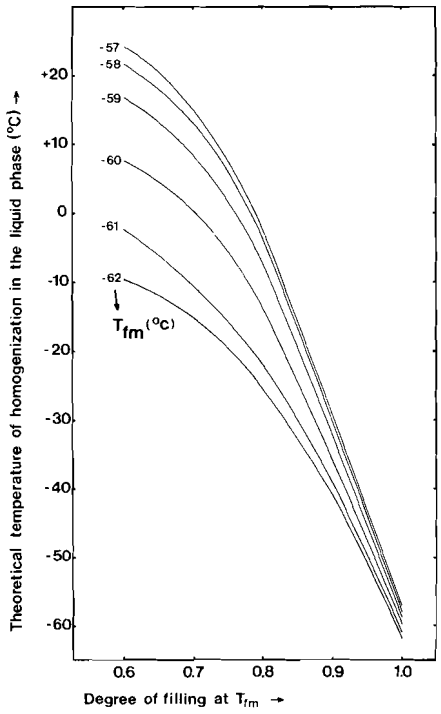

FIG. 15 Theoretical temperatures of homogenization (liq. phase) at given final melting temperature (T_{fm}) and degree of filling with liquid at T_{fm} (system CO_2-CH_4). In part after Swanenberg (1979).

temperature of CO_2 and the degree of filling at that temperature are known. In other words, theoretical temperatures of homogenization can be calculated, provided a sufficient number of boundary curves are known. Figure 15 is a diagram for homogenizations in the liquid phase. It should be stressed that theoretical homogenization temperatures are only rough estimates because the degree of filling cannot be accurately determined. A comparison with the observed homogenization temperature may, however, provide an additional 'inconsistency test' for the system CO_2-CH_4 (see also Hollister & Burruss, 1976).

I.7 THE SYSTEM CO_2-N_2

I.7.1 THE LOW-TEMPERATURE REGION

I.7.1.1. Melting phenomena

The effect of N_2 on the melting temperature of CO_2 is not directly known from experimental work. Data by Davis *et al.* (1962) suggest that in the presence of CH_4 and N_2, CO_2 melts at a higher temperature than in an equimolar mixture of CO_2 and CH_4 but still at temperatures below $-56.6^{\circ}C$.

Guilhaumou *et al.* (1978) and Dhamelincourt *et al.* (1979) combined Raman spectroscopy and microthermometry on mixed CO_2-N_2 inclusions. These

data indicate that in the presence of an N_2-rich phase, the melting point of CO_2 is depressed with respect to the triple point value of pure CO_2, albeit to a smaller extent than in an equimolar mixture of CO_2-CH_4.

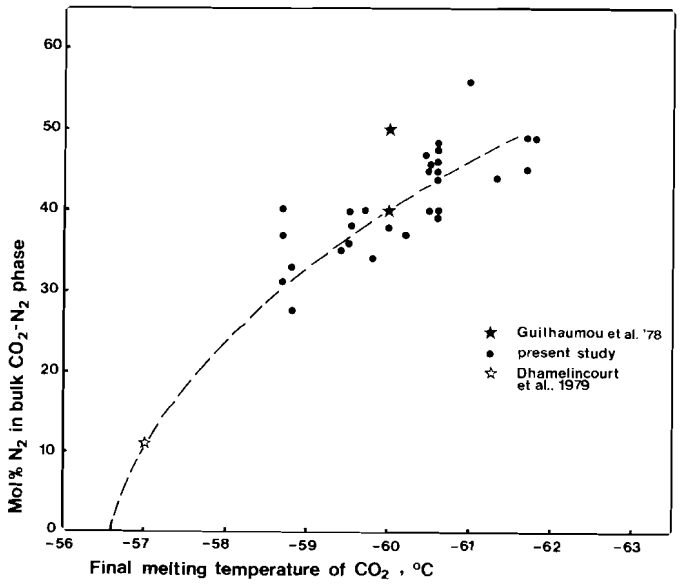

FIG. 16 Relation between molar percentage of N_2 in a bulk CO_2-N_2 fluid and final melting temperature of CO_2. Based on microthermometric data of fluid inclusions from S.W. Norway (cf. Pt.II) as well as on Raman-spectroscopic data by Guilhaumou et al. (1978) and Dhamelincourt *et al.* (1979).

Provided the concentration of N_2 is sufficiently high, cooling of CO_2-N_2 inclusions down to -180°C generates a liquid-gas equilibrium within the N_2-rich phase in addition to solid CO_2. An approximate composition in terms of CO_2 and N_2 can be obtained by estimating the relative volumes and densities of the phases involved (the density of solid CO_2 is 1.56 g/cc; the N_2-density is given by the homogenization temperature (figure 5)). Such procedure has been followed for a number of inclusions where (near-) critical behavior of the N_2-rich fluid phase in the inclusions, or in adjoining inclusions of the same configuration, indicates a relatively pure N_2 fluid (figure 16).

I.7.1.2. Homogenization phenomena

A limited number of volumetric measurements at +15°, 0°, and -20°C have been carried out by Arai *et al.* (1971). Their experimental data, including the position of the boundary curves, have been rearranged to molar compositions X_{N_2} = 0.1 and 0.2. The results are depicted in figure 17. Systematic differences have been found in the data by Arai *et al.* (1971) on the one hand, and Vagarftik (1972) and Kennedy & Holser (1966) on the other, as far as the end member CO_2 is concerned (table 1). At given temperatures of homogenization in the liquid phase, the corresponding densities given by Arai *et al.* (1971) are higher by about 4%.

As no experimental data at temperatures below -20°C are available at

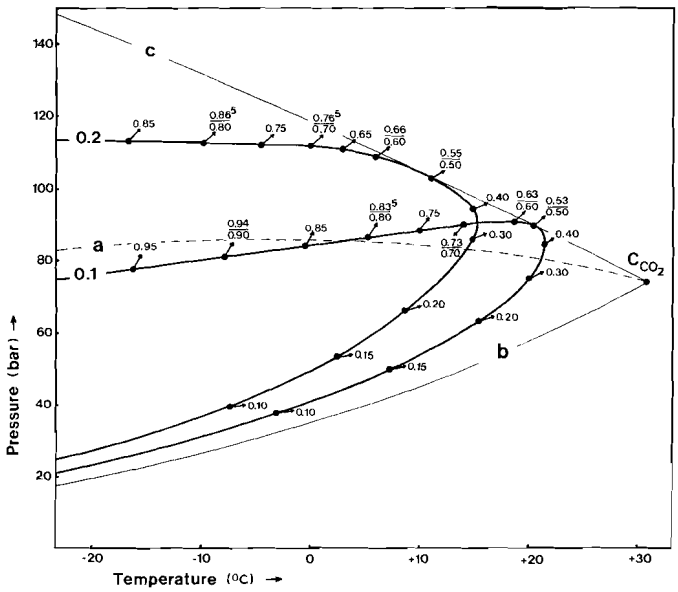

FIG. 17 Isocompositional sections and volumetry of the system CO_2-N_2 at low temperatures. Heavy lines refer to boundary curves X_{N_2}=0.1 and X_{N_2}=0.2. Numbers at bubble- and dew points refer to bulk density if single or under bar, and to equivalent CO_2-density if above bar. Curve labeled "b" is the boiling curve of pure CO_2. C_{CO_2} is the critical point of CO_2. Curve "c" is the critical curve of the system CO_2-N_2. Curve "a", the critical curve of the system CO_2-CH_4, is added for comparison. Rearranged from Arai *et al.* (1971).

present, the positions of bubble-points in this field of temperatures must be approached theoretically. This is achieved by intersecting (high-density) isochores (to be calculated with the MRK) with extrapolations of known bubble-point curves. The parameters a^{MRK} and b^{MRK} for CO_2 and N_2 given in table 1 have been extracted from the available experimental data of Vagarftik (1972). In the mixing rule for a_{12}, $a^{o}_{CO_2}$ = 46 (de Santis *et al.*, 1974).

The isochores, thus calculated, show a slight misfit with the isochores calculated from the data by Arai *et al.*(1971). This effect is not unexpected because the 'Arai'-isochores are known to be situated at a lower pressure level than the 'Vagarftik'-isochores (Table 1). Consequently, intersection of calculated isochores with the bubble-point curves yields densities that are systematically lower than the bubble-point densities that have been derived from Arai *et al.* (1971).

In order to obtain low-temperature bubble-point densities that *fit* the 'Arai'-data, only the relative positions of the MRK-isochores were taken into account. The extrapolated extensions of the bubble-point curves below -20°C were inferred from comparable phase boundaries in the system CO_2-CO (Christiansen *et al.*, 1974). The final results of this procedure have been incorporated in figures 18 and 19 whose construction will be dealt with in the next section.

I.7.2 THE HIGH-TEMPERATURE REGION

As far as is known to the present author, the only volumetric data available on CO_2-N_2 mixtures are those by Haney & Bliss (1944) for molar fractions X_{N_2} = 0.2 and 0.5 at pressures up to 500 bars and temperatures of 25°, 50°, 75°, 100°, and 125°C. Such data are of limited value to geological problems. Therefore the MRK was invoked to allow the construction of binary CO_2-N_2 isochores.

The value of F (section I.1), calculated for the system CO_2-N_2, following Pesuit (1978), is 1.001154. This is probably sufficiently close to unity to suggest that mixing rule 4, based on F = 1, will still be valid at closer molecular packing. In addition, it is assumed that the value of b_{CO_2} in a mixture of CO_2 and N_2 equals the value of b_{CO_2} in pure CO_2 which is at the same temperature and pressure as the mixture. Such a way of calculating binary isochores requires an iteration procedure. An initial estimate

of the pressure P^1_{MRK} is made on the basis of approximate values for a and b. Subsequently, the values for b_{CO_2} and b_{N_2} are corrected according to P^1_{MRK} after which P^2_{MRK} is obtained. Parameters b_{CO_2} and b_{N_2} are thus being repeatedly adjusted. The iteration is stopped when P^n_{MRK}-P^{n-1}_{MRK} is sufficiently small.

Following this procedure, isochores have been calculated for molar compositions X_{N_2} = 0.1, 0.2, 0.3, and 0.4; the results are presented graphically in figures 18, 19, 20, and 21 respectively. By combining the results of section I.7.1.2, the isochores in figures 18 and 19 are related to homogenization temperatures. It should be emphasized that the high-density isochores are approximations. Based on the definition of $b^{MRK}_{CO_2,N_2}$

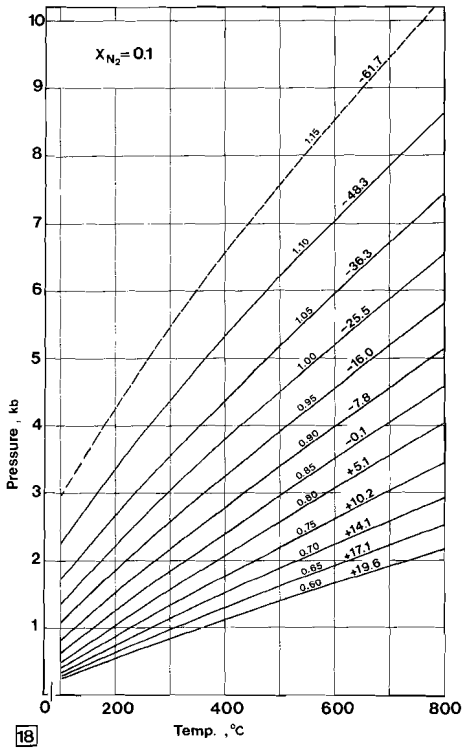

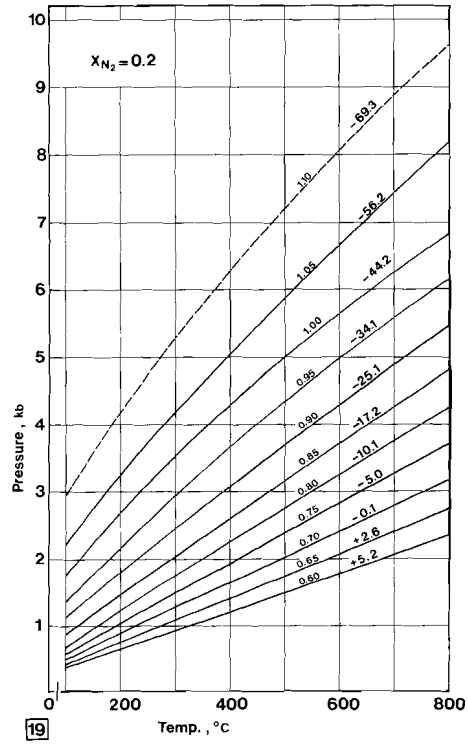

FIGS 18-19 MRK-derived isochores in the system CO_2-N_2 for compositions X_{N_2}= 0.1 and 0.2. Isochores are given by bulk density (g/cc) and temperature of homogenization in the liquid phase (°C). Broken lines are isochores of extremely dense fluids; their position is somewhat uncertain. Based on Arai *et al.*(1971).

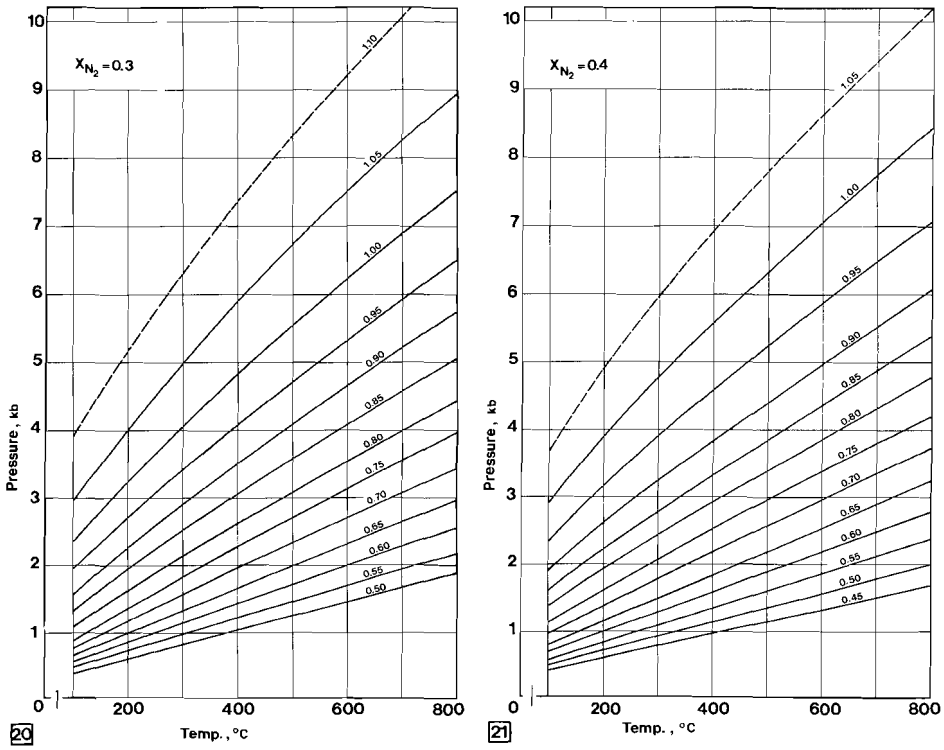

FIGS 20-21 MRK-derived isochores of the system CO_2-N_2 for compositions X_{N_2}= 0.3 and 0.4. Numbers attached to isochores are bulk densities (g/cc).

is believed, however, that the high-density isochores represent at least minimum pressures at given temperatures.

I.8 THE SYSTEM H_2O-CO_2

The binary system H_2O-CO_2 is one of the fundamental binary systems in geochemistry. P-T-X relations up to 350°C and 2500 bars have been determined experimentally by Tödheide (1963), and up to 2500 bars by Takenouchi & Kennedy (1964). A rearrangement of the data by Takenouchi & Kennedy (1964) yields boundary curves in the P-T plane (figure 22). P-V-T-X relations given by Khitarov & Malinin (1956), Franck & Tödheide (1959), Ypma (1963), Greenwood (1969), and Ryzhenko & Malinin (1971) largely apply to low-pressure conditions and are thus of limited interest to

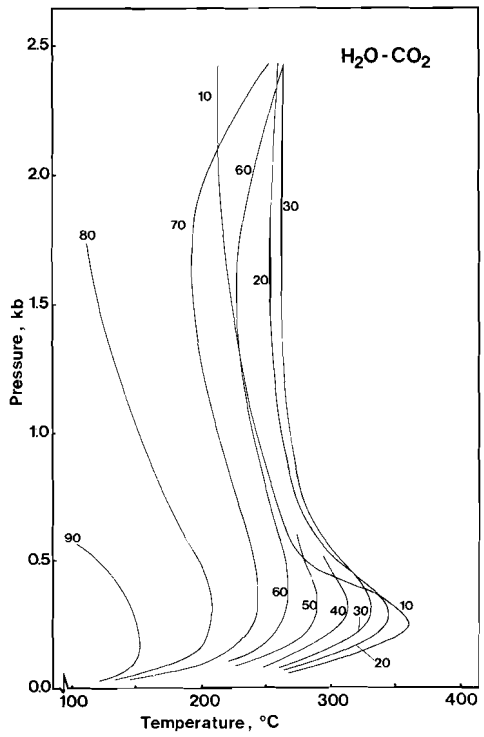

FIG. 22 Isocompositional curves of the system H_2O-CO_2 according to Takenouchi & Kennedy (1964). Numbers at boundary curves refer to molar percentages of CO_2.

the present fluid inclusion study.

The MRK (Eq.(1)) has been employed to calculate isochores in the field of geologically interesting temperatures and pressures. The following parameters and cross-parameters, in addition to those given in section I.1, have been used:

$$a_{H_2O}(T)=1.01325\times(166.8\times10^{6}-193080T+186.4T^{2}-0.071288T^{3}) \quad \text{(Holloway, 1977)}$$

$$a_{CO_2}(T)=1.01325\times(73.03\times10^{6}-71400T+21.57T^{2}) \quad \text{"}$$

$$a_{12}=(a^{o}_{H_2O}\cdot a^{o}_{CO_2})^{\frac{1}{2}}+\tfrac{1}{2}R^{2}T^{5/2}.K \quad \text{(de Santis } et\ al.\text{, 1974)}$$

$$\ln K=11.071+5953/T-2746\times10^{3}/T^{2}+464.6\times10^{6}/T^{3} \quad \text{"}$$

$$b_{H_2O}=0.0146 \quad \text{"}$$

A constant value for b_{CO_2} (0.0297 l/mole) such as proposed by de Santis *et al.* (1974) will yield erroneous isochores at elevated densities and high concentrations of CO_2 (section I.2.3). It is, therefore, proposed to define b_{CO_2} of the mixture in the same way as has been done for the system CO_2-N_2 (section I.7.2). In other words, it is assumed that the H_2O molecules have the same effect on b_{CO_2} in the mixture as a substitute number of CO_2 molecules would have at the same temperature and pressure. The calculation of

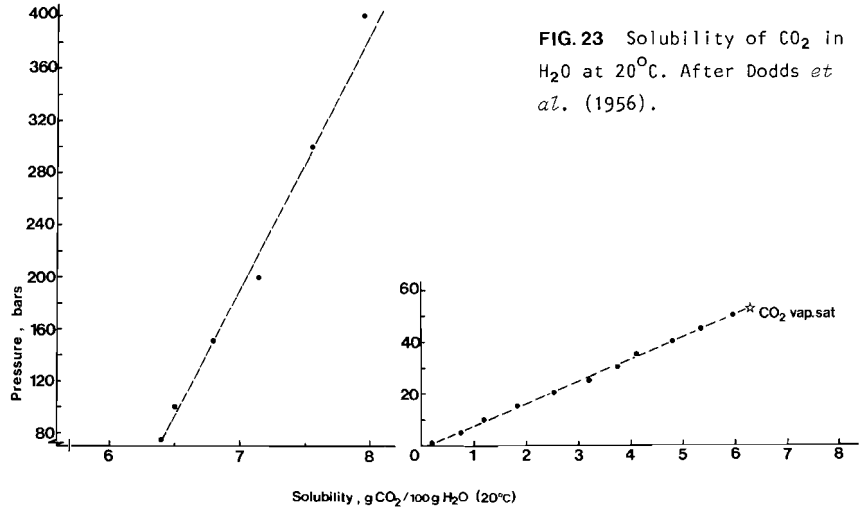

FIG. 23 Solubility of CO_2 in H_2O at 20°C. After Dodds *et al.* (1956).

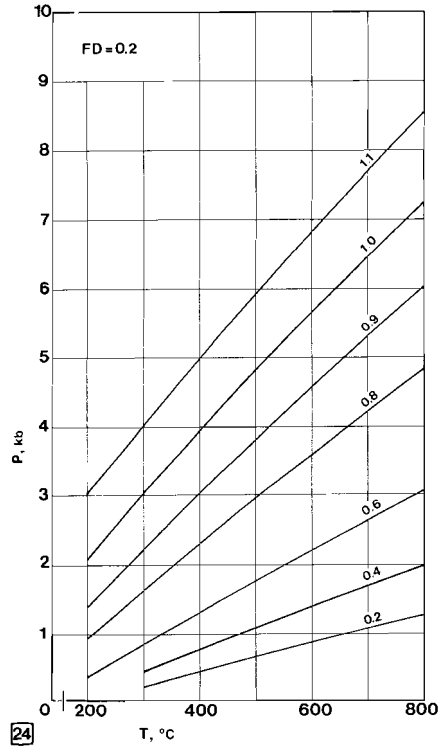

24

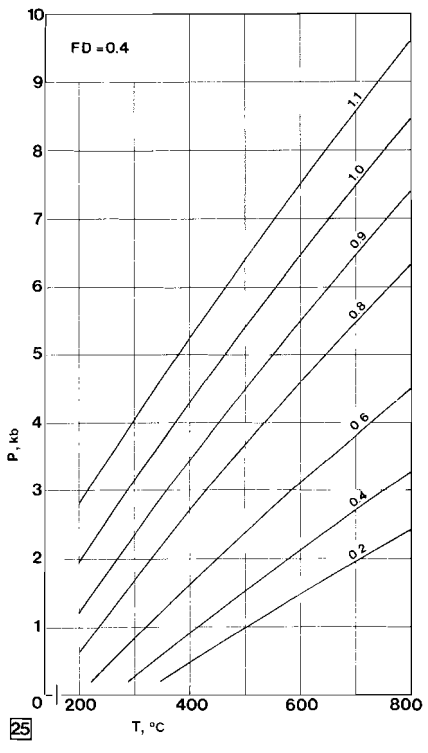

25

FIGS 24-27 MRK-derived isochores of the system H_2O-CO_2. Each diagram applies to a given degree of filling V_{H_2O}/V_{total}, estimated at about +21°C. Numbers along isochores are densities of CO_2 in the bubble at 21°C.

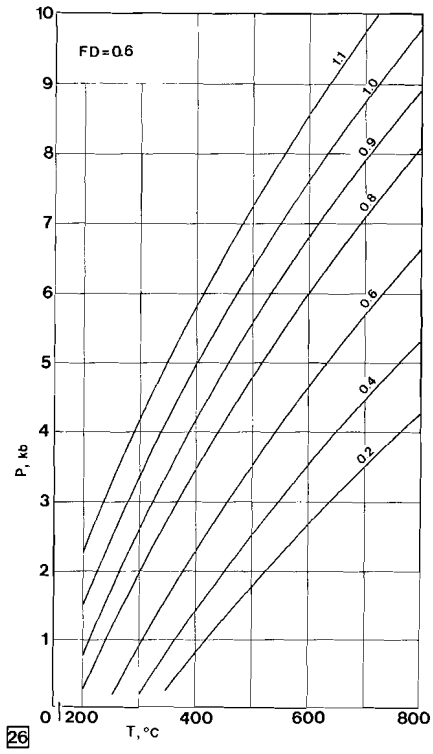

26

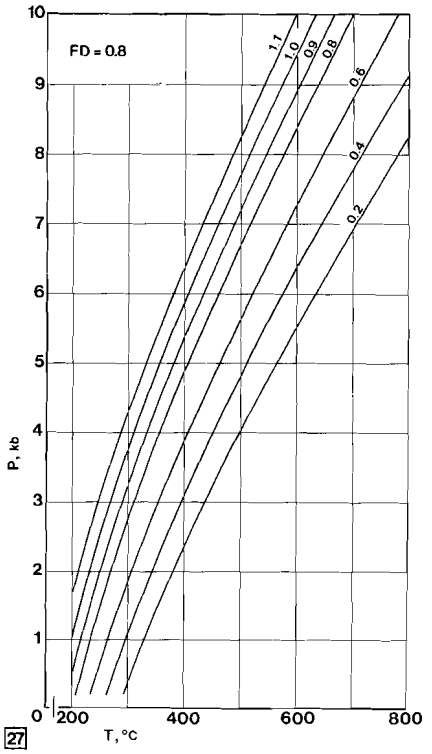

27

MRK-isochores, knowing the degree of filling with H_2O and the density of CO_2 in the bubble, is based on the following additional assumptions:

- the solubility of H_2O in CO_2 is very low (Wiebe & Gaddy, 1941) and has, therefore, been neglected.
- the solubility of CO_2 in H_2O is appreciable at high pressures (figure 23) and has, therefore, been considered in the calculations.
- the degree of filling with H_2O is estimated at about 21°C, because at that particular temperature the partial molal volume of CO_2 in H_2O (affecting the bulk density of the aqueous solution) is nearly independent of the pressure (Parkinson & De Nevers, 1969; Malinin, 1974).
- the density of H_2O-rich phase is 1.00 g/cc (Parkinson & De Nevers, 1969).

A graphical presentation of the MRK-isochores is given in figures 24, 25, 26, and 27.

Alternatively, it may be assumed that b_{CO_2} in the mixture varies according to the partial pressure of CO_2 rather than the total pressure. In this way, somewhat higher pressures are eventually obtained (in particular with the high-density isochores). A comparison with the (low-density) data of Franck & Tödheide (1959), however, does not permit a choice between the two hypotheses because both result in MRK-pressures that are in good agreement with the experimental data (Table 5)

X_{H_2O}	Number of moles/l	Pressure (F&T,bars)	Pressure (MRK-1)bars	ΔP (%)	Pressure (MRK-2)bars	ΔP (%)
0.822	6.4	396	395	-0.2	395	-1.0
0.705	7.4	459	466	+1.5	466	+0.9
0.619	8.4	533	546	+2.4	546	+2.5
0.551	9.5	620	631	+1.8	631	+2.2
0.498	10.5	723	730	+1.0	730	+1.4
0.453	11.5	821	837	+1.9	837	+2.6
0.416	12.5	946	956	+1.1	956	+2.0
0.385	13.6	1089	1100	+1.1	1101	+1.1
0.358	14.6	1253	1253	+0.1	1258	+0.4
0.335	15.6	1423	1424	+0.1	1435	+0.8
0.314	16.6	1631	1642	+0.7	1629	-0.1
0.296	17.6	1836	1870	+1.8	1852	+0.9

TABLE 5 Comparison of MRK-derived pressures with experimental data by Franck & Tödheide, 1959 (F&T) at 500°C. MRK-1 pressures have been derived with the assumption that b_{CO_2} is determined by the total pressure exterted by the mixture. MRK-2 are the results if b_{CO_2} is related to the partial pressure of CO_2. See text for discussion.

1.9 CONCLUSIONS

1. Application of the Modified Redlich-Kwong equation of state to the systems CO_2, CH_4, N_2, N_2-CH_4, CO_2-N_2, and H_2O-CO_2 allows the P-T interpretation of homogenization temperatures of fluid inclusions at known compositions. Using the concept of "CO_2-equivalent density" (cf. Swanenberg, 1979) it should be possible to derive approximate isochores for CO_2-CH_4-H_2O and CO_2-N_2-H_2O inclusions as well.

2. The melting point depression of CO_2 by N_2 is much less compared with the effect of CH_4. This implies that compositions, acquired by assuming that CH_4 rather than N_2 is the main depressor of the CO_2 triple-point temperature, are seriously in error. In addition to this, the corresponding homogenization temperatures (liquid phase), expressed in the system CO_2-CH_4, define isochores that, at given temperature, are too high in pressure.

3. The temperature of homogenization in the liquid phase of a CH_4- or N_2-bearing carbonic inclusion, compared to an equimolar pure CO_2 inclusion, is invariably lower. At given homogenization temperature (liquid phase), the bulk- and CO_2-equivalent density of a mixed CO_2-(N_2-CH_4) inclusion are both less than the density of a pure CO_2 inclusion homogenizing at the same temperature. By neglecting the presence of CH_4 or, in particular, N_2 in a CO_2-rich inclusion the pressure estimates will be too high.

4. In the system H_2O-CO_2 the isochores at high density of CO_2 and low degrees of filling with H_2O (up to 0.2) are not markedly different from isochores that are based on the homogenization temperature of CO_2 only. This implies that only small errors are introduced if a (usually invisible) small amount of H_2O is not taken into account and the inclusion is regarded as a pure CO_2 inclusion. Similarly, isochores for high degree of filling are no sensitive function of the CO_2-density in the bubble.

Part II

FLUID INCLUSION STUDY

II.1 GEOLOGIC SETTING

The high-grade metamorphic Precambrian of south-west Norway consists of anorthosite masses and the lopolith of Bjerkreim-Sokndal (fig. 28; Hermans *et al.*, 1975). Intrusion of the lopolith, about 1000-1050 Ma ago, gave rise to contact metamorphism (high-temperature, low-pressure granulite-facies metamorphism which affected a pre-existing high grade metamorphic terrane (Wielens, 1979; Maijer *et al.*, 1980). Rb-Sr whole rock age determinations suggest additional igneous or metamorphic events at about 1500 and 1200 Ma (Versteeve, 1975).

The high-grade metamorphic envelope largely consists of charnockitic and granitic migmatites (banded as well as massive parts are discerned). In addition, augen gneisses, syenitic and basic intrusions, and (largely) metasedimentary sequences are present. In the migmatitic rocks the leucocratic parts are generally medium-grained charnockites and charnoenderbites (or their "granitic" equivalents in the eastern part of the region) whereas the darker components comprise (leuco)norites, amphibolites, monzonorites, and enderbites.

Two types of metasedimentary rocks occur:

1. Garnetiferous migmatites, mainly composed of metapelitic gneisses and granofelses, containing mineral assemblages of almandine-rich garnet, biotite, sillimanite, spinel, cordierite, and orthopyroxene, besides quartz and feldspars. Locally, osumilite and sapphirine are present (Hermans *et al.*, 1976; Maijer *et al.*, 1980).
2. Faurefjell metasediments, mainly composed of quartzites, marbles, diopside rocks, diopside gneisses, and rocks of (alkali)granitic composition in sequences up to 40 meters thick and with varying relative proportions of the constituent rock types.

The local presence of sapphirine and osumilite in the Garnetiferous migmatites suggests minimum temperatures of 800-900°C at a total pressure of 3-6 kbars (Hermans *et al.*, 1976; Maijer *et al.*, 1980). Geothermometry based on pyroxene and oxide equilibria in metabasites gives 800-900°C whereas garnet-cordierite pairs point to 700-750°C (Jacques de Dixmude, 1978). Temperatures of pyroxene crystallization in the top of the lopolith and in one of the syenitic intrusions enclosed in the metamorphic envelope are between approximately 900 and 1050°C while the total pressure variation is 5-7 kbars in the top of the lopolith (850-950 Ma, Versteeve, 1975,

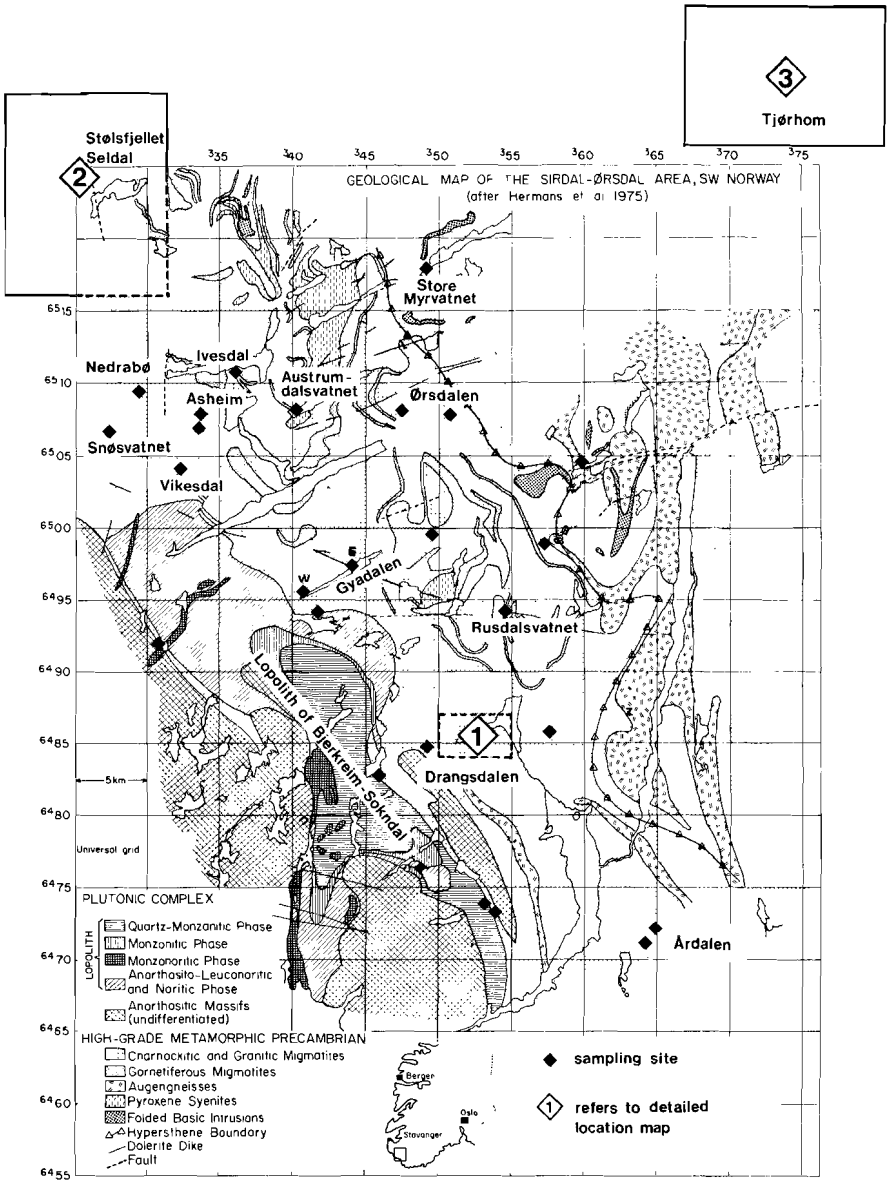

FIG. 28 Geological map of Rogaland/Vest-Agder, showing sample locations. Insets 1, 2, and 3 are expanded in figures 75, 29, and 30 respectively. Geology simplified after Hermans *et al.* (1975).

Pasteels *et al.*, 1979) and 7-10 kbars in a syenitic intrusion (1200 Ma, Wielens, 1979). Studies based on Fe-Mg partitioning in orthopyroxene-garnet-cordierite assemblages from an intercalation in Garnetiferous migmatites give temperatures of 720-770°C and about 1000°C at a lithostatic pressure of 6-7 kbars (Brons, 1975; pers.comm. Jansen). In the Faurefjell metasediments the maximum amount of $MgCO_3$ in calcite points to minimum temperatures of 670° and 750°C at two different localities (Sauter, pers. comm.) while phase theoretical work on mineral assemblages yields a minimum temperature of 650-700°C at a fluid pressure of 5-7 kbars (Teske, 1977a).

The large-scale deformation comprises at least four phases: D1= isoclinal folding; D2= rather indistinct, locally NE-SW folding; D3= recumbent folding with axes trending NW-SE to N-S (most important phase of folding); D4= open folding, possibly in conjunction with an updoming of the anorthosite masses. Fold axes in the north of Rogaland are N-S whereas in the south they are E-W. Most phases of deformation predate the latest phase of high-grade metamorphism (Hermans *et al.*, 1975; Maijer, pers.comm.)

The area is transected by ENE-WSW and WNW-ESE trending dolerite dikes which may have intruded about 900 Ma ago, the last-mentioned being younger although the exact age is unknown (Versteeve, 1975).

Retrogressive activity, well developed in fault zones, is reflected by the presence of minerals such as stilpnomelane, prehnite, pumpellyite, green biotite, chlorite, epidote, serpentine, and carbonate. In part, the assemblages of secondary minerals may result from Caledonian overthrusting.

II.2 PETROLOGY OF THE SAMPLING SITES

Sampling sites in the Rogaland/Vest-Agder region of S.W. Norway have been selected in charnockitic and granitic migmatites (comprising pegmatites) and in metasedimentary rocks (including quartz pods). The location of the sampling sites and the descriptions of individual samples are given in the Appendix.

I.2.1 DRANGSDALEN

Drangsdalen is located northwest of Moi, NGO sheet Sokndal 1311 IV (fig. 28, inset 1). Geologically, it forms part of a dome-shaped structure in charnockitic migmatites (with orthopyroxene in leucogranitic components, Hermans *et al.*, 1975). Although quartz-rich samples were selected for fluid inclusion studies it was tried to sample a possible contact-zone with a meso/melanocratic rock as well. This procedure is based on the hypothesis that such a contact-zone is the most suitable locus of finding evidence for possible mineral reactions. Because a large part of the area is, or has been, migmatitic, dehydration reactions involving quartz and hydrated ferro-magnesian silicates will preferentially occur along the contact, where volatiles can be removed effectively.

After a preliminary sampling, thin sections that were prepared in the field camp, facilitated the interpretation of megascopically visible phenomena.

Structurally, the oldest rocks of the Drangsdal area form part of the so-called "*Early Migmatite*", predominantly fine-grained rocks with diffuse nebulitic to schlieren-like structures; locally, the appearance is massive (Mehnert, 1968). The general direction of the foliation or banding is difficult to establish but the strike is approximately N-S with steep dips between 50° and 90°E. Coarse-grained quartzofeldspathic rocks are locally intercalated in the Early Migmatite. Although gradual transitions have been observed, a number of contacts show a convex form of the coarse-grained rock towards the parent rock, suggesting a "front-like advance of the mobilisate" (Mehnert, 1968). At the scale of an outcrop, thin discordant biotite-feldspar veins produce a diktyonitic structure in the Early Migmatite. Because the parent rock bends flexure-like towards the veins, this structure probably involves shear movement.

A vaguely- to well-banded sequence of rocks, locally showing discor-

dant relations with the Early Migmatite is called "*Late Migmatite*". Banding is caused by compositional variations and/or variation in grain size.

The "*Pegmatite Phase*" comprises discordant pegmatites and pegmatoid bodies as well as discordant biotite-feldspar veins (mainly found in the Early Migmatite).

In the leucocratic components of the Early and Late Migmatite (charnockites- leuconorites) large crystals of quartz may be observed (locally up to 30 mm in the longest dimension) in a relatively fine-grained matrix with variable proportions of plagioclase, K-feldspar, and quartz. Quartz may show preferred form orientation. In the mafic components, greenish-brown amphibole is locally present.

Compositions in the Pegmatite Phase range from alkalifeldspar charnockite to enderbite (or their granitic equivalents). The border zones of discordant leucocratic veins may contain appreciable amounts of ilmenite/magnetite, zircon, monazite, and apatite. One of these veins was dated by Wielens (1979) at 880 Ma (U-Pb zircon, upper intercept with Concordia).

As a rule, quartz-bearing leucocratic rocks, in particular when coarse grained , are devoid of biotite. In Early Migmatite rocks, typically composed of anhydrous mineral assemblages, thin intercalations containing fine-grained biotite have been observed (zones with local high P_{H_2O}?). A limited number of rocks, medium-grained charnockites, contain biotite in contact with quartz. Here, the biotite occurs in flakes with some preferred orientation (40-30SE). This biotite may be secondary, being related to the "shearzones". In general, however, *biotite and quartz display an antipathetic relation* : contacts between quartz-bearing leucocratic rocks and biotite-bearing mafic rocks invariably show an orthopyroxene-rich rim.

As opposed to the frequently observed assemblages of anhydrous minerals in the coarse-grained leucocratic rocks, the finer grained meso/melanocratic rocks commonly contain biotite. As this biotite is probably not a secondary phase it is suggested that during high-grade metamorphism coarse-grained rocks have behaved more like an open system than the adjacent finer grained meso/melanocratic rocks, where volatiles could less easily escape. The anhydrous mineral assemblage in the coarse-grained rocks could, however, equally well result from a meltphase produced under conditions of low P_{H_2O}.

The generally observed antipathetic relation between biotite and quartz together with the presence, in stead, of orthopyroxene, strongly suggest a metamorphic reaction. It remains, however, difficult to explain the (frequently observed) absence of K-feldspar at the reaction site. This absence could perhaps in part be attributed to the formation of a melt

which takes up H_2O, thus promoting the orthopyroxene-forming reaction and the concomitant removal of alkalifeldspar. Discordant orthopyroxene syenites in the Early Migmatite as well as rocks from the Pegmatite Phase indicate that melts have been produced at granulite-facies conditions.

In contact specimens the An-content of plagioclase in the leucocratic biotite-free quartzofeldspatic rock is slightly less (4-9%) than in the plagioclase of the adjacent biotite-bearing mafic rock. The An-content in orthopyroxene-bearing rocks without biotite-quartz contacts is generally higher than in charnockitic rocks where biotite is found in contact with quartz. The highest An-contents have been determined in a noritic body in the eastern part of Drangsdalen: a fine grained biotite-amphibole-bearing gabbro-norite (An-content ranging from 64 to 73%) locally contains coarser grained segregations composed of plagioclase (52-56% An), orthopyroxene, and clinopyroxene which are rimmed by a zone rich in orthopyroxene and plagioclase (59-65% An). This phenomenon resembles the bimetasomatic rims that have been reported by Schrijver (1973) from a hornblende granulite-facies terrane in the Grenville Province (Canadian Shield). Such rims are ascribed by Schrijver (1973) to simultaneously operative "desilication" of metabasite and metamorphic reactions between hydrous mafic minerals and quartz.

Versteeve (1975) has obtained a 1485 Ma Rb-Sr whole rock age for a restricted area in Drangsdalen. This isochron is based on datapoints from six rocks, three of which (Versteeve's samples Rog 212, 213, and 215) almost certainly belong to the Early Migmatite whereas one sample (Rog 214) may be Late Migmatite. From the samples that produce "off-isochron" points (Rog 54, 56, 211, 216, 217, and 218) only Rog 216 almost certainly belongs to the Early Migmatite. In addition to this, Rog 216 is the only deviating datapoint above the isochron as opposed to the other samples. It is thus suggested that the 1485 Ma isochron in Drangsdalen is essentially based on rocks from the Early Migmatite, occurring preferentially in the core of a dome-shaped structure.

Most rocks show low to intermediate degrees of post-crystalline deformation. Large crystals of plagioclase may show curved twin lamellae. Quartz commonly shows more or less intense undulatory extinction; occasionally, deformation lamellae may be observed in subbasal section (fig. 45). An extremely high degree of deformation is shown by a strongly retromorphosed quartzofeldspathic rock in a noritic body in the eastern part of Drangsdalen.

Local retromorphic activity (greenschist facies) is not uncommon in Drangsdalen. It is particularly widespread in the western part, along

joints. In general, coarse-grained leucocratic rocks are altered more extensively than the adjacent finer grained mesocratic rocks. This suggests again a more open behavior of coarse-grained rocks, in this case with respect to late-stage fluids.

II.2.2 FAUREFJELL METASEDIMENTS

An account of the petrology of the Faurefjell metasediments is given by Sauter (1980). Samples have been collected from the "basal" part of the formation (a norite or a quartzite), from a number of quartz veins and -pods in forsterite-phlogopite marbles (4-5 m thick) and from diopside-bearing gneisses and -quartzites.

The basal quartzite that has been sampled near Asheim (fig. 28) is 4-6 m thick and consists mainly of coarse-grained bluish-gray quartz. Locally, a distinct banding, caused by thin layers (about 1 mm) of cordierite and alkalifeldspar, has been observed. Grain sizes range up to 3-4 mm. The degree of deformation is generally low. Most grains contain a relatively high number of small rutile(?) needles, probably responsible for the bluish-gray macroscopic color.

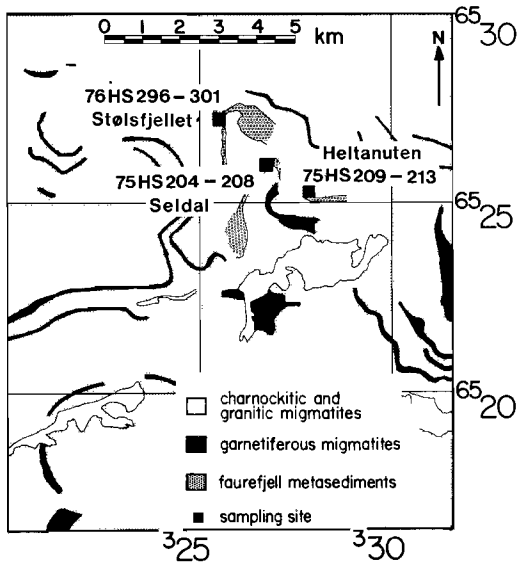

FIG. 29 Sample locations in northern occurrences of the Faurefjell Metasediments (inset 2, figure 28). Geology after Morroy (1974), Teske (1977), and Wegelin (1979).

The quartz pods are usually lensoid bodies, about 10 cm. thick, which are locally folded. They are separated from the host marble by a 1-3 cm thick rim of diopside. The quartz is typically white or gray, very coarse (up to 20 mm) and may contain solid inclusions of diopside, carbonate, and tremolite (replacing diopside). Rutile is not common. The degree of deformation is generally low but some crystals show well-developed mosaic textures. In a northern occurrence of the Faurefjell metasediments near Seldal (fig.

28 (inset 2); fig. 29) the marble carries calcite (locally calcite-dolomite symplectites), forsterite, phlogopite, plus a minor amount of diopside. A large body of quartz is present in the crest of a fold near Stølsfjellet. The quartz has been sampled because it has almost certainly been emplaced at retrograde greenschist facies conditions, as evidenced by the presence of a talc-rich level between the quartz body and a talc-tremolite-bearing marble. Within the main mass of quartz, clear streaks and vugs filled with euhedral crystals point to dissolution and (re)precipitation.

The quartz-diopside gneisses, sampled near Nedrabø (fig. 28), comprise quartz-rich alkalifeldspar granites or-charnockites. Relatively large crystals of titanite are not uncommon. In general, quartz displays a moderate to high degree of deformation. Quartz crystals size up to 20 mm , the average value being 4-6 mm. Retrogressive alteration is quite common.

II.2.3 GARNETIFEROUS MIGMATITES

Near Austrumdalsvatnet (fig. 28) a number of graphite-bearing quartzofeldspathic rocks have been sampled for the purpose of studying the relations between the presence of graphite and the composition of fluid inclusions. The graphite-bearing rocks are largely concordantly intercalated (although locally discordant off-shoots have been observed) in garnet-cordierite gneisses and -granulites that may contain sillimanite and/or spinel in addition.

Near Vikesdal (fig. 28), coarse-grained quartzofeldspathic rocks are interlayered with dark streaks containing quartz, orthoclase-mesoperthite, strongly pleochroic orthopyroxene, garnet, spinel, and *osumilite*. Spinel is not in contact with quartz; garnet is rimmed by plagioclase and orthopyroxene and is not in contact with quartz (cf. Maijer *et al.*, 1977). A similar type of rock, without osumilite, but containing cordierite, has been collected in Gyadalen. In the associated fine-grained rocks spinel (hercynite) is in contact with quartz.

Near Ivesdal (fig. 28), a quartz enderbite has been sampled close to *sapphirine*- bearing rocks (cf. Hermans *et al.*, 1976).

II.2.4 THE HIGH-GRADE AMPHIBOLITE FACIES AREA AROUND TJØRHOM

In the high-grade amphibolite facies area around Tjørhom, samples were collected to establish a possible relation between the grade of metamorphism and the composition of the fluid inclusions (following Touret, 1974a). A simplified geological map of the area including the location of samples, is given in fig. 30 (see also inset 3 in fig. 28). Granitic migmatites,

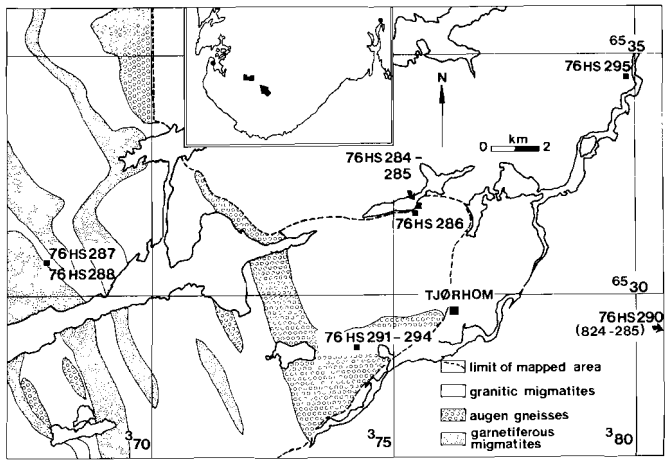

FIG. 30 Index map (inset 3 in fig. 28) showing sample locations in the region near Tjørhom. Geology after Kars *et al.* (1977).

augengneisses, pegmatitic granites, and garnetiferous migmatites ("Hunnedalen type", Hermans *et al.*, 1975) are present. In the granitic migmatites near Tjørhom, the boundary between mobilisate and restite is devoid of orthopyroxene (as opposed to the charnockitic migmatites) but contains, in stead, concentrations of biotite and amphibole. Five kilometers to the west, however, orthopyroxene has been found along the contact of a quartz vein with an amphibolite. In a nearby collected enderbitic rock, on the other hand, (primary?) biotite has been found in contact with quartz, while orthopyroxene is present in the leucocratic rock. Local recurrences of charnockitic rocks within the Tjørhom area are not uncommon (Sauter, pers. comm.)

II.2.5 ROCKS ADJACENT TO A DOLERITE DIKE

In order to eventually determine superheated fluid inclusions (Lokerman (1962), rocks adjacent to a dolerite dike were sampled. Contacts between

a WNW-ESE running dike (Egersund system) and the country rock have been sampled at two localities (Rusdalsvatnet and Gyadalen-E, fig. 28). The dike has an extension of at least 50 km., its thickness is variable and amounts up to 30 m locally. It has been described earlier by Antun (1956) as an olivine-bearing (trachy)dolerite, composed of plagioclase, augite, olivine, K-feldspar, opaques, and apatite.

As opposed to the "reversed" magnetization of the basement rocks and the "Hunnedalen" dolerites (striking ENE-WSW) the "Egersund" dolerites display a "normal" magnetization. This precludes their emplacement at a time when the basement rocks were still at a temperature of 550-650°C (Poorter, 1972). Owing to relaxation effects upon slow cooling, this blocking temperature of the basement rocks may drop to 300-350°C (Poorter, pers.comm.). The presence of chilled margins and microporphyritic vitreous rims (Antun, 1956) also indicates relatively low ambient temperatures in the order of 300°C (compare Wiebe, 1979). Palaeomagnetic data by Poorter (1972), however, still indicate a Precambrian pole position for the Egersund dolerite dikes.

Extensive hydrothermal alteration (carbonate, prehnite, chlorite, saussurite) is common. Antun (1956) refers to "autometamorphic alteration", caused by volatiles that are released by the doleritic magma.

II.3 FLUID INCLUSIONS - ANALYTICAL PROCEDURE

II.3.1 CRUSHING TESTS

In the present study the crushing stage has been used in a semi-quantitative way following Al-Khatib & Touret (1973). Grains of quartz, dimensions about 0.5-0.7 mm, are weighed and crushed in anhydrous glycerine between two glass plates (3 mm thick). Number and sizes of the bubbles that result from opening inclusions with gas under pressure (or liquid), are measured. A number of 10 crushing runs is performed on each sample. If the liberated gas is assumed to be CO_2, a valid assumption for most rocks, the weight percentage gas in quartz (W) can be determined from:

W= total volume bubbles x 0.2/ (volume grain x 2.65)

As a rule, the quantities of gas are quite variable. An index I, defined by:

I= 1/ ((standard deviation/mean) + 1)

reflects this variability for individual samples in a relative way.

An approximate bulk ratio CO_2 / n.c. (=non-condensable gasfraction at liquid nitrogen temperature) of fluid inclusions can be obtained by crushing quartz grains under vacuum in steel tubes. After removal of adsorbed water by pumping, the sample is crushed at room temperature with the aid of a hydraulic press (10 ton) which opens part of the inclusions. Separation of CO_2 and non-condensable gases is achieved by successively applying melting acetone (-90°C) and boiling nitrogen (-196°C) to the cold trap of a vacuum system. Respective pressures are measured with a McLeod manometer. Non-condensable gases can be collected on molsieve 5Å at -196°C for gaschromatographic analysis.

II.3.2 GASCHROMATOGRAPHIC ANALYSIS AND STABLE ISOTOPES

The non-condensable gases (O_2, N_2, CH_4, and CO) have been analyzed with the aid of a simple gaschromatographic set-up, essentially composed of a 1 m long stainless steel column (I.D. $^1/_8$"), packed with molsieve 5Å, and a Carle (thermal conductivity) Microdetector. Carrier gas is He, flowing at a rate of about 30 ml/min. Effective detection of CO requires minimum temperatures of about 50°C. The gaschromatographic set-up is connected with a vacuum system where a precolumn, packed with molsieve 5Å, at liquid

nitrogen temperature allows the freezing out of gas samples. Next, the cold trap is switched in series with the analytical column and is brought quickly to a temperature of about 50°C.

It is assumed that all O_2 that appears in the analysis is due to leakage. The quantity of N_2 has, therefore, been corrected relative to the amount of O_2 , taking into account that the molar ratio of N_2-O_2 in air has a value of 3.731 (Weast, ed., 1975).

Correction for selective adsorption of CO_2 (and to a lesser extent CH_4) relative to N_2 (Barker & Torkelson, 1975) has not been made because in the present experiments the pressures are extremely low (molsieve at liquid nitrogen temperature!).

Isotope ratios were measured on a Micromass 602C mass-spectrometer, equipped with an inlet system suitable for handling small samples. 44-45 ratios of CO_2 were corrected for coincidence of $^{12}C^{16}O^{17}O$ ions and 46/(44+45) ratios for the contribution of mass 45 to the major peak. Isotope ratios are reported in the usual δ-notation as ‰ deviations relative to PDB. The uncertainty is probably in the order of 0.5-1.0 ‰ .

II.3.3 SAMPLE PREPARATION FOR MICROTHERMOMETRY STUDIES

Rock specimens are sawn with a diamond blade (Ø 250 mm, 2000 r.p.m.), ground flat with carborundum and polished with Tonerde 1 (5 microns). Next, the chips are mounted on object glass using a two-component Loctite-Locquic cement curing in about 10 seconds, followed by grinding and polishing of the other side. Considerable care is taken not to overheat the sample. Depending on the transparancy of the sample, the final thickness is set at 60-150 microns.

For routine optical studies mounted sections are most practical but accurate heating-freezing work requires unmounted sections, readily obtained by dissolving the cement in H_2O. When a long time has elapsed since the preparation, the section can be unmounted by using concentrated HNO_3 at room temperature.

II.3.4 ESTIMATING RELATIVE PROPORTIONS OF INCLUSION TYPES

Optically, three main types of fluid inclusions may be recognized: 1. monophase carbonic or N_2-rich. 2. biphase with an intermediate to large

bubble (H_2O-CO_2 or H_2O-N_2). 3. aqueous, monophase or biphase. Relative proportions of inclusion types in a given sample are obtained by taking the average value of a number (20-50) of visual estimates in the field of a 25x objective.

It should perhaps be emphasized that all descriptions of fluid inclusions, unless stated otherwise, strictly apply to the phenomenology at room temperature.

II.3.5 MICROTHERMOMETRY

Measurements of phase transitions in fluid inclusions as a function of the temperature were carried out with a commercially available Chaixmeca heating-freezing stage (Poty *et al.*, 1976). At low temperatures the stage is calibrated against methylcyclopentane (m.p. -142.4°C) and pure CO_2 (m.p. -56.6°C; contained in natural quartz crystals).

In order to prevent condensation of water on optical surfaces during freezing experiments, nitrogen gas is allowed to pass through rubber bellows placed between the stage and the microscope light window.

A number of freezing experiments (in particular the determination of homogenization temperatures of carbonic inclusions) have been carried out on glass-mounted sections. Such samples are easy in operation and allow the observation of fluid inclusions approximately in the focal plane of the condensing system (about 1.2 mm above the upper condensing lens of the stage). In view of the relatively small size of the inclusions (fig. 47), a large number of freezing runs required the use of a (Leitz) P50x -0.85 standard objective. The use of a short-focus objective and/or glass-mounting implies an additional calibration.

For that purpose a droplet of mercury is brought to the sample, if possible in tiny holes or fractures. Mounted sections are covered with glycerine and coverglass, whereas unmounted sections are embedded in glycerine between two round cover glasses, Ø 15 mm, thickness 0.13 mm. Subsequently, sets of calibration curves are constructed from observed melting temperatures of CO_2 and mercury using both a P50x and a L32x objective (fig. 31). Melting of mercury in a routine freezing run, using a L32x objective, has been observed between -38.7° and -38.9°C (literature value = -38.85°C according to Weast (ed.), 1975). When using a P50x objective, selection of the specific calibration curve is based on the observed melting temperature of mercury. It should be noted that the good optical quality

of a P50x objective permits the observation of phase changes in inclusions with sizes of about 1 micron.

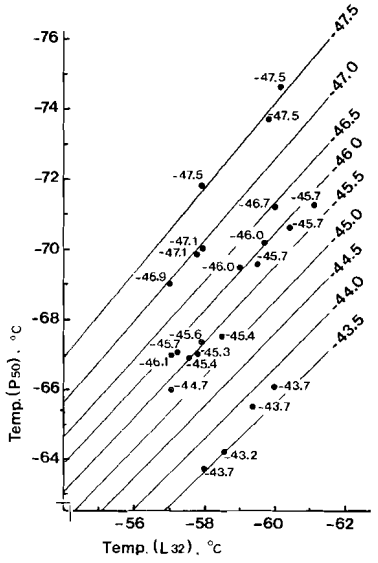

FIG. 31 Calibration curves for freezing runs using a Leitz P50x objective. Points indicate relation between melting point determination of CO_2 observed with P50x and L32x at given melting temperature of mercury (numbers attached to points, determined with L32x). Straight lines are "best fit" approaches.

The uncertainty in the freezing temperatures, using a P50x objective, is estimated at about 0.5° at temperatures around $-60^{\circ}C$. Although such error is appreciable for CO_2 melting temperatures, it is still acceptable for homogenization temperatures of carbonic inclusions. Accurate determinations of CO_2 melting temperatures as well as homogenization temperatures of N_2-rich and CH_4-rich inclusions clearly require a long-distance objective (estimated uncertainty 0.2°). This procedure has been followed for all datapoints that have been assembled in fig. 63 (a "T_f-T_h-diagram") and for many that constitute the "T_f-histograms".

The determination of homogenization temperatures of the carbonic phase in biphase H_2O-CO_2 inclusions is hampered by formation of hydrate after having cooled down to about $-100^{\circ}C$. The presence of hydrate will cause a departure from the homogenization temperature as recorded at hydrate-absent conditions. Formation of the hydrate phase may be prevented by cooling down to temperatures of about $-25^{\circ}C$ followed by quickly raising the temperature to within a few degrees of the homogenization temperature. Temperatures of homogenization at hydrate-absent conditions are invariably lower than those measured at hydrate-present conditions (fig. 32). The differences amount up to 15°, implying that it is important to state the conditions during homo-

genization. So far, it has not been possible to find a relation between the magnitude of the effect and any significant property of the inclusion. Simple arithmetic shows that the presence of only 10 vol.% hydrate at an average CO_2-density of ca.1.00 g/cc, could easily give rise to differences in CO_2 density of 5% between hydrate-absent and hydrate-present conditions.

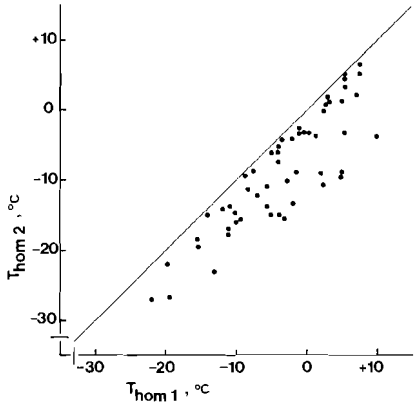

FIG. 32 Homogenization temperatures of the carbonic phase in biphase H_2O-CO_2 inclusions at hydrate-present (T_{hom1}) and hydrate-absent (T_{hom2}) conditions.

In addition, CO_2-densities in H_2O-CO_2 inclusions, derived from homogenization temperatures below 22°C, should be corrected for the increase in CO_2 solubility at lower temperatures (Dodds *et al.* 1956) in order to use them in the binary H_2O-CO_2 isochore diagrams (cf. Section 1.1.8) On the other hand, a complete quantification of hydrate- and solubility effects seems unnecessary in view of the gross error commonly made in estimating the degree of filling with H_2O.

Temperatures of total homogenization of H_2O-CO_2 inclusions have not been obtained because of decrepitation prior to homogenization. Decrepitation temperatures range from about 150° to 304°C.

First melting temperatures of aqueous inclusions were not determined in the usual way by recording the temperature of sudden translucency. Initially, the inclusions are cooled down sufficiently to nucleate ice. If the temperature drop does not bring about visible solidification (apart from the possibility of forming a vitreous solid (Hobbs, 1974)), warming up from -190° to -100°C is generally sufficient to produce a crystalline solid. Next, the fine-grained crystalline aggregate will recrystallize upon rising temperatures, thus eventually giving rise to a single, rounded crystal of ice. After renewed cooling, one or more sharply faceted crystals of ice Ih

(hexagonal) are formed. First melting is detected by observing the rounding of the edges of the hexagons.

II.4 FLUID INCLUSIONS - RESULTS

II.4.1 CRUSHING TESTS

The crushing test has been performed on 100 samples from various geologic environments. The results are presented in fig. 33. In groups 1 and

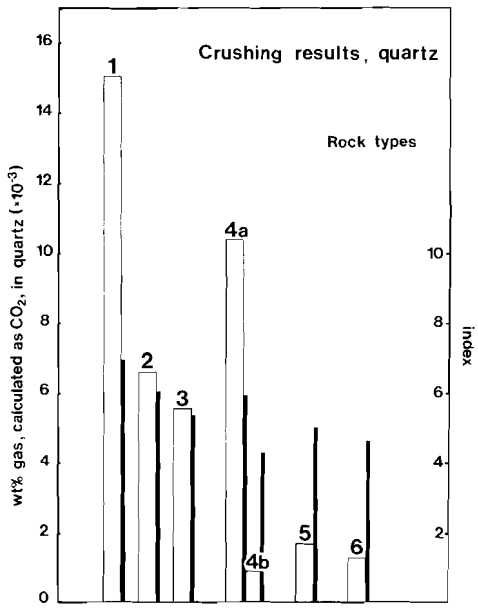

FIG. 33 Crushing results on quartz from various geologic environments (open columns, left scale). Solid bar (scale at the right) represents index I, defined in section II.3.1). 1: rocks in the vicinity of a dolerite dike (180 grains). 2: strongly retromorphosed rocks in anorthosite and norite (20 grains). 3: rocks adjacent to amphibole-bearing mafic rocks (180 grains). 4: Faurefjell Metasediments; 4a: quartz pods (50 grains), 4b: remainder of quartz-rich rocks (160 grains). 5: rocks from Garnetiferous Migmatites (130 grains). 6: concordant and discordant pegmatoid rocks (280 grains).

3 the conversion to weight percentage CO_2 is not completely correct as gaschromatographic analyses and microthermometric studies showed the presence of N_2. Nevertheless it is apparent that high amounts of gas have been liberated from rocks in groups 1-4a, particularly group 1, which comprises rocks adjacent to or in the vicinity of a dolerite dike. The index I is high, indicating a regular distribution of the CO_2-rich inclusions in individual samples.

In fig. 34 the results of group 1 have been plotted as a function of the distance from the contact. In general, gas liberations are highest at or close to the contact, amounting up to 10-20 times the average value in the remainder of the Rogaland samples. The high amounts of gas found in samples 242 and 243 cannot positively be ascribed to the presence of a

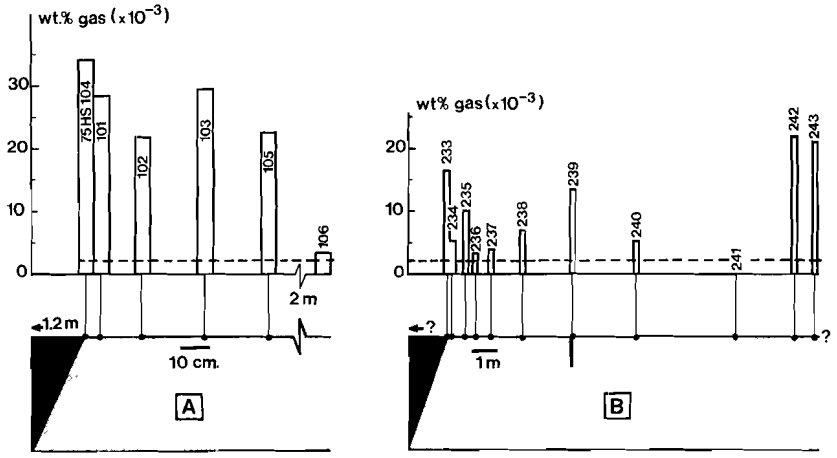

FIG. 34 Crushing results on quartz in the vicinity of a dolerite dike. Contacts sampled in Gyadalen (A) and at Rusdalsvatnet (B). At (B) all samples have been collected from a given subhorizontal quartzofeldspathic band. Liberated gas has been calculated as CO_2. Broken line represents the mean value in the remainder of the Rogaland samples. Numbers attached to boxes refer to sample numbers. Only samples 75HS102-104-106-233-243 have been described petrographically (Appendix)

second dolerite dike because the area in the vicinity of these sampling sites is not exposed. Collectively, however, the observations strongly suggest a genetic relationship between the inclusions in the country rock (mainly CO_2) and the dolerite (or the fracture). In addition to this, the frequent occurrence of relatively small and irregular inclusions in crystallographically non-rational trails as well as the relatively low densities of the fluids (cf. sections II.4.5 and II.4.9) are properties that are different from most other samples.

II.4.2 GASCHROMATOGRAPHIC ANALYSES AND $\delta^{13}C$- VALUES OF CO_2

Only a limited number of gaschromatographic analyses have been carried out. In table 6 the results are presented, along with manometrically determined amounts of CO_2 and non-condensable gases (N_2, O_2, CH_4, and noble gases) as well as $\delta^{13}C$- values of CO_2. CO has not been detected. High amounts of CH_4 are present in graphite-bearing rocks and in a pegmatite, belonging to a mafic intrusion, where it has been recognized as low-densi-

Sample code	Provenance	CO_2	CH_4	N_2	$\delta^{13}C$
75HS102	contact between dolerite and country rock	42.8	8.6	48.6	-7.6
75HS191	quartz-rich band adjacent to amphibole-bearing leuconorite	45.8	10^{-3}	54.2	-8.7
75HS199	diopside quartzite in Faurefjell Metasediments	28.6	n.c.=	71.4	n.d.
75HS207	quartz pod in the vicinity of marble (Faurefjell Metas.)	93.2	0.1	6.7	-3.3
76HS250	basal quartzite Faurefjell Metasediments	65.3	-	34.7	-7.4
76HS256	coarse grained pegmatite in lopolith of Bjerkreim-S.dal.	13.8	47.0	39.2	n.d.
76HS274	folded quartz lens in diopside rock (Faurefj. Metased.)	57.2	0.4	42.4	-6.0
76HS276	cordierite-bearing basal quartzite Faurefj. Metased.	83.3	0.3	16.4	n.d.
76HS277	large concordant body of quartz in Charnock. Migm.	99.0	-	1.0	-3.1
76HS287	narrow, concordant quartz vein adjacent to amphibolite	-	-	100.0	n.d.
76HS298	quartz pod enclosed in marble (Faurefjell Metasediments)	81.2	4.5	14.3	+0.0
76HS306	graphite bearing quartz-feldspar rock (Garnet. Migm.)	8.7	48.7	42.6	n.d.
76HS311	graphite bearing quartz-feldspar rock (Garnet. Migm.)	1.0	44.8	54.2	n.d.

TABLE 6 Manometrically determined amounts of CO_2 and n.c. gasfraction (analyzed by gaschromatography), expressed in molar percentages. $\delta^{13}C$-values are presented in the last column.
n.c.= gasfraction, non-condensable at -196°C
n.d.= not determined
— = not detected

ty, late-stage inclusions. In the remainder of the samples, the composition of the non-condensable fraction is N_2-rich.

In spite of their limited number, the $\delta^{13}C$-values of CO_2 in quartz pods associated with marbles seem to be relatively high. This might indicate that these CO_2-rich fluids are in part derived from decarbonation reactions.

II.4.3 COMPOSITIONAL TYPES OF FLUID INCLUSIONS

Most fluid inclusion in rocks from S.W. Norway occur in quartz. Occasionally, carbonic and aqueous inclusions have been recognized in apatite, calcite, diopside, and K-feldspar.

The main types of fluid inclusions are:

1. *Carbonic* (CO_2-rich); essentially monophase at room temperature; some contain an isotropic or birefringent solid phase (daughter mineral or captive). Examples: figs 39, 41, 61.
2. *Aqueous* (H_2O-rich); generally two phase liquid + vapor at room temperature; monophase inclusions, however, may locally be abundant; some contain daughter phases or captives (isotropic and/or birefringent). Examples: fig. 53.
3. *H_2O-CO_2*; inclusions composed of a CO_2-rich phase (liquid or liquid + vapor) and an aqueous phase; solid phases may be present in addition. Examples: figs 39, 52.
4. *N_2-rich*; inclusions, rather similar in appearance as CO_2-rich inclusions although perhaps somewhat darker; identification without using a freezing stage almost impossible; frequently, however, their arrangement in cluster-like configurations and their absence in well-defined trails is distinctive; for convenience, H_2O-N_2 inclusions have also been called N_2-rich. Examples: figs 35, 36
5. *CH_4-rich*; the low-density variety is dark-looking, has a thick rim of total reflection, contains up to 30 vol% H_2O, and may show a well-developed negative crystal shape; the variety with medium density is rare and has only been observed in sample 76HS270, a strongly retromorphic rock with bluish-gray quartz. Example (low-density variety): fig. 48.
6. *Multiphase*; composed of solid(s), liquid $\pm$ vapor; recognized in many retromorphic rocks; the ratio of solid phase volume- total volume shows a wide range.

   In a quartz pod enclosed in Faurefjell marbles large inclusions, possibly primary, contain several solid phases with a relative volume up to about 90% (!). Clusters composed of multiphase inclusions with variable phase ratios have also been found.

   Another quartz pod (Faurefjell metasediments) contains secondary multiphase inclusions with at least three different solid phases (all bire-

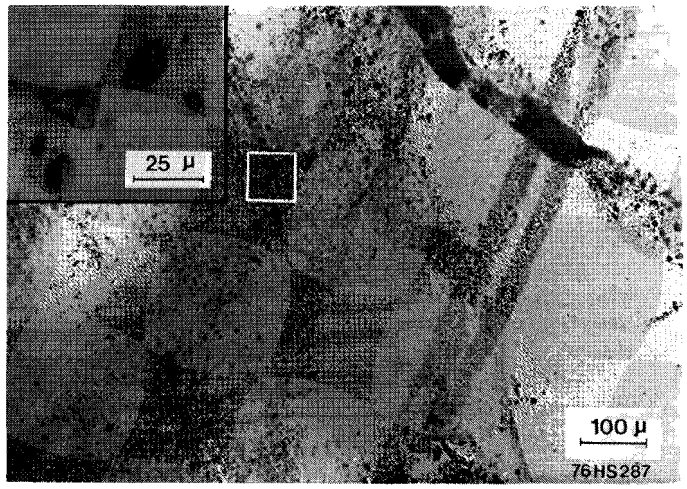

FIG. 35 Photomicrograph showing well-defined trails composed of biphase aqueous inclusions (right-hand side) and ill-defined configurations (left part), mainly composed of N_2-rich inclusions (see also inset top left). Quartz-rich intercalation adjacent to an amphibolite in the Tjørhom area.

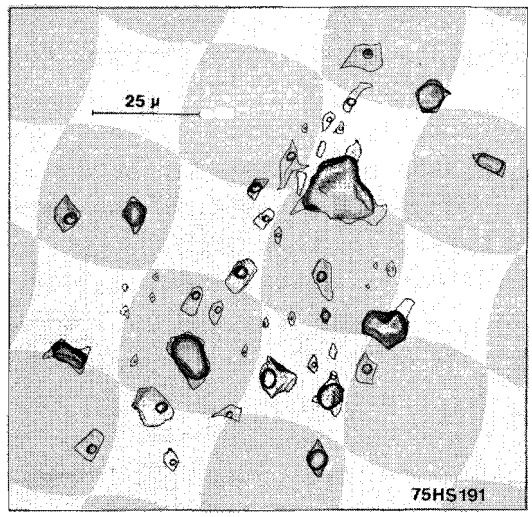

FIG. 36 Camera lucida drawing showing cluster of biphase H_2O-N_2 inclusions with variable phase ratios. In part discordant quartz-rich vein close to amphibole-bearing norite in Drangsdalen.

fringent) and a CO_2-H_2S gasbubble (about 10 vol.%). H_2S has been detected by the fetid odor that is emitted upon scratching or crushing the host quartz. In addition to this, homogenization of the CO_2-H_2S phase occurred at temperatures well above the critical temperature of pure CO_2.
In a large number of retromorphosed rocks where the irregular shapes of many inclusions suggests decrepitation-like events (cf. II.4.5), multiphase inclusions with a high number of small solid phases in a highly saline liquid have been found. Locally, such solid phases are needle-like (dawsonite ?) and occur in large concentrations.
Most multiphase inclusions, however, contain only a limited number of solid phases and are associated with "common" two- or monophase aqueous inclusions. Apart from their relative abundance in retromorphosed rocks (compare Crawford *et al.*, 1979a) they have frequently been observed in rocks from Gyadalen "West".
No serious effort has been undertaken to identify the solid phases. An isotropic phase is tentatively interpreted as NaCl; birefringent phases may be carbonate, anhydrite, or nahcolite (?).

II.4.4 REGIONAL DISTRIBUTION OF INCLUSION TYPES

At a regional scale the average volumetric ratio of CO_2 and H_2O in rocks sampled within a distance of 10 km from the Lopolith of Bjerkreim-Sokndal is 53/47 whereas in rocks at least 10 km away this ratio has an average value of 28/72. The significance of these values is not known because the H_2O-CO_2 ratio may vary widely within the confinement of an outcrop, sample, or even host crystal (Cf. Appendix).

A high proportion of carbonic inclusions is found in diopside quartzites and quartz-diopside gneisses of the Faurefjell metasediments immediately north of the lopolith. Aqueous inclusions are relatively abundant in a number of rocks from the Tjørhom area (mainly amphibolite facies), in an extensive quartz body near Stølsfjellet (crystallization or recrystallization at low-grade conditions), and in amphibole-free rocks from the Store Myrvatn area (high-grade amphibolite facies).

In Drangsdalen, the relative abundances of fluid inclusion types, expressed as the volumetric ratio of monophase carbonic, biphase H_2O-CO_2 and aqueous inclusions (cf. Section II.3.4) are distributed as follows (82 rocks):

enderbites (N=35): 57/11/32; when excluding discordant rocks and rocks showing biotite-quartz contacts: 64/09/27 (N=24)

charno-enderbites (N=13): 46/10/44

charnockitic and granitic rocks (N=34): 33/18/49

The spatial distribution of fluid inclusion types in Drangsdalen, Årdalen, and Gyadalen should preferably be related to geochronological work by Versteeve (1975).

> Versteeve (1975) suggests that open- and closed system behavior of Rb-Sr whole rock systems is a function of the "partial pressure of the fluid phase (pH_2O and/or pCO_2). A higher partial pressure would create conditions favorable to Rb and/or Sr migration while a (slightly) lower partial pressure would prevent such migrations, thus promoting the inheritance of older ages.

In Drangsdalen (fig. 37) the rock samples that define the 1485 Ma isochron ("age asylum") have been collected in outcrops where, in general, carbonic inclusions are relatively abundant and the net amount of free

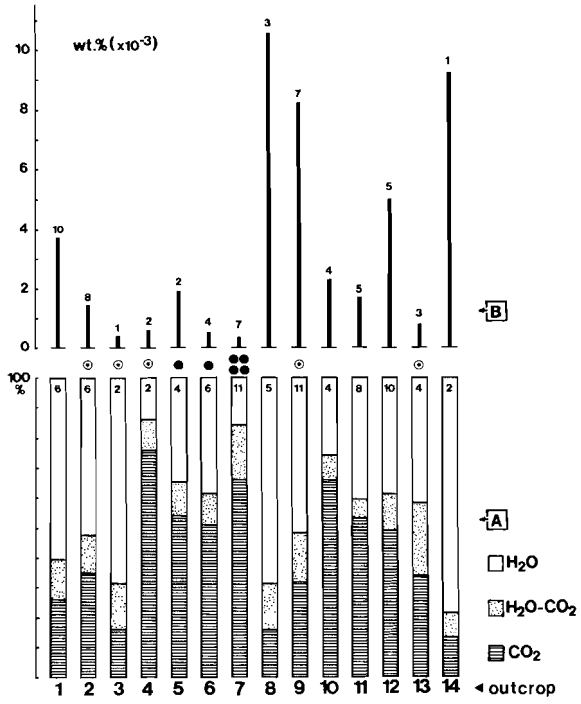

FIG. 37 Relative proportions of fluid inclusion types (A) and weight percentage of free H_2O and CO_2 (B), based on crushing results, in quartz from Drangsdalen. Numbers inside boxes refer to the number of samples whereas the number of crushing runs is indicated by a number on top of the bar.

◉ "off isochron"

● "on isochron"

fluid phase is low. Conversely, most datapoints situated off the 1485 Ma isochron have been obtained on samples collected in outcrops where aqueous inclusions are predominant.

Despite its low content of free fluid phase and the predominance of carbonic inclusions, outcrop 4 does not provide a datapoint on the isochron (Versteeve's sample *Rog 216* is the only deviating datapoint situated *above* the isochron). The petrographic description of Rog 216, however, fits most of the other rocks that have produced datapoints *on* the isochron. The position of this particular sample thus remains somewhat enigmatic.

In the area of Årdalen most inclusions are of the aqueous type and occur abundantly (fig. 38A). Rb-Sr isotope datapoints obtained on rocks from a nearby site (Flikka) did not produce a well-defined isochron.
In Gyadalen (fig. 38B) the contents of free fluid phase are rather variable but the proportions of the various types remain fairly constant. Both Gyadalen "East" and "West" produced in part well-defined Rb-Sr whole rock isochrons of 1004 and 947Ma respectively.

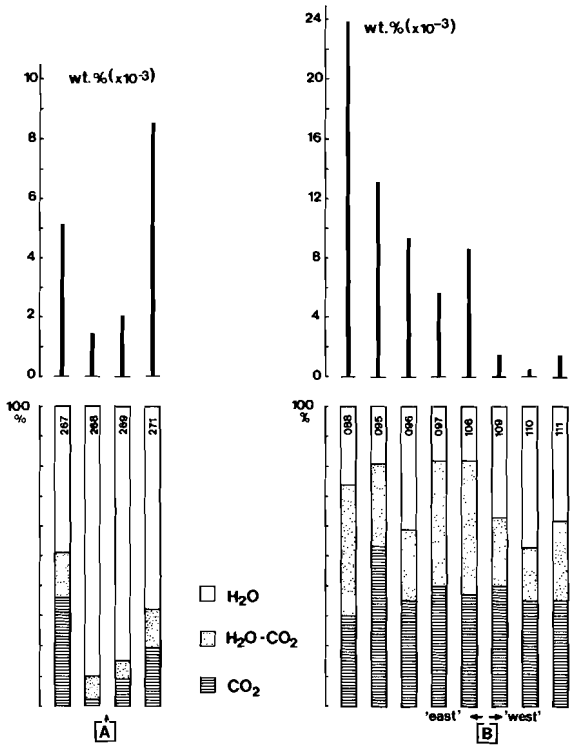

FIG 38 Relative proportions of fluid inclusion types (lower part of the figure) and content of free fluid phase (H_2O+CO_2) as derived from crushing results on quartz from Årdalen (A) and Gyadalen (B). Sample no. inside box. Årdalen is close to Flikka, which did not produce a Rb-Sr isochron; Both Gyadalen "East" and "West" produced well-defined isochrons, about 1000Ma and 950Ma respectively, but deviating datapoints were also present (Versteeve, 1975).

By interpreting the expression "partial pressure" of the fluid phase (Versteeve, 1975) in terms of "partial pressure of H_2O" the distribution of fluid inclusion types in Drangsdalen and Årdalen (perhaps also in Gyadalen) seems to be in support of the hypothesis invoked by Versteeve (1975). In addition to this, the abundance of fluid inclusions, when reflecting the net amount of fluid that has passed the rocks, may also be an important parameter in this respect. It should be stressed, however, that the relation between fluid inclusion properties and Rb-Sr behavior need not be a primary one. Most of the rocks in or adjacent to the "age asylum" outcrop are relatively fine-grained. Here, percolation of fluids may have been less than in the coarser grained rocks.

II.4.5 DISTRIBUTION OF INCLUSIONS IN THE HOST MINERAL

A distinction has been made between *isolated* inclusions, inclusions arranged in *cluster-like configurations*, and inclusions confined to more or less well-defined arrays or *trails*. Transital configurations are possible.

Inclusions that are randomly distributed over the host crystal or occur in isolated position are rare and have only been observed in quartz

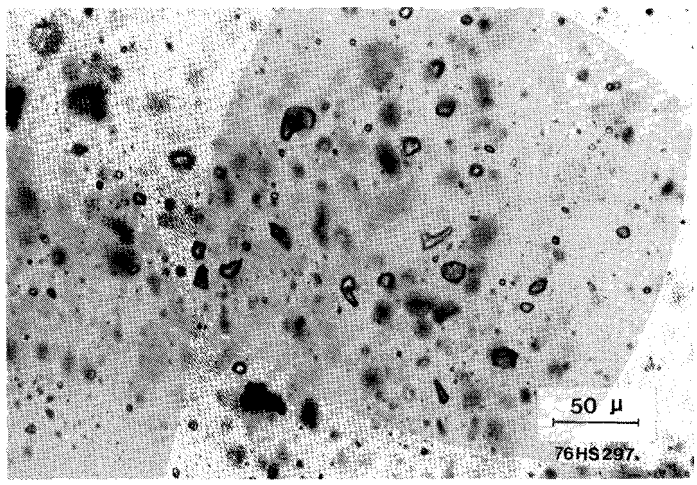

FIG. 39 Photomicrograph showing dispersed carbonic inclusions (monophase as well as biphase H_2O-CO_2) in quartz pod from Faurefjell Metasediments at Stølsfjellet.

bodies in the Faurefjell metasediments (fig. 39). Such inclusions are considered *primary* (Roedder, 1977).

Cluster-like configurations are essentially non-planar arrangements of spatially associated inclusions. According to Hollister & Burruss (1976) and Konnerup-Madsen (1977; 1979) inclusions situated in clusters should in general be considered as earlier secondary than those confined to trails ("healed fractures"). In the present study, however, it is not *a priori* assumed that all features of a cluster-like configuration are necessarily "early secondary". In particular those configurations that remind of partial decrepitation (called "decrepitation clusters") suggest that the final geometry of the cluster may be due to late stage processes (figs 40, 61).

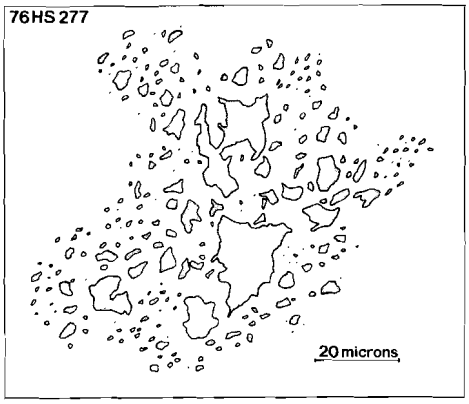

FIG. 40 Camera lucida drawing showing a "decrepitation cluster" composed of monophase carbonic inclusions. Note the large number of small inclusions. Coarse grained quartzite from Snøsvatnet.

In general, however, fluid inclusions are arranged in trails, which are two-dimensional expressions of planar arrangements. When observed with crossed polars a slight misfit between the orientation of the "trail-quartz" and the bulk may be observed.

> For practical purposes the trail terminology has in part been derived from Simmons & Richter (1976). *Intragrain* trails are situated completely within a grain and do not reach a grain boundary. *Intergrain* trails start at a grain boundary and peter out in the interior part of the grain or extend to another grain boundary. *Multigrain* (or *transgranular*) trails are equivalent to so-called "*Tuttle lamellae*" which have been described by Hobbs *et al.* (1976) as "more or less planar arrays of inclusions that cross many grains with the same spatial orientation independent of the crystallographic orientation of the grains (cf. Tuttle, 1949).

Preferred orientation of intergrain trails has been observed frequently (fig. 42) and may even be visible megascopically.

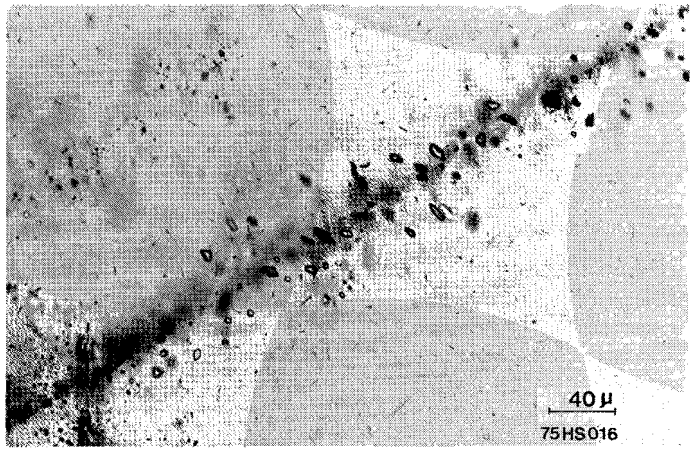

FIG. 41 Photomicrograph showing subbasally oriented, relatively well-defined trail composed of monophase carbonic inclusions. View almost perpendicular to the plane of fluid inclusions. A number of inclusions are situated "off" the median zone of the trail. Charnockitic migmatite from Drangsdalen.

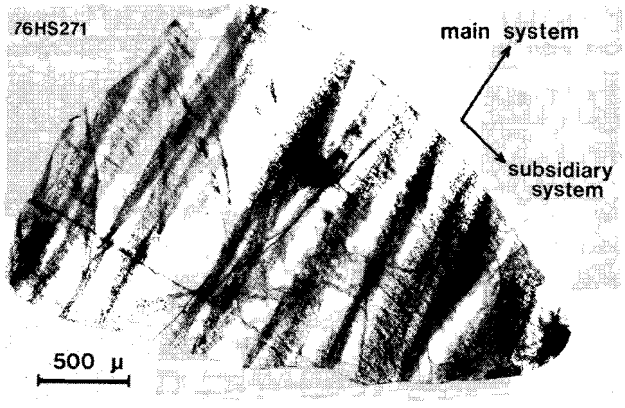

FIG. 42 Photomicrograph showing subbasally oriented trails, mainly composed of carbonic inclusions. A subsidiary system of trails is present in addition. Charnockitic migmatite from Årdalen.

The results of universal-stage measurements on fluid inclusion planes in a sample from Drangsdalen (fig. 43) illustrate the (frequently observed) subbasal orientation of CO_2-rich trails as opposed to the more randomly orientation of H_2O-rich trails. Notable exeptions, however, do exist (such as CO_2-rich trails with random orientation in quartz near a dolerite dike).

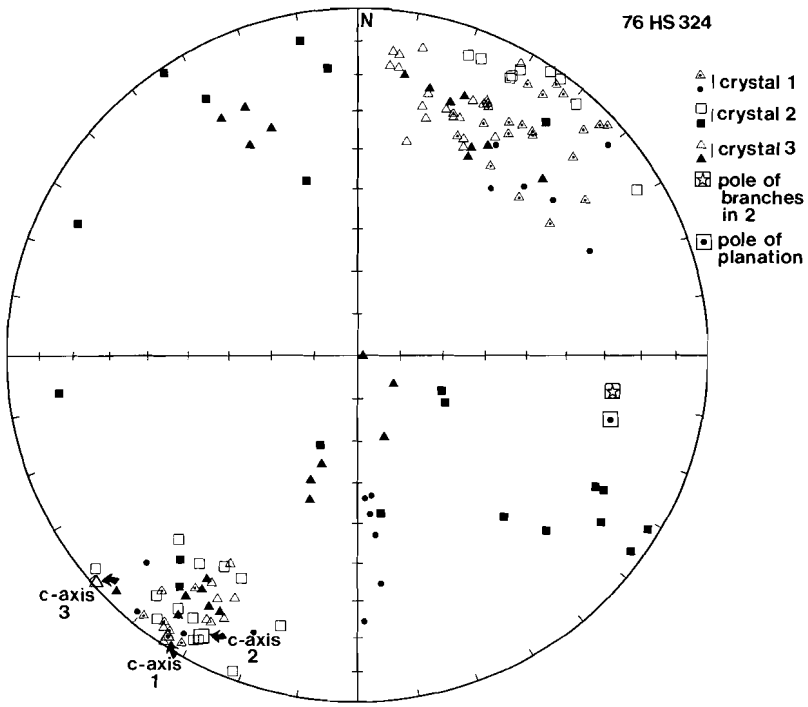

FIG. 43 Equal area, lower hemisphere projection of poles of planar features in Drangsdalen rock. Squares, points, and triangles indicate planes of fluid inclusions. "Branches" refer to subsidiary planes of fluid inclusions. Open symbols designate carbonic and/or mixed H_2O-CO_2 inclusions. Closed symbols represent aqueous inclusions. C-axis orientations of quartz crystals (enlarged symbols) are indicated by arrows.

In a given sample large numbers of subbasally oriented trails may be present in certain grains while being absent in adjacent grains with different lattice orientations.

At intersections of H_2O-rich and CO_2-rich trails, mixed H_2O-CO_2 inclusions may be encountered in the CO_2-rich trail; mixed inclusions. however,

are not found in the H_2O-rich trail. In many CO_2-rich trails that peter out in the interior part of the grain, the monophase carbonic inclusions are largely confined to the tip region whereas mixed H_2O-CO_2 inclusions are present in that part of the trail close to the grain boundary. Multigrain trails consist typically of aqueous inclusions; carbonic inclusions are rarely found in such trails.

Collectively, the observations strongly suggest that at least part of the aqueous and mixed H_2O-CO_2 inclusions *postdate* the carbonic inclusions.

The trails are probably most effectively being dealt with in terms of healed microfractures (cf. Chapter II.6.1) A ductile origin, particularly for the subbasally oriented ones, however, cannot be excluded a priori.

According to Wilkins & Barkas (1978) healing of microcracks results in "brittle-deformation inclusions" whereas decoration of deformation lamellae, subgrain- and deformation band boundaries yields "ductile deformation inclusions". Simmons & Richter (1976) discuss various kinds of microcracks. A few relevant types will be briefly mentioned:

dP-dT cracks are produced where the local linear strain in the vicinity of a grain boundary exceeds the average linear strain of the rock. The development of such grain boundary cracks is a function of the relative orientation, the linear thermal expansion, the compressibility, and the grain-boundary strength of the mineral grains involved. Grain boundary cracks may be numerous in a certain grain and be absent in an adjacent one. Most of them start at the grain boundary and propagate into the interior part of the grain.

Stress-induced cracks are related chiefly to the principal directions of a non-hydrostatic stress field and seem to be largely independent of the crystallographical orientation of the host mineral. The initial fracture planes will develop in the shear or tensional directional direction of the deforming stress pattern. Not uncommonly, cracks of this type are found to be transgranular.

Thermal gradient cracks are formed because of differences in the thermal contraction coefficients between adjacent units of different lithology.

The dP-dT cracks most closely approach the definition of intergranular trails that are oriented subbasally. Such trails are generally composed of carbonic and/or mixed H_2O-CO_2 inclusions. The definition of stress-induced cracks clearly fits at least part of the trails that are composed of H_2O-rich inclusions. Thermal gradient cracks have probably been induced in the country rock during intrusion of a dolerite dike.

Healing of the cracks is accomplished by introduction of fluid and

subsequent dissolution and precipitation of material, thereby effectively reducing the surface free energy of the original fluid-filled crack. Aspects of the healing process are discussed by Lemmlein (1929, 1956), Tuttle (1949), Lemmlein & Klya (1960), Wise (1964), Roedder (1967), and Carstens (1969).

Among the first changes that occur when a new stress field is imposed on the rocks is the re-opening of healed cracks, probably because there is less material to break (Wise, 1964; Paterson, 1978). In addition to this Wise (1964) observed that older sets of (healed) microcracks controlled at least some of the younger generations of microcracks. Both effects may have played a role during introduction of H_2O after trapping of N_2-rich and CO_2-rich fluids.

Transposition and degeneration of trails

When observed exactly along the "plane", most fluid inclusion trails appear to somewhat diffuse because a number of inclusions, obviously related to the trail, are situated off the median plane (fig. 41). If it is assumed that the trail results from fracture-healing, apparently some inclusions have moved away from the original plane.

Blurring of original fluid inclusion trails is also illustrated in fig. 44. In fig. 44A, part of the inclusions decorate subgrain boundaries.

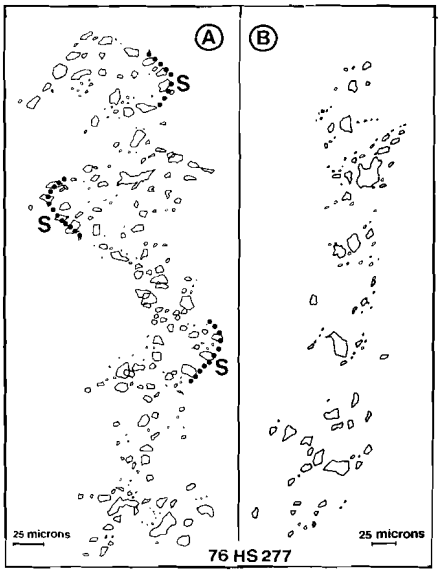

FIG. 44 Camera lucida drawings of poorly defined trails composed of rearranged monophase carbonic inclusions.
A. Transposition of a pre-existing N-S trail by decoration of subgrain boundaries (S)
B. Array of "decrepitation clusters".

The configuration in fig. 44B is probably best explained by initial migration of fluid inclusions approximately along the median plane, accompanied by coalescence (Wise, 1964; Roedder, 1971), followed by partial decrepitation of the larger sized inclusions in a later stage.

FIG. 45 Photomicrograph showing transposition of carbonic inclusions from a pre-existing planar arrangement into subsidiary planes that constitute a pervasive system oriented NE-SW. Note presence of deformation lamellae. Subbasal section of quartz in a discordant rock from Drangsdalen. Crossed polars.

Not infrequently, trails are accompanied by a set of small-sized trails in approximately parallel arrangement (fig. 42). A very pronounced subsidiary system has been observed in plastically deformed quartz (fig. 45). Large-scale obliteration of original trails as the result of advanced transposition into a subsidiary system with different orientation is shown in fig. 46. In extreme cases such a subsidiary system takes over completely without leaving a trace of the pre-existing trail. In those samples where the inclusions in the subsidiary system are extremely small (< 1 micron), this effect has given rise to a "pseudo-cleavage" of the quartz. In general, the subsidiary system is penetrative, showing a uniform direction all over the section and being non-rational with respect to the crystallography of the host.

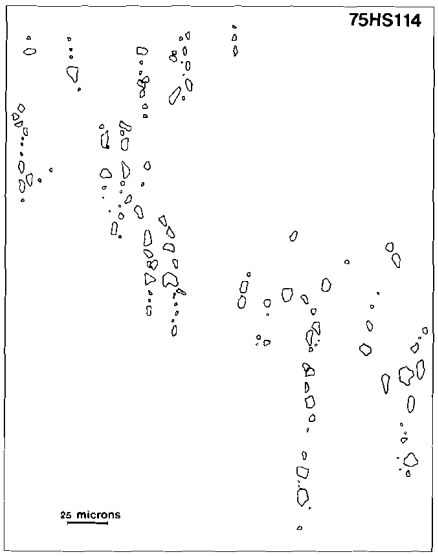

FIG. 46 Camera lucida drawing showing advanced transposition of a preexisting NW-SE oriented trail into short, subsidiary N-S trails. Drangsdalen charnockitic migmatite.

The transposition of trails clearly involves (stress-induced) migration of fluid inclusions. Migration as a result of thermal gradients is considered to be unlikely as the magnitude of such gradients at the scale of a grain are small. Roedder (1971) has suggested that fluid inclusion migration is facilitated in zones of enhanced solubility but owing to the absence of distinctly crystallographic controls of the transposed trails these effects are probably not significant.

The exact mechanism of fluid inclusion migration and the possible role of dislocations is not yet fully understood but probably involves dissolution and (re)precipitation. Owing to the enhanced solubility of SiO_2 in H_2O as opposed to CO_2 (Shettel, 1973), aqueous inclusions probably respond easier to varying conditions of stress than carbonic inclusions. This could effectively explain the occurrences of isolated aqueous inclusions and the poor definition - in general - of configurations composed of aqueous inclusions. Chronological differences of inclusion generations as deduced from cluster-like or trail-like aspects of the configurations may thus be in error if inclusions with widely different compositions are involved.

II.4.6 SIZE AND SHAPE

The upper size limit for irregular inclusions is 150 microns in the longest dimension (aqueous inclusion in a discordant rock from Drangsdalen). The upper size limit for more or less isometric inclusions is about 40 mi-

crons. Commonly, the range is about 2-20 microns.

For a number of carbonic inclusions, a histogram of the sizes is presented in fig. 47. It shows that over 75 percent of the inclusions are less than six microns.

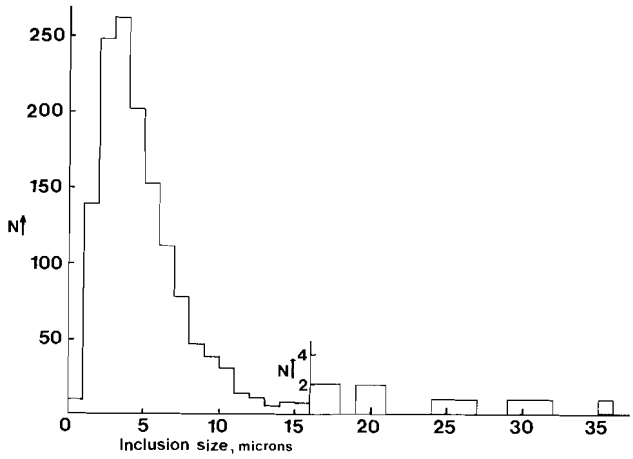

FIG. 47 Histogram, showing the size distribution of carbonic inclusions selected for freezing studies.

Relatively large inclusions have been found in cluster-like configurations, which occur frequently in coarse-grained rocks. Small inclusions are abundant in most configurations that result from late-stage processes, for instance "decrepitation clusters" (figs 40, 61). Small inclusions are by definition absent in so-called "mature configurations", which originated in a relatively early stage and have remained largely unaffected since. Mature trails thus typically consist of inclusions with well-developed negative crystal shapes, separated from each other at relatively large distances, possibly indicating coalescence and elimination of the smaller inclusions.

Commonly, small inclusions have regular shapes. They are somewhat oblong with a general tendency towards a rounded negative crystal shape. Large carbonic inclusions with well-developed negative crystal shapes have only been observed frequently in quartz pods and quartz-diopside gneisses of the Faurefjell metasediments. Both the α- and β negative crystal shapes have been found in random distribution. Remarkably well-developed negative crystal shapes are found on a number of low-density, CH_4-

rich inclusions (fig. 48). Similar observations on CH_4-rich inclusions with higher densities have been made by Touray & Jauzein (1967), Touray & Sagon (1967), Touray (1969), Stalder & Touray (1970), Mullis *et al.* (1973), and Mullis (1976).

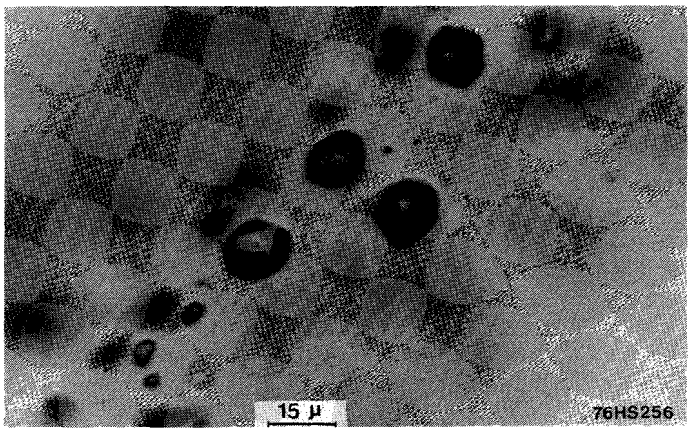

FIG. 48 Photomicrograph of a well-defined planar arrangement (obliquely intersected) of low-density, CH_4-rich inclusions with well-developed negative crystal shapes. Pegmatite at the base of the Bjerkreim-Sokndal lopolith.

The negative crystal shapes of CH_4-rich inclusions could result from a relatively large anisotropy of the specific surface energy which, at declining temperature, gives rise to equilibrium shapes with sharply defined crystal faces. A more isotropic specific surface energy promotes the development of isometric, rounded equilibrium shapes (Hartman, 1979). Such equilibrium shapes would preferably develop in CO_2-rich and H_2O-rich inclusions where the net decrease in SiO_2 solubility with temperature allows the precipitation of silica in the edges of pre-existing negative crystals.

Theoretically, the negative crystal shapes of the CH_4-rich inclusions could be regarded as an original growth- or dissolution habit (Hartman, pers. comm.). Such a shape would require a rise in temperature after entrapment of the CH_4-rich fluid. There is, however, no direct geological evidence for a rise in temperature during the late-stage history of the rock complex (although a Caledonian effect could be envisaged).

Re-equilibrated shapes

Superimposed on natural effects of equilibration, as decribed in the previous paragraph, the shape of an inclusion may change as a result of varying conditions of temperature, pressure or stress, set up after entrapment.

In a (small) number of inclusions the incomplete negative crystal shapes suggest transfer (inflow?) of silica (fig. 49) and possibly illustrate the results of re-equilibration towards higher densities (cf. Chapter II.6)

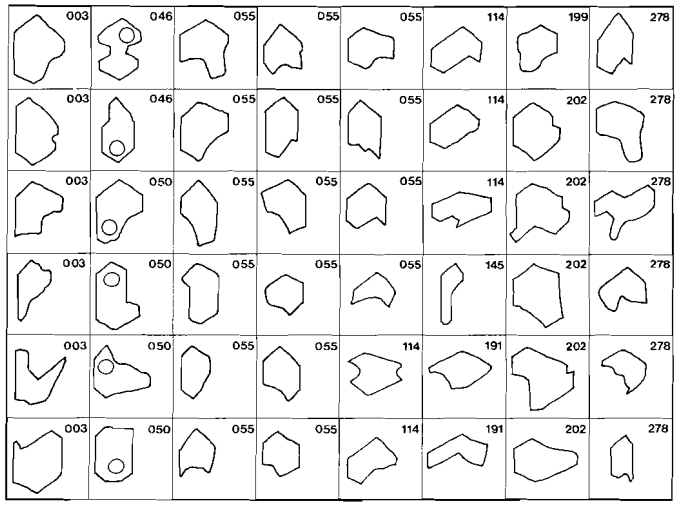

FIG. 49 Outlines of fluid inclusions with incomplete negative crystal shape. Blank: CO_2-rich; bubble: aqueous inclusion. Numbers denote sample number.

A certain preferred form orientation of fluid inclusions has frequently been observed in subsidiary trails and occasionally in separate trails (fig. 50). Probably the elongated inclusions are due to recrystallization of the host phase in response to a stress gradient.

The phenomenon of partial decrepitation ("superheating") has already been touched upon in Section II.4.5 dealing with "decrepitation clusters". Although indications for partial decrepitation are found in almost any rock, classic examples with extension fractures and satellite inclusions are rare

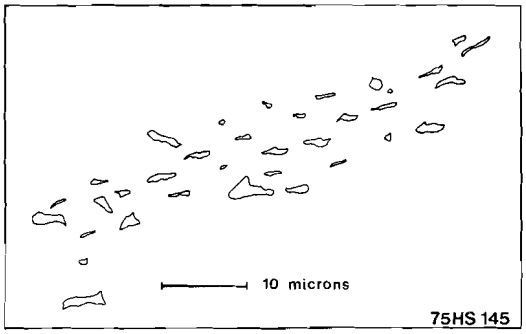

FIG. 50 Camera lucida drawing of flattened, monophase inclusions containing a high-density N_2-rich fluid. Drangsdalen charnockitic migmatite.

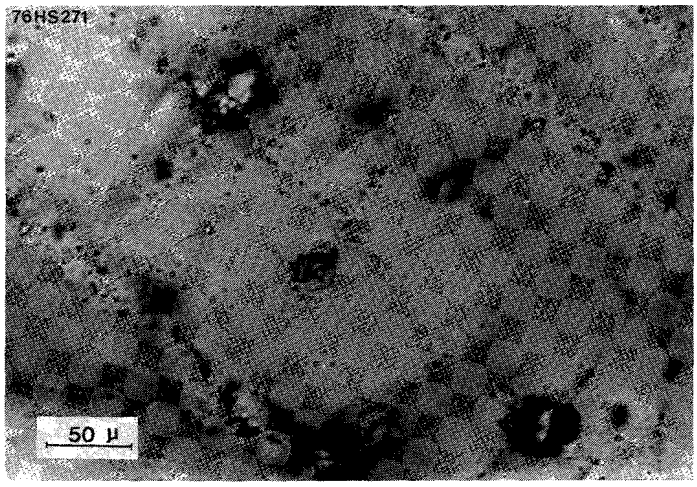

FIG. 51 Photomicrograph of aqueous and biphase H_2O-CO_2 inclusions showing more or less "classic" partial decrepitation. Quartz from Årdalen.

(fig. 51).

Inclusions with off-shoots (fig. 52) resemble "superheated" H_2O-CO_2 inclusions from Naxos (Greece), discussed by Kreulen (1977). He suggests a low ambient pressure as the main cause for the expansion of the fluid. In a wider context, decrepitation-like events will be discussed in Chapter II.6.5.

In retromorphic or strongly tectonized rocks fluid inclusions may be highly irregular (including the small ones). Even within a single grain

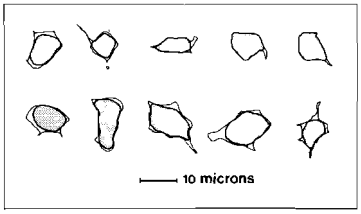

FIG. 52 Sketches of individual biphase H_2O-CO_2 inclusions from cluster-like configurations. Offshoots may indicate partial decrepitation. Note low degree of filling. Drangsdalen pegmatite.

the regularity in shape of a given fluid inclusion type may vary considerably. In the neighborhood of hydrothermally altered minerals for instance, highly irregular shapes are not uncommon. Probably, such shapes result from late-stage processes at relatively low temperatures.

Occasionally, large, irregular and dark-looking carbonic inclusions have been found at junctions of trails with multiphase and carbonic inclusions. This observation suggests that the irregular inclusions have formed as a result of (partial) decrepitation under conditions of relatively low temperatures and pressures.

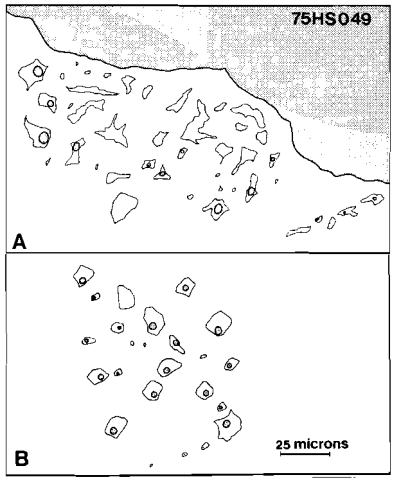

FIG. 53 Camera lucida drawings showing:
A. irregular aqueous inclusions close to an extensively altered plagioclase (gray). Note high proportion of monophase inclusions.
B. Aqueous inclusions with regular shapes at about 1.2 mm distance from altered plagioclase.
Drangsdalen pegmatite.

II.4.7 MICROTHERMOMETRY

Aqueous inclusions

Heating-freezing studies of aqueous inclusions have only been performed on rocks from Drangsdalen and Stølsfjellet. Most temperatures of first melting in the presence of vapor are below the eutectic temperature of the system NaCl-KCl-H_2O (-22.9°C); they reach a minimum value of -87°C (fig. 54). Between the temperatures of first and final melting no other phase

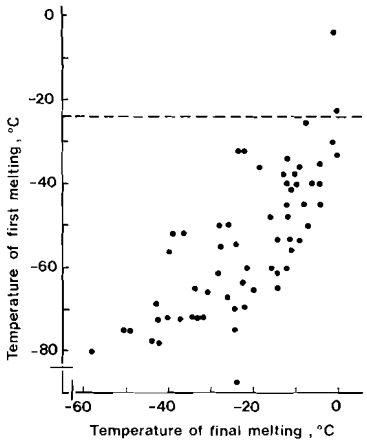

FIG. 54 Microthermometry of aqueous inclusions in Drangsdalen rocks. Relation between temperatures of first and final melting of ice in the presence of a vapor phase.

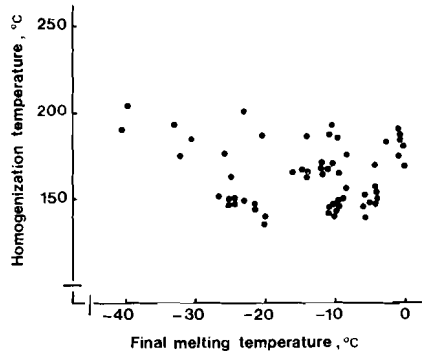

FIG. 55 Microthermometry of aqueous inclusions in Drangsdalen rocks. Relation between final melting temperature of ice and homogenization temperature.

change has been observed. This indicates that the temperatures of final melting (ranging from 0 to -59°C) cannot be expressed properly in terms of equivalent weight percentage NaCl and, in addition, suggest that varying but significant amounts of Ca^{2+} and/or Mg^{2+} are present in the aqueous solution (Konnerup-Madsen, 1979; Crawford *et al.*, 1979a). In a number of inclusions a metastable equilibrium of liquid H_2O and ice has been maintained at temperatures above 0°C, up to a maximum of +5.9°C indicating appreciable negative pressures (Roedder, 1967a).

Homogenization temperatures of aqueous inclusions are generally between 130° and 200°C (fig. 56). There is no clear relation between the ho-

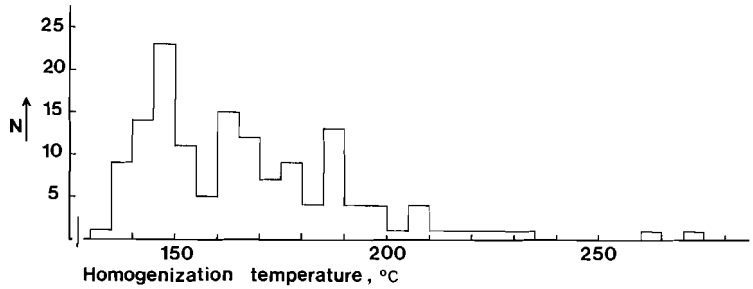

FIG. 56 Homogenization temperatures of aqueous inclusions in Drangsdalen rocks.

mogenization temperature and the final melting temperature (fig. 55).

In a quartz body from Stølsfjellet, probably emplaced at greenschist-facies conditions, the final melting temperatures of the primary inclusions range from -15° to 0°C (first melting from -50° to -22.5°C) whereas homogenizations in the liquid phase have been recorded between 157° and 166°C.

N_2-rich inclusions

The cooling of N_2-rich inclusions down to -190°C will bring about a liquid-vapor separation. Additional cooling (using liquid He) would be required for solidification of N_2 but in view of the experimental difficulties such method has not been followed for routinely made freezing runs. Hence, the compositions of N_2-rich inclusions cannot be determined directly (except perhaps in case of critical homogenization) and should be obtained from gaschromatographic analysis of the gases released upon crushing fragments of the host mineral.

A compilation of homogenization temperatures of N_2-rich inclusions is given in fig. 57. The uncertainty is estimated at about 1°, based on the calibration with methyl-cyclopentane (melting temperature= -142.4°C). Homogenizations in the liquid phase are largely restricted to inclusions with low contents of CO_2. Homogenizations in the gas phase have mainly

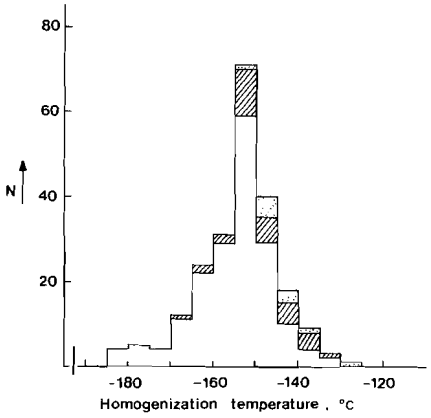

FIG. 57 Microthermometry of N_2-rich inclusions in various rocks. Blank: homogenization in the liquid phase. Shaded: homogenization in the gas phase. Stippled: critical homogenization.

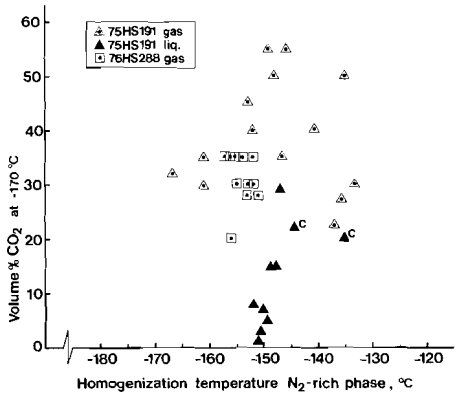

FIG. 58 Relation between temperature of homogenization (to gas- or liquid phase), volume percentage of solid CO_2 (estimated at -170°C), and homogenization temperature of the N_2-rich phase. "C" denotes critical homogenization.

been observed on inclusions with substantial amounts of CO_2 (fig. 58). Extremely low temperatures of homogenization in the liquid phase (down to -181°C!) have been recorded for elongated inclusions (fig. 50), forming part of a configuration where most inclusions remained monophase upon cooling to -190°C (very high densities). Dense N_2-rich inclusions have also been found in rocks from Ørsdalen (in a retromorphic environment).

Homogenizations above -147°C indicate the presence of constituents with a higher critical temperature than N_2, such as CH_4. In this respect, CO_2 has only have a minor effect on the phase equilibria because at temperatures of about -130°C the amount of CO_2 dissolved in an N_2-rich fluid is very small.

Dissociation temperatures of N_2-hydrate cover a range between -5 and +8°C. Their practical value, however, is negligible because the equilibria involved are presssure-dependent (Marshall *et al.*, 1964).

CH_4-rich inclusions

Two types of CH_4-rich inclusions have been distinguished (cf. Section II.4.3). The low-density type homogenizes in the gas phase between -100°

and -110°C (10 determinations). Gaschromatography has confirmed the presence of CH_4. The intermediate-density type homogenizes in the liquid phase between -120° and -84°C (commonly between -90° and -85°C) and (rarely) in the gas phase at temperatures between -86° and -84°C. Extreme cooling (using the vapor of boiling He as a refrigerant) caused solidification of CH_4 at about -215°C. The solid filled about 50% of the inclusion volume and melted in the presence of vapor at about -187°C (uncorrected temperature). In conjunction with observed near-critical behavior at about -84°C these data point to relatively pure CH_4.

Carbonic inclusions

Most carbonic inclusions show a melting interval (difference between first and final melting temperature), ranging from 0.1 to 3.5° (168 determinations) with a common value between 0.2 and 0.6°. Melting intervals have been theoretically explained in the system CO_2-CH_4 by Swanenberg (1979) but an analogous approach can be made for the system CO_2-N_2, known to be the main reference system for carbonic inclusions in S.W. Norway (cf. Section II.5.5).

Monophase carbonic inclusions

Results of freezing studies on inclusions from migmatites and related rocks are presented in fig. 59. Although the range in homogenization temperatures for individual sites is appreciable, most histograms are uniform and show a more or less distinct frequency peak, generally between -10° and -20°C. Inclusions in strongly deformed or retromorphosed rocks from Drangsdalen (fig. 59-2) display a large range in homogenization temperatures without a distinct frequency peak. These homogenization temperatures, however, contribute for at least 75% to all homogenization temperatures lower than -40°C. In conjunction with the values of the melting temperatures a high density for these (generally small) inclusions is suggested. Relatively low homogenization temperatures have also been recorded for inclusions situated "off-trail" ("isolated" in fig. 59-2) as opposed to those situated closer to the median zone of a trail. Fig. 59-4 illustrates the presence of high-density carbonic inclusions in Garnetiferous migmatites from Vikesdal and their absence in similar rocks collected in Gyadalen.
High homogenization temperatures (frequency peak between +10 and +20°C)

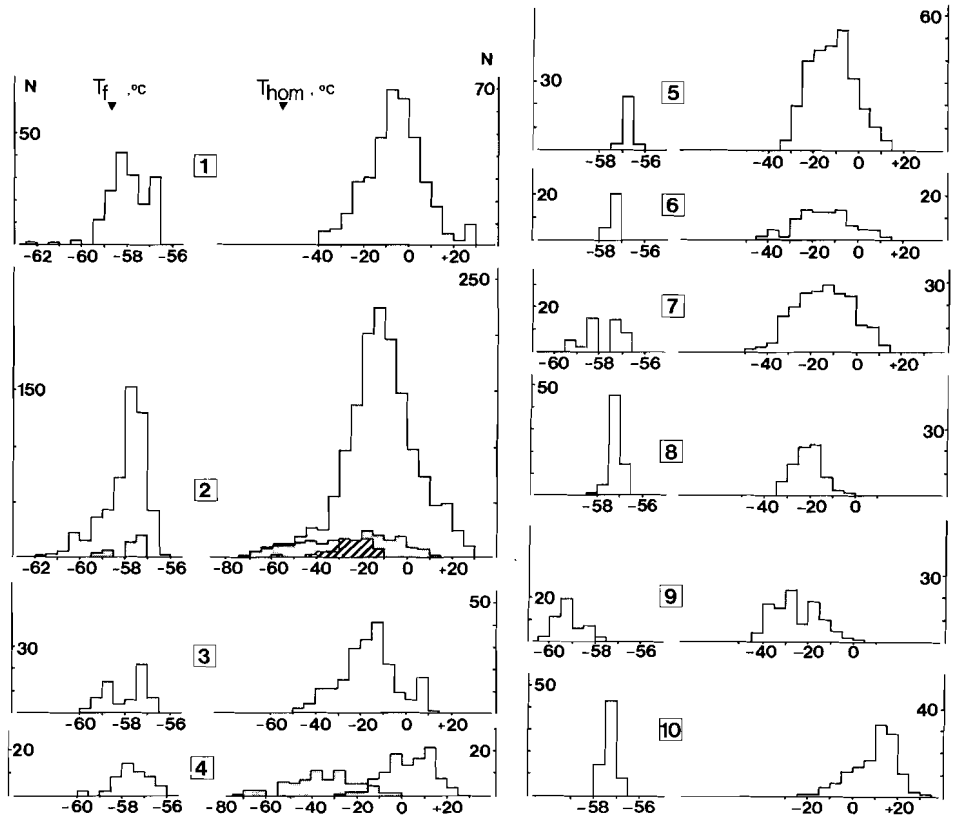

FIG. 59 Microthermometry of monophase carbonic inclusions in migmatites and related rocks from Rogaland/Vest-Agder.
1. Rocks in the vicinity of the Bjerkreim-Sokndal lopolith. 2. Charnockitic migmatites from Drangsdalen. 3. Charnockitic migmatites from Årdalen. 4. Garnetiferous migmatites from Gyadalen (blank), and Vikesdal (gray). 5. Charnockitic migmatites from Snøsvatnet. 6. Garnetiferous migmatites from Ivesdal. 7. Charnockitic migmatites from Ørsdalen. 8. Granitic migmatites from Store Myrvatnet. 9. Granitic migmatites from Tjørhom. 10. Country rock adjacent to a dolerite dike near Rusdalsvatnet.
Stippled: retromorphosed or strongly deformed rocks ; shaded: "isolated" inclusions.

are found in rocks adjacent to or in the vicinity of a dolerite dike (fig. 59-10).

Freezing data of monophase inclusions in Faurefjell metasediments are presented in fig. 60. Compared with the Drangsdalen rocks for instance,

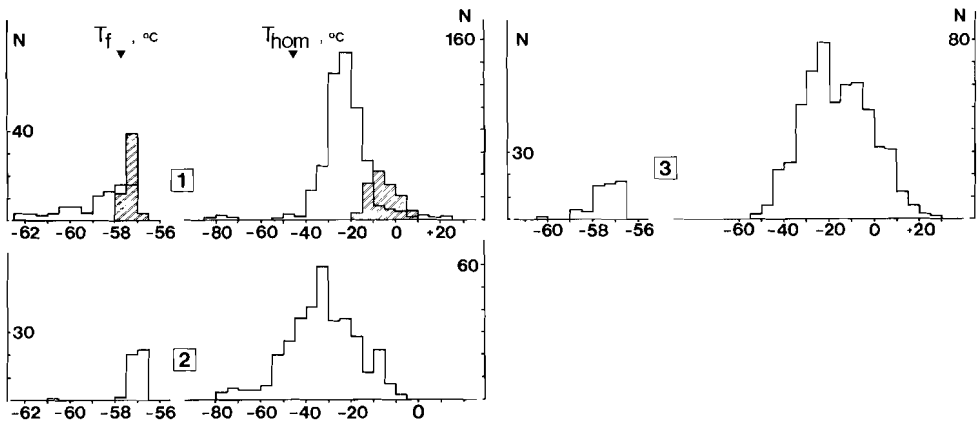

FIG. 60 Microthermometry of monophase carbonic inclusions in Faurefjell Metasediments. T_f= final melting temperature of CO_2. T_{hom}= homogenization temperature. 1. Quartz pods in marble and diopside rock. 2. basal quartzite at Asheim. 3. Quartz-diopside gneisses from Nedrabø .

the homogenization temperatures of inclusions in both the quartz-diopside gneisses/ quartzites (fig. 60-3) and the basal quartzite (fig. 60-2) are lower. As final melting temperatures of CO_2 below -58° are relatively rare in these rocks, a large proportion of the low homogenization temperatures must be ascribed to high densities.

A number of monophase carbonic inclusions shows metastable homogenization in the liquid phase at temperatures below the triple-point value of pure CO_2 ($-56.6^{\circ}C$) (cf. Section I.2.2). The volume of solid CO_2, present at $-100^{\circ}C$, occupies approximately 70-80 percent of the inclusion volume. Melting temperatures of CO_2 are invariably higher than $-57.5^{\circ}C$. Collectively, these data indicate an extremely high equivalent CO_2-density up to about 1.23 g/cc. Many of these "superdense" carbonic inclusions occur in configurations that have been described earlier as decrepitation clusters (cf. Section II.4.5; fig. 61).

Compared with the inclusions in the metasediments proper, the range in CO_2-equivalent densities of monophase inclusions in the quartz pods and veins is more restricted. This effect might indicate that quartz bodies, wholly enclosed in marble (and perhaps also in diopside rock) are less sensitive to post-entrapment processes which, in general, tend to increase the range in densities (compare fig. 59-2; cf. Chapter II.6.5).

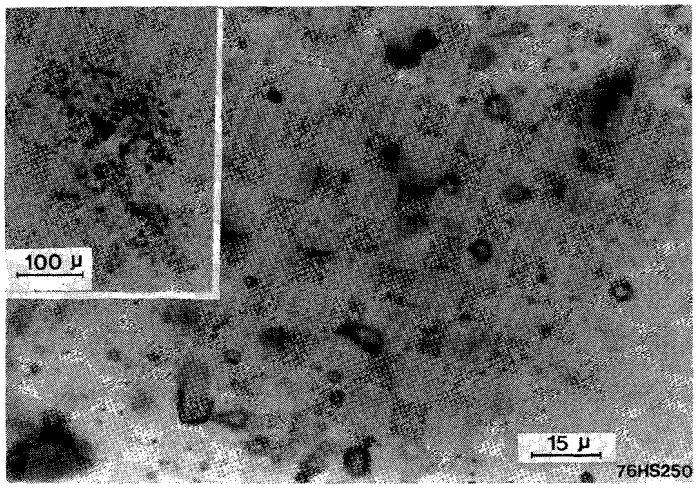

FIG. 61 Photomicrograph of high-density carbonic inclusions, forming part of a "decrepitation cluster" (see also inset top left). Basal quartzite of Faurefjell Metasediments at Asheim.

In graphite-bearing quartzo-feldspathic rocks (Garnetiferous migmatites) dark-looking carbonic inclusions have been found (carbonaceous material?). Upon sufficient cooling these inclusions develop a crystal mush which, as opposed to CO_2 crystals in pure CO_2 vapor, is rather reluctant to recrystallize into a smaller number of larger crystals. Because homogenization temperatures are lower than -80°C (fig. 62) melting of CO_2 does not occur in the presence of a liquid and vapor but should preferably be described as "dissolution of CO_2 in a fluid mixture of N_2, CH_4, and CO_2 .

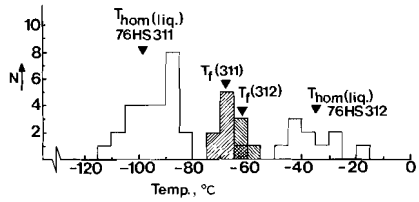

FIG. 62 Microthermometry of monophase carbonic inclusions in quartzofeldspathic rocks from the Garnetiferous migmatites near Austrumdalsvatnet. Sample 76HS311 contains graphite whereas 76HS312 (same locality) is virtually devoid of graphite.

A graphite-free sample, collected in the immediate vicinity (76HS312 in fig. 62) contains relatively clear carbonic inclusions, which melt in the

presence of liquid and vapor at temperatures of about -60°C. Such temperatures still indicate considerable amounts of CH_4 and/or N_2. This is confirmed by gaschromatography (cf. Section II.4.2).

Relation between the final melting- and homogenization temperature of the carbonic phase.

Plots of final melting temperatures versus homogenization temperatures of the carbonic phase show a positive correlation (fig. 63). This relation

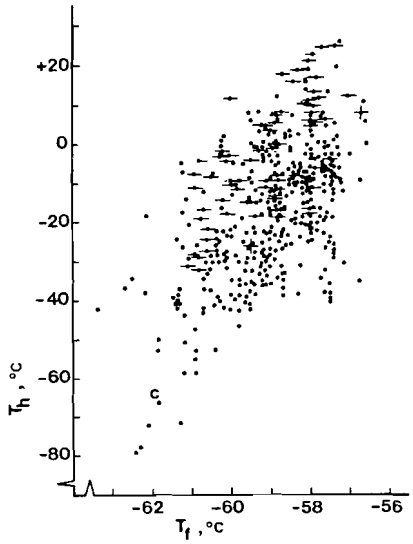

FIG. 63 Relation between temperatures of final melting of CO_2 (T_f) and homogenization of the carbonic phase (T_h). ● : monophase; ⊷: biphase H_2O-CO_2; ✚: biphase H_2O-CO_2, hydrate-absent. C: critical homogenization.

indicates that at least part of the range in homogenization temperatures is due to compositional effects. The decrease in homogenization temperatures of the carbonic phase is theoretically predictable (Swanenberg, 1979; cf. Chapter I.9) if at constant equivalent CO_2-density the composition is introduced as a variable.

H_2O-CO_2 inclusions.

Homogenization temperatures of the carbonic phase in mixed H_2O-CO_2 inclusions are given in fig. 64. Compared with the values for the monophase inclusions the homogenization temperatures are, in general, about 20-25° higher.

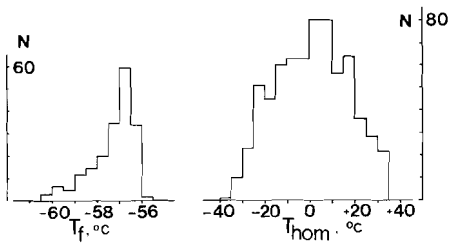

FIG. 64 Temperatures of final melting (T_f) and homogenization in the liquid phase (T_{hom}) of the carbonic phase in H_2O-CO_2 inclusions.

A positive correlation has been established between the homogenization temperature of the carbonic phase and the degree of filling with H_2O (fig. 65). Part of the variation in vertical sense is due to compositional effects (cf. fig. 63). The significance of this relation with respect to temperatures and pressures of geologic interest will be dealt with in Section II.5.5.

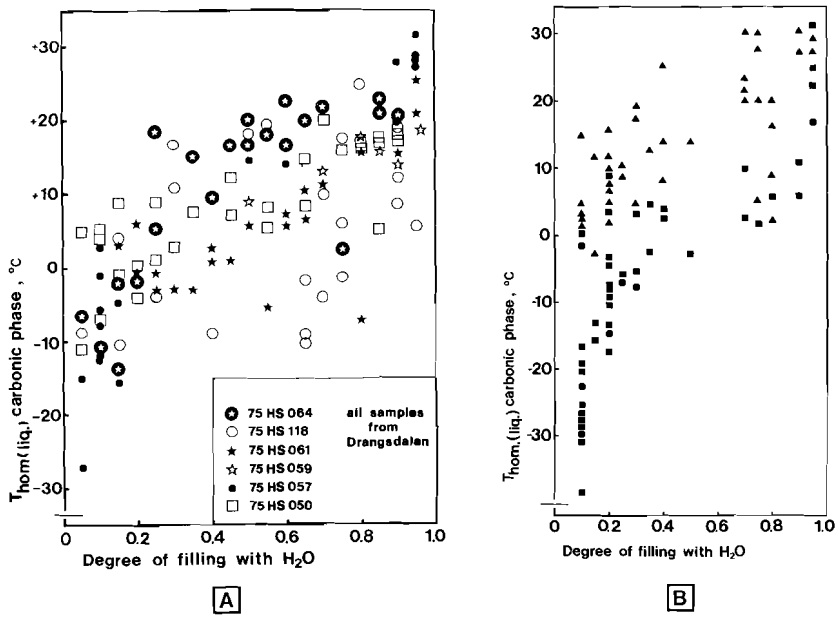

FIG. 65 Homogenization temperatures of the carbonic phase in biphase H_2O-CO_2 inclusions as a function of the degree of filling with H_2O. Hydrate may be present. A: Drangsdalen; B. Faurefjell Metasediments (excluding quartz pods).

CO_2-hydrate dissociation

In the mixed H_2O-CO_2 inclusions, dissociation of the CO_2-rich hydrate start 1-9° before final dissociation. It should perhaps be stressed that the dissociation of CO_2-hydrate is difficult to observe, thus introducing considerable errors (probably at least ± 0.5°C). One of the criteria used is the degree of roundness of the CO_2-rich bubble during dissociation. Because the carbonic phase commonly homogenizes at relatively low temperatures, only a liquid (fluid) phase is present at the temperature of final dissociation. Data on hydrate-dissociation are given in fig. 66.

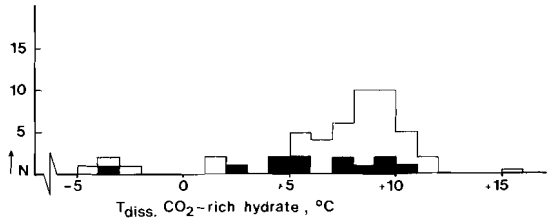

FIG. 66 Dissociation temperatures of the CO_2-rich hydrate. In black: dissociation in the presence of liquid + vapor. Blank: dissociation in the presence of liquid only.

In conjunction with the fact that the salinity of the aqueous phase cannot be determined correctly (part of the H_2O is bound to the hydrate) it is believed that the data on hydrate dissociation are of limited value in determining the composition of H_2O-CO_2 inclusions.

II.5 FLUID INCLUSIONS - INTERPRETATION

II.5.1 BASIC ASSUMPTIONS

It is assumed that the species presently found in the inclusion are the same as those present in the fluid that was trapped once. Perchuk (1976) states that species such as CO_2 and H_2O can be derived by oxidation of reduced species such as H_2, CH_4, and CO, possibly present in deep metamorphic zones with low oxygen fugacity. With regard to fluid inclusions this hypothesis would envisage trapping of reduced species followed by oxidation if H_2 is allowed to diffuse out of the inclusions. In case the inclusions contain graphite (fig. 62) H_2-diffusion may have been prevented but reactions between graphite and fluid will certainly change the composition.

Because any effect of post-entrapment re-equilibration will be superposed on a pre-existing variation in fluid inclusion properties, this must be taken into account when interpreting heating-freezing data in trapping temperatures and pressures.

The basic assumption of non-leakage (Roedder & Skinner, 1968) is probably valid for most inclusions in hydrothermal vein minerals or in minerals associated with ore deposition. It may be questioned, however, in case the rocks have suffered post-crystalline deformation (Kerrich, 1976; Wilkins & Barkas, 1978). Post-entrapment changes may, therefore, produce fluid inclusions whose density and composition do not or do only in part reflect the original conditions during trapping.

Finally, volumetric corrections resulting from precipitation of SiO_2 in H_2O or CO_2-rich inclusions at decreasing temperatures have not been made. According to Shettel (1973) the solubility of SiO_2 in a 50 % molar H_2O-CO_2 fluid at 700^{o}-5kb is only 0.2 wt% ; with this order of magnitude solubility effects are not significant in CO_2-rich inclusions.

Corrections for dilatancy and compressibility of the host mineral (for instance applied by Touret, 1971) have not been considered in view of the large error already made in the interpretation of the microthermometric data (cf. Section II.5.5).

II.5.2 AQUEOUS INCLUSIONS

By selecting the system H_2O-$CaCl_2$ as the reference system for aqueous

inclusions (cf. Section II.4.7) final melting temperatures of ice indicate 0-30 equivalent weight percent $CaCl_2$ (Weast, ed., 1975). Because high-temperature volumetric data of the system H_2O-$CaCl_2$ are not available, approximate isochores have been obtained by converting weight percentages $CaCl_2$ to weight percentages NaCl in such a way that the bulk density remains the same. Such a procedure has been carried out for inclusions homogenizing between 130° and 200°C with salinities ranging from 10 to 25 wt% $CaCl_2$, a common range for inclusions in rocks that have not suffered intense retromorphism or deformation (figs 55, 56). The isochores can be obtained with the aid of Potter II (1977), a study on the system H_2O-NaCl; the results are depicted in fig. 67. At pressures exceeding 2 kb the isochores have been extrapolated linearly.

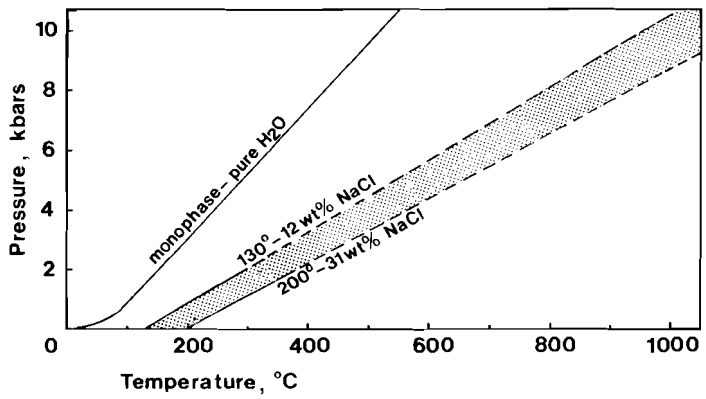

FIG. 67 Isochores for aqueous inclusions (Drangsdalen, Stølsfjellet). Stippled area reflects the most common range in homogenization temperatures and salinities. Note that salinities are equivalent weight percentages only with respect to the density (see text). Isochores are based on Fisher (1976) and Potter II (1977).

II.5.3 N_2-BEARING INCLUSIONS

Critical homogenizations between -145° and -130°C (cf. fig. 57) indicate CH_4-contents up to 20 molar percent. In terms of CO_2 and N_2, compositions can be approached from an estimate of the volumetric portion of solid CO_2 at about -170°C in conjunction with the density of the N_2-rich phase.

Compositions, derived from N_2-CO_2 inclusions showing liquid-vapor separation at very low temperatures, range from 4 to 90 mole% CO_2. The N_2-bearing CO_2-rich inclusions have provided the datapoints of fig. 16 (Pt.I).

N_2-rich inclusions (< 4 mole% CO_2) homogenize between -152° and -181°C. These temperatures correspond to a density-range of about 0.50-0.74 g/cc (fig. 5), the most common range being 0.53-0.63 g/cc. The isochores are obtained using figs 6 and 9; the results are depicted graphically in fig. 68. High-density N_2 has been found in Drangsdalen and in Ørsdalen (in a retromorphic environment, cf. Heier, 1956).

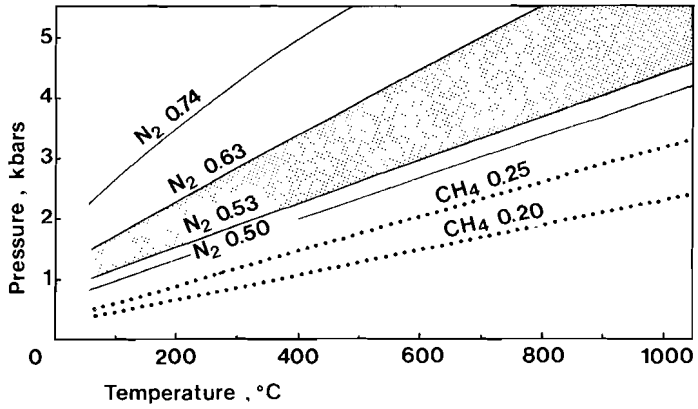

FIG. 68 Isochores for N_2-rich and CH_4-rich inclusions (density ranges of 0.50-0.74 and 0.20-0.25 g/cc respectively). Stippled area encompasses the most common range in densities of N_2-rich inclusions.

II.5.4 CH_4-RICH INCLUSIONS

Homogenization temperatures of the gaseous phase in dark-looking CH_4-rich inclusions (cf. Section II.4.7) reflect CH_4-densities in the range 0.03- 0.04 g/cc (Mullis, 1979). An aqueous phase, which is occasionally present in amounts up to 30 volume percent, would increase the bulk density. Despite their well-developed negative crystal shapes, the inclusions have probably been trapped at low temperatures as is suggested by their occurrence in well-defined planar arrays. If temperatures of trapping are assumed to be between 200° and 300°C (cf. Mullis, 1979), the corresponding pressures would be 93-125 bars. The presence of additional H_2O (applying Dalton's law) would raise the pressures to 110-215 bars.

The homogenization temperatures of the intermediate-density type reflect a density range of 0.10-0.35 g/cc, the most common range being 0.20-0.25 g/cc. The corresponding isochores are depicted in fig. 68.

II.5.5 CARBONIC AND MIXED H_2O-CO_2 INCLUSIONS

Selection of the reference system for the carbonic phase

In Chapter I.6 (fig. 15) a method has been outlined to check homogenization temperatures in terms of the system CO_2-CH_4 if the melting temperature and the associated degree of filling with liquid are known. The results of this procedure, carried out for a number of inclusions from Drangsdalen rocks are depicted in fig. 69. Most observed temperatures of homogenization are higher than those theoretically predicted and could be considered "inconsistent" in the system CO_2-CH_4. Unfortunately, lack of accurate and complete experimental data precludes a similar test with the system CO_2-N_2. Based on the small value of the freezing point depression by N_2 compared with CH_4, the homogenization temperatures, however, would be even more inconsistent in the system CO_2-N_2. This is the only serious objection against the interpretation of homogenization temperatures in terms of CO_2 and N_2.

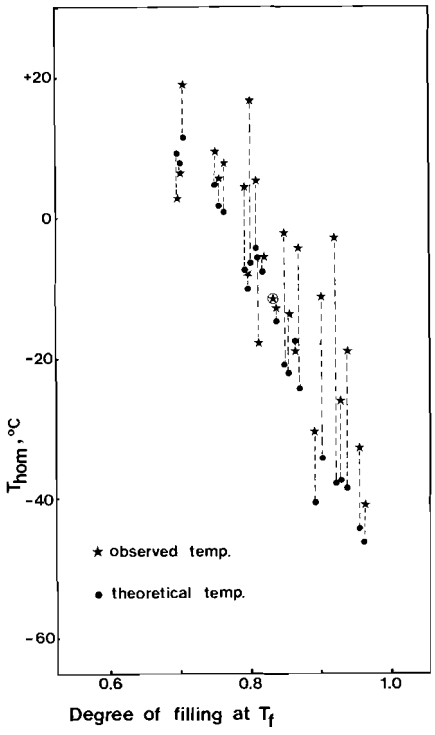

FIG. 69 Inconsistency test for carbonic inclusions (system CO_2-CH_4), based on fig. 15 (Pt.I).

Dissociation temperatures of the CO_2-rich hydrate are generally below +11°C (fig. 66) indicating that substantial amounts of CH_4 in the carbonic phase are not likely (Hollister & Burruss, 1976).

Evidence in favor of N_2 as the principal contaminant in the carbonic

phase is provided by microthermometry of the residual phase left over after solidification of CO_2 at sufficiently low temperatures (cf. Sections II.4.7 and II.5.3)

> In a CO_2-N_2-(CH_4?) inclusion (75HS191) homogenization of the residual phase (left over after solidification of CO_2) occurs in the liquid phase at -143°C. This temperature indicates that, in addition to N_2 , another component with a higher critical temperature must be present (CH_4, NH_3). The carbonic phase of the inclusion homogenizes critically at -37°C. In terms of the system CO_2-N_2 this temperature would point to about 0.48 mole N_2 and 0.52 mole CO_2 whereas in the system CO_2-CH_4 these values would be 0.61 and 0.39 respectively (interpolated from Zagoruchenko & Zhuravlev, 1969 and Arai *et al.*, 1971). The CO_2-CH_4 composition does not comply with the observed final melting temperature of CO_2 at -60.9 (this value should be about -70°C according to Donnelly & Katz, 1954). In conjunction with the observed low contrast between the gas bubble and the liquid at temperatures of about -145°C the data are in support of an N_2-rich residual phase.

In addition, gaschromatographic analysis of the gases released upon crushing in vacuum revealed N_2 as the predominant component of the non-condensable phase (cf. Table 6).

In summary, the data suggest that the depression of the melting point of CO_2 is generally due to N_2 rather than to CH_4 . Consequently, homogenization temperatures of the carbonic phase are expressed in terms of CO_2-N_2, using figs 16, 18, and 19 (Pt.I). For convenience, the bulk densities are converted to "CO_2-equivalent densities", which produce approximately the same isochore as the one derived from the bulk density (with binary composition).

The optical error, made by not being able to observe a 5 vol.% rim of H_2O introduces an uncertainty of about 200 bars. Interpretation in terms of CO_2-N_2, using fig. 16, adds about 350 bars to the uncertainty while the isochores are accurate up to $\pm$ 150 bars. Instrumental errors are not significant. By taking the square root of the sum of squares of the individual errors the final estimated uncertainty is 500 bars. This error becomes significantly lower if a large body of data is available. In that case, however, the main error resides no longer in the mean or mode of the histograms but is essentially determined by the way these histograms are being interpreted in geologic parameters.

Monophase carbonic inclusions

The total range in CO_2-equivalent densities in various rocks from Rogaland/Vest-Agder, based on about 4800 homogenization temperatures that have been interpreted in the system CO_2-N_2 is 0.70-1.23 g/cc, the most common value being about 0.95 g/cc. A comparison with fluid inclusion data obtained from other granulite-facies rocks (fig. 73) reveals that most CO_2-equivalent densities in S.W. Norway are high, some are even extremely high ($d > 1.10$ g/cc).

The high-density inclusions, however, do not represent a synmetamorphic fluid phase in terms of pressure and temperature. This hypothesis is in part substantiated by the following arguments:

- the preferential occurrence of extremely dense carbonic inclusions in

Occurrence	CO_2-equivalent density (g/cc)	
	average	maximum
Rocks in the vicinity of the lopolith of Bjerkreim-Sokndal		
- concordant	0.82	1.01
- discordant	0.88	1.07
Charnockitic Migmatites		
- Snøsvatnet	0.96	1.07
- Drangsdalen	0.89	1.19
- Gyadalen ("East")	0.94	1.02
- Årdalen	0.94	1.07
- Ørsdalen	0.93	1.04
Granitic Migmatites		
- Store Myrvatnet	0.98	1.07
- Tjørhom	0.85	0.93
Garnetiferous Migmatites		
- Gyadalen	0.82	0.98
- Vikesdal	1.02	1.17
- Ivesdal	0.96(?)	1.11
Faurefjell Metasediments		
- Quartz lenses at Asheim, Seldal, and Stølsfjellet	0.94	1.08
- Quartz-diopside gneisses at Nedrabø	1.03	1.15
- Basal quartzite at Asheim	1.07	1.23
Rocks in the vicinity of a dolerite dike at Rusdalsvatnet	0.80	0.99

TABLE 7 Approximate CO_2-equivalent densities of monophase carbonic inclusions, based on interpretation in the system CO_2-N_2 of appropriate histograms of homogenization temperatures.

in rocks affected by retromorphism or plastic deformation (fig. 59-2)
- the presence of extremely dense carbonic inclusions (CO_2-equivalent densities up to 1.17 g/cc) in or adjacent to rocks containing typically HT-LP minerals such as osumilite or cordierite.
- the presence of high-density carbonic inclusions in a discordant vein , dated at 880Ma (Wielens, 1979).
- the occurrence of a high-density carbonic phase in inclusions with the negative crystal shape of α-quartz, indicating maximum temperatures of entrapment or equilibration in the order of 700°C at 5 kb (Frondel, 1962).
- the presence of extremely dense CO_2-rich inclusions in decrepitation - clusters (probably rather late-stage phenomena)(figs 60-2 and 61).
- the absence of extremely dense carbonic inclusions in quartz pods, enclosed in marbles.

This leaves the frequency maximum, found in most T_{hom}-histograms if based on a sufficiently large number of data, to be explained. In Drangsdalen, for instance, the average CO_2-equivalent density of about 0.89 g/cc (Table 7) gives an isochore that intersects values of 4.8 and 5.3 kb at 800° and 900° respectively (fig. 74). These values are compatible with independently determined P-T estimates of the main phase of granulite-facies metamorphism (cf. Chapter II.1).

In the basal quartzite and in the diopside gneisses/quartzites of the Faurefjell metasediments, the average CO_2-equivalent densities are about 1.07 and 1.03 g/cc respectively (Table 7). For these inclusions the corresponding isochores (fig. 74) are clearly not in agreement with the P-T estimates of high-grade metamorphism in this region.

In summary, the frequency peak in the T_{hom}-histograms could reflect the P-T conditions of high-grade metamorphism but, taking into account the possibility of post-metamorphic changes, it might equally well result from prolonged post-entrapment re-equilibration at high-density isochores. Although many of the carbonic inclusions with relatively low densities would be potential candidates for a synmetamorphic fluid, at least those with irregular shapes result from low-temperature re-equilibration, possibly involving (partial) leakage.

Mixed H_2O-CO_2 inclusions

Essentially two types of mixed H_2O-CO_2 inclusions have been found.

In the first type the degree of filling with H_2O is fairly constant, ranging from 0.6 to 0.9 while homogenization temperatures of the carbonic phase are measured between +15.9 and +31.0°C (liquid phase). It has been found in relatively well-defined trails in a restricted number of samples. Because final melting temperatures of CO_2 range from -56.6° to -56.9°C and those of ice are about -3.5°C, the microthermometric data have been expressed in the system H_2O-CO_2 . Molar percentages of CO_2 in these H_2O-CO_2 inclusion range from 3 to 17%. Isochores have been obtained using figs 26 and 27 (Pt.1). The possible P-T conditions of formation of the inclusions are situated in the area limited by the curves 0.9-0.69 and 0.6-0.60 (denoting degree of filling and CO_2-density respectively) in fig. 70. Unfortunately, the MRK-isochores are not accurate at temperatures lower than 400°C and extrapolation from the low-density data by Khitarov & Malinin (1956) is not possible. In the region between 200° and 400°C the isochores have, therefore, been dashed. Below 200°C the pressure exerted by a H_2O-CO_2 inclusion

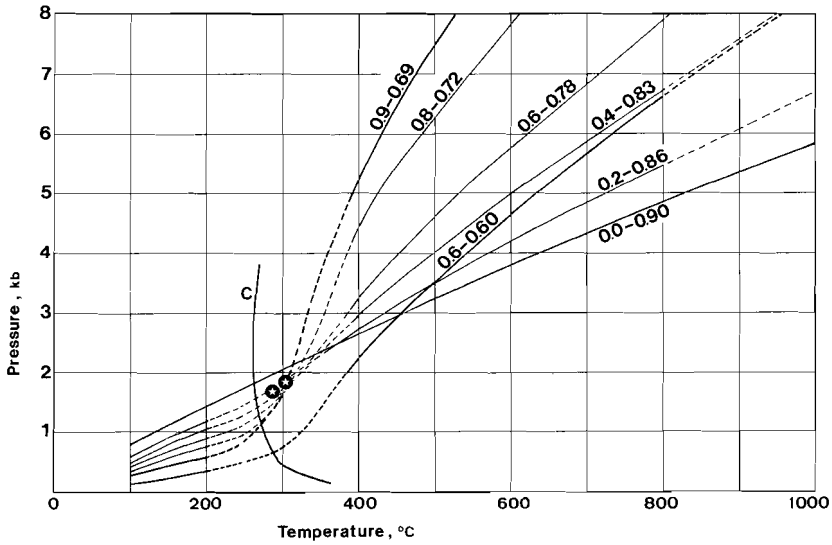

FIG. 70 Isochores for biphase H_2O-CO_2 inclusions with given degree of filling at room temperature (first number) and density of CO_2 in the bubble (last number) corresponding to the upper row of datapoints in fig. 65-AB. C= critical curve of the system H_2O-CO_2 (Tödheide, 1963). ✪ = decrepitated inclusion.

may be approximated by the isochore that corresponds to the CO_2-equivalent density of the bubble at room temperature. If it is assumed that this type originated from a homogeneous H_2O-CO_2 phase, lower temperature limits of trapping for at least two representative inclusions are given by their decrepitation temperatures (282° and 304°C), prior to homogenization (fig. 70).

The second type of mixed H_2O-CO_2 inclusions is found in cluster-like configuration and in trails, otherwise composed of monophase carbonic inclusions. A positive correlation was found between the degree of filling with H_2O and the homogenization temperature of the carbonic phase (fig. 65). Thus, in the upper part of the broad zone of datapoints in fig. 65 (where the carbonic phase is probably least contaminated), each pair of filling degree and CO_2-homogenization temperature will produce an isochore. Along these isochores temperatures and pressures of final equilibration of the individual inclusions are located. For degrees of filling 0.0, 0.2, 0.4, 0.6, 0.8, and 0.9 (aqueous phase is considered as pure H_2O) and their corresponding CO_2-densities the isochores (excluding 0.6-0.60) are depicted in fig. 70.

The intersection of isochores suggests that mixed H_2O-CO_2 inclusions with a wide range in compositions may have been generated within a relatively narrow field of low temperatures and pressures. Entrapment or re-equilibration at higher temperatures is possible but would require a larger pressure interval in order to satisfy the general relation between filling degree and CO_2-density.

As indicated by the position of the critical curve ("c" in fig. 70), the intersection point is situated in the monophase fluid region of the system H_2O-CO_2 . Although the assumption of pure H_2O probably does not introduce significant errors in the isochore construction, its validity with regard to the position of the critical curve and hence, boundary curves may be questioned. As pointed out by Hollister & Burruss (1976) relatively small amounts of salt may raise the critical temperature of H_2O-CO_2 fluids considerably. This implies that type 2 H_2O-CO_2 inclusions could originate from an unmixed fluid.

> Because of the hydrate-effect (cf. Section II.3.5) binary isochores based on CO_2-densities above 0.88 g/cc should be corrected. Such correction would add at least 0.03 g/cc to the CO_2-densities. In terms of isochores this would result in a pressure correction of at least 250 bars at temperatures above 400°C.

Isochores of H_2O-CO_2 inclusions with higher CO_2-densities than those mentioned in fig. 70, would intersect at higher pressures. The isochores of inclusions with a high degree of filling with H_2O are, however, no sensitive function of the CO_2-density. This indicates that the 0.9-0.69 isochore approximately defines un upper pressure limit for all H_2O-CO_2 inclusions.

II.6 DISCUSSION

II.6.1 THE TRAIL PROBLEM

The presence of carbonic inclusions as a characteristic feature of granulite-facies rocks (Touret, 1970, 1971, 1972, 1974ab; Bilal, 1976; Bilal & Touret, 1976; Konnerup-Madsen, 1977, 1979) has in part been confirmed by the present study. Their general occurrence in trails, however, suggests that they are trapped after (re)crystallization of the host mineral, at post-metamorphic conditions (cf. Section II.4.5). If, on the other hand, the carbonic inclusions are *synmetamorphic* it would imply brittle behavior of quartz under high-grade metamorphic conditions. Although it is believed by many geologists that rocks in granulite-facies environments yield by plastic deformation, quartz is known to remain brittle up to high temperatures (Verhoogen *et al.*, 1970), particularly under anhydrous conditions (Griggs, 1967). In addition to this, CO_2-bearing healed fractures have been reported from mantle-derived olivine (Roedder, 1965) and from several minerals in catazonal xenoliths (Bilal, 1976; Bilal & Touret, 1976).

Fracture-healing at relatively low temperatures and pressures is, however, more acceptable from a mechanical point of view but leaves the question on the origin of the CO_2-rich fluid unanswered. According to Touret (1971, 1974a), Hoefs & Touret (1975), Schuiling & Kreulen (1979) and Kreulen (1980), CO_2-rich fluids could have a deep-seated origin. Thus, the fluid would be retained in the rocks during part of the post-metamorphic history of the rock.

> A juvenile origin of CO_2 in granulite-facies rocks from S. Norway is proposed by Hoefs & Touret (1975) on the basis of relatively low $\delta^{13}C$-values (about -15‰). In the present study, however, most values are between -6 and -9‰ (Section II.4.2). Such values are, in general, still considered as representative of juvenile C.

An alternative hypothesis for the occurrence of fluid inclusions in trails, particularly the subbasally oriented ones, may be derived from Wilkins & Barkas (1978). According to Wilkins & Barkas (1978), aqueous inclusions that are associated with ductile deformation lamellae could result from precipitation of structurally bound H_2O or from external pore fluids. Although the first-mentioned possibility is difficult to envisage for CO_2-

rich inclusions, a more or less alternative reading would be the formation of (subbasal) trails from pre-existing arrangements by migration of inclusions and their subsequent decoration of slipplanes ("Boehm" lamellae, Gary *et al.*, eds., 1974). Subbasally oriented deformation lamellae (reflecting slipplanes) have been produced experimentally at temperatures up to 850°C depending on pressure, strain rate and OH-content (Avé'lallement & Carter, 1971). The hypothesis of decoration of ancient slipplanes by carbonic inclusions is in part substantiated by observations on the transposition of fluid inclusion trails (cf. Section II.4.5).

It is suggested that Transmission Electron Microscopy could aid in defining criteria for the distinction between fluid inclusion trails that have originated from brittle deformation and those that are somehow related to ductile deformation processes.

II.6.2 RELATION FLUID INCLUSIONS - PETROLOGY

The distribution of various types of fluid inclusions as related to the composition or metamorphic grade of the host rock does not produce a consistent picture. For instance, in Drangsdalen thin layers containing an apparently stable biotite-quartz assemblage may show the same fluid inclusions as the anhydrous assemblages in the neighboring rocks (Section II.2.1.). Statistically, however, carbonic inclusions are more abundant in enderbitic rocks than in (alkali)granitic rock, where most of the biotite - quartz contacts have been found (cf. Section II.4.4). More or less simi-

lar phenomena were observed by Konnerup-Madsen (1977) in the Kleivan granite (S.Norway) where a high proportion of carbonic inclusions is found in the plagioclase-rich pyroxene- and hornblende-bearing parts (plagioclase/total feldspar= 0.47) as opposed to the biotite zone (plagioclase/total feldspar= 0.27) where such inclusions are practically absent.

On a more expanded scale, the estimates of CO_2-H_2O ratios seem to be relatively high in rocks from the Charnockitic migmatites whereas this number for rocks of the Granitic migmatites is somewhat lower (Section II. 4.4). This resembles the results of Touret (1972) who established a similar relation between the distribution of inclusion types and the location of the samples with respect to the orthopyroxene-isograd.

Most fluid inclusions consist of H_2O or CO_2 or both. Additional non-ionic species may comprise CH_4 or N_2. CO_2-rich inclusions in graphite-bearing rocks contain a relatively high amount of CH_4 (Sections II.4.2 and II.4.7). The presence of CH_4 in graphite-bearing rocks has also been reported by Touret (1972), Bilal (1976), and Crawford *et al.* (1979); local buffering by graphite also follows from stable isotope work by Kreulen (1980).

As far as is known to the present author, N_2-rich inclusions have not been reported earlier. Although N_2 has frequently been analyzed upon heating rocks in vacuum (Roedder, 1972), the existence of N_2-rich fluid inclusions seems to be largely unknown.

Most N_2-rich inclusions have been found in quartz-rich rocks adjacent to or in the vicinity of mafic rocks (many of which are clinopyroxene- or amphibole-bearing) and in a number of pegmatites.

The relatively rare occurrence of mixed CO_2-N_2 inclusions with more or less uniform intermediate compositions seems to preclude a large-scale simultaneous trapping of CO_2 and N_2 , implying that CO_2 and N_2 were introduced at different times. Although H_2O-rich and N_2-rich inclusions have been found associated in cluster-like configurations this need not necessarily imply a late-stage origin of the N_2-rich inclusions. In stead, a number of arguments are in favor of an "early-secondary" trapping:

i. the occurrence of N_2-rich inclusions in cluster-like trails, probably pointing to a relatively long history of the original configuration.
ii. the overlap of the N_2-isochores with those of CO_2, suggesting a similar postmetamorphic development.

iii. the occurrence of N_2-rich inclusions in high-grade pegmatites and quartz veins.

Arguments in favor of trapping after the CO_2-rich inclusions are:

i. the locally observed preferred contamination of CO_2-rich inclusions in the grain-boundary region of a trail whereas the tip region in the interior part of the grain remains largely unaffected by N_2.

ii. the (unique) occurrence of N_2-rich inclusions (together with H_2O-rich inclusions) in a quartz vein while CO_2 inclusions are absent.

Little can be said about the origin of N_2. N_2 may be a primary (residual?) phase in the crust or upper mantle (cf. Wlotzka, 1961). Ammonia may substitute for potassium in phyllosilicates (Vedder, 1965). Biotites from migmatitic rocks in the Ryoke Belt (Japan) contain up to 500 ppm ammonium (Itihara & Honma, 1979). This suggests that, depending on the distribution-coefficient of NH_4 over products and reactants, nitrogen may be released from pre-existing NH_4-rich biotites that decompose during high-grade metamorphism. Decomposition of ammonia-bearing feldspars could also give rise to the development of an N_2-rich phase (Althaus, pers.comm.).

II.6.3 COMPARISON WITH OTHER METAMORPHIC TERRANES

Bilal (1976) has demonstrated that granulite-xenoliths from the Massif Central, brought rapidly to the surface by volcanic activity, exclusively contain carbonic inclusions as opposed to rocks from granulite-complexes that crop out at the surface. This is a strong argument in favor of the currently accepted hypothesis (proposed by Touret, 1971) that carbonic inclusions are typical for granulite-facies metamorphism whereas aqueous inclusions represent a later phase.

Konnerup-Madsen (1977, 1979) has described fluid inclusions in post-kinematic granites from S. Norway. Most of his observations with regard to mixed H_2O-CO_2 inclusions are more or less similar to those made in the present study. His data point to trapping temperatures of about 300^{o} at about 1 kbar for inclusions with variable phase ratios (unmixed fluid). H_2O-CO_2 inclusions with rather uniform phase ratios (suggesting a homogeneous fluid at the time of trapping) have also been observed.

With regard to homogenization temperatures of (largely) monophase carbonic inclusions, a comparison with the data from Touret (1971), Bilal

(1976), and Konnerup-Madsen (1977) is presented in fig. 71. Apart from their variation, most homogenization temperatures of CO_2 in the Rogaland

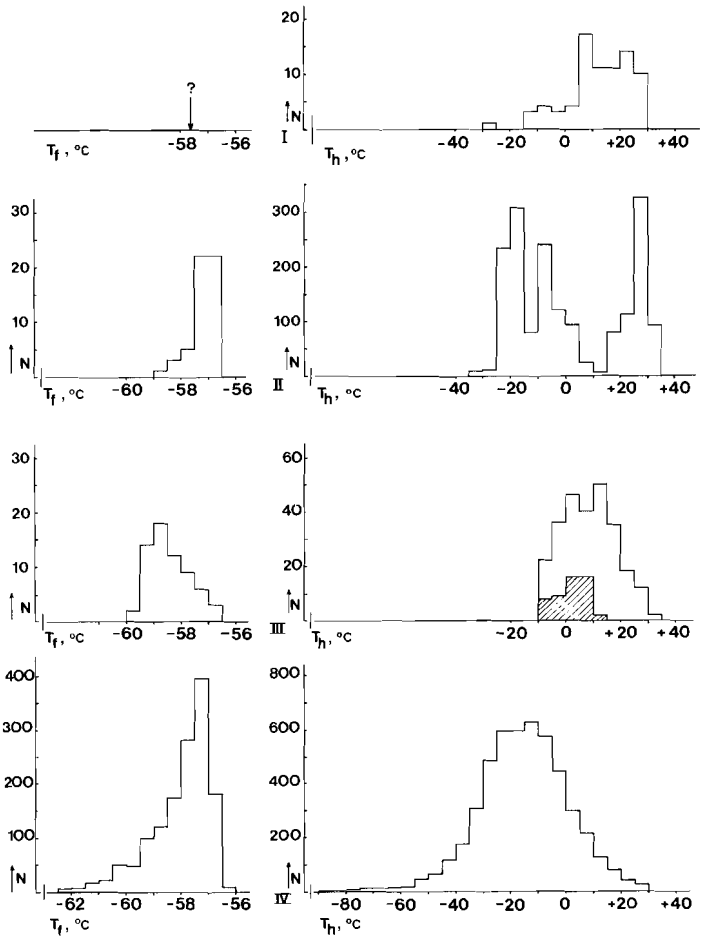

FIG. 71 Comparison between microthermometric data of carbonic inclusions (monophase, unless stated otherwise) in high-grade metamorphic and related igneous rocks. T_f= final melting temperature of CO_2 . T_h= homogenization temperature of the carbonic phase. I= Touret, 1972 (perhaps part of the inclusions is biphase H_2O-CO_2). II= Bilal, 1976 (regrouped histograms) III= Konnerup-Madsen, 1977 (regrouped histograms; shaded area refers to isolated inclusions). IV= present work; a compilation.

area are considerably lower than those in the Bamble area of S. Norway (Touret, 1971) and in the Kleivan granite, a post-kinematic pluton in S. Norway (Konnerup-Madsen, 1977). In terms of CO_2-equivalent densities, the differences between Rogaland and the (nearby) Kleivan granite are even more pronounced. The results of Bilal (1976) most closely approach the Rogaland data but a distinct peak at relatively high homogenization temperatures, interpreted as the result of a high-grade retrogressive event in the Massif Central area, is not present in the Rogaland histogram.

When comparing seemingly objective data such as homogenization temperatures, an element of subjectivity is introduced by the different aims that have been set by the various investigators. Depending on the way certain significant parameters of the host rock or the inclusions have been accounted for, the final selection of the inclusions may be widely different. Such parameters may comprise the structural state of the sample, the degree of retrogressive metamorphism, the number, and the size of the inclusions.

II.6.4 THE SIZE EFFECT

During the freezing studies of monophase carbonic inclusions in rocks from the Faurefjell metasediments, it appeared that in a given configuration of inclusions the lowest homogenization temperatures were invariably recorded for small inclusions. For a number of freezing runs both the homogenization temperatures and the sizes of the inclusions were registered. The idealized shape of plots of homogenization temperature (X-axis) versus inclusion size (Y-axis) is a quadrilateral figure. For practical purposes, only datapoints constituting the left-hand side of the quadrilaterals are presented (Fig. 72, interconnected points).

Although compositional effects may in part account for the horizontal variation and the variation in the average slope of the lines, the diagrams indicate that - in general - higher densities may preferably be found in smaller inclusions. Such a relation between size and homogenization temperature has also been established by Bilal (1976).

If it is assumed that a size effect is operative, we have to account for possible differences in size when comparing homogenization temperatures of carbonic inclusions from different areas or sites. For instance, in Drangsdalen the most common size of the inclusions selected for freezing

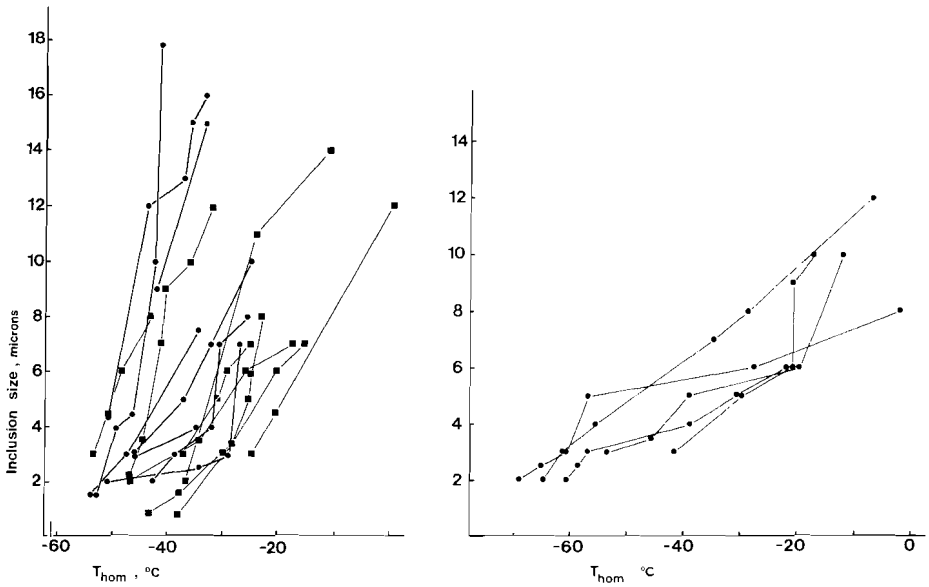

FIG. 72 Relation between homogenization temperature and inclusion size. Lines connect datapoints of individual runs. A. Quartzitic rocks from Faurefjell Metasediments. B. Tectonized and/or retromorphosed, discordant rocks from Drangsdalen. See text for discussion.

work is about 4.0 microns (N=364) whereas in the Asheim-Nedrabø area this value is about 2.8 microns (N=416). This difference in size (1.2 microns) implies that the relatively low homogenization temperatures in the Asheim-Nedrabø area are only significantly lower if the difference with the Drangsdal area exceeds 5^{o}, a value derived from the average slope of the appropriate lines in fig. 72AB. Because the observed difference is about 14^{o} (figs 59-2 and 60-2,3) and the CO_2 melting temperatures in Drangsdalen are about 0.5^{o} lower than those in the Asheim-Nedrabø area, a true difference in terms of average CO_2-equivalent density exists between the two areas.

Apparently, the relation between inclusion size and homogenization temparature reflects the enhanced mechanical strength of smaller sized inclusions during the post-entrapment period. Relatively large inclusions are more likely to undergo decrepitation and subsequent leakage.

Preliminary experiments, carried out by the present author, show that the quartz around inclusions of about 1 micron is able to sustain pressures in the order of 5-6 kbars (fig. 73). The upper datapoints in fig. 73 have been determined by stepwise heating of carbonic inclusions up to 900°C. After each step, inclusions of given sizes were checked for their densities at the freezing stage.

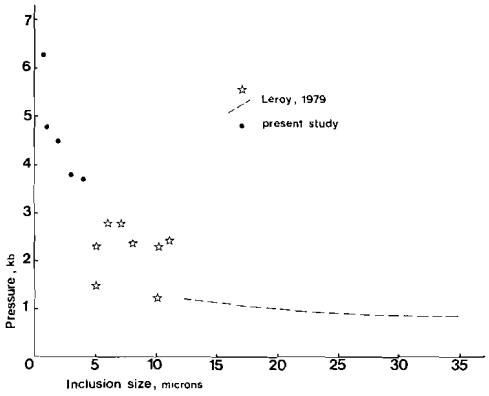

FIG. 73 Maximum pressure in fluid inclusions as a function of inclusion size (up to five microns). Experimentally determined values, obtained by stepwise heating of carbonic inclusions up to 900°C. Based on isochores of fig. 2. Data by Leroy (1979) refer to aqueous inclusions and have been added to complete the diagram for sizes up to 35 microns.

II.6.5 FLUID INCLUSIONS IN RELATION TO THE POST-METAMORPHIC HISTORY OF THE ROGALAND/VEST-AGDER ROCK COMPLEX

If it is assumed that the carbonic inclusions represent the fluid phase present during granulite-facies metamorphism their densities do not or only partly reflect the conditions of high-grade metamorphism in terms of pressure and temperature (cf. Section II.5.5). The possibility of a premetamorphic origin (i.e. before the latest phase of granulite-facies metamorphism) for the high-density carbonic inclusions is thought unlikely because this is only possible if the host phase (quartz) does not recrystallize at high-grade conditions. Although the P_{H_2O} may have been low under granulite-facies conditions even minor amounts of an aqueous phase could induce recrystallization if sufficient time is available. In addition to this, many arguments are in favor of a late-stage "origin" for the high-density carbonic inclusions (cf. Section II.5.5).

In conjunction with the P-T estimates for the Rogaland area and the assumed deep-seated origin of the CO_2-rich phase, the high-density carbonic inclusions strongly suggest a *post-entrapment re-equilibration of pre-existing inclusions towards higher densities.*

Such re-equilibration could result from (A) near-*isobaric* cooling, when isochores of increasing density are intersected at decreasing temperatures (e.g. down to 550-500°C) and from (B) Caledonian *overthrusting,* when high-density isochores are reached in the early stages of overthrusting at relatively high pressures and low temperatures.

A number of petrological arguments point to a near-isobaric cooling in the early post-metamorphic history of the Rogaland complex:

1. Pyroxene subsolidus relations indicate that at temperatures of 800-600 °C the pressure was in the order of 5 kbars, while the P_{H_2O} was relatively low (Rietmeijer, 1979).
2. Rims of garnet that are locally found around amphibole, pyroxene, and olivine indicate that at temperatures between about 900 and 700°C the pressure must have remained approximately constant.
3. During formation of secondary amphibole, temperatures were relatively low (about 600°C) while pressures were still about 5 kbars (Dekker, 1978).

This near-isobaric cooling probably reflects the return to P-T conditions appropriate to a shield area (low geothermal gradients) after the intruding lopolith had caused a major disturbance by imposing high geothermal gradients. In general, the retrograde P-T loop of the Rogaland area is curved concave towards the temperature axis. This situation is fundamentally different from many other metamorphic terranes such as the Coast Mountains in British Columbia (Hollister *et al.*, 1979), the Massif Central area (Albarède, 1976; Bilal & Touret, 1976), and the Haas Schists in New Zealand (Norris & Henley, 1976).

Because there is not necessarily a communication with external fluids, an important consequence of this type of re-equilibration is the possible preservation of the original compostion. Subsequent events, however, such as a decrease in ambient pressure, could induce selective decrepitation of the inclusions, depending on their size and position in the host. Eventually, a wide range in compositions and densities could result.

The possible effect of isobaric cooling on the volumetry of the inclusions is outlined fig. 74 (high-temperature part of the "lithostatic loop"). The density maximum of the lithostatic loop is based on the highest density (about 1.07 g/cc) found for isolated inclusions with well-developed negative crystal shapes, occurring in mature configurations (cf. Section II.4.6).

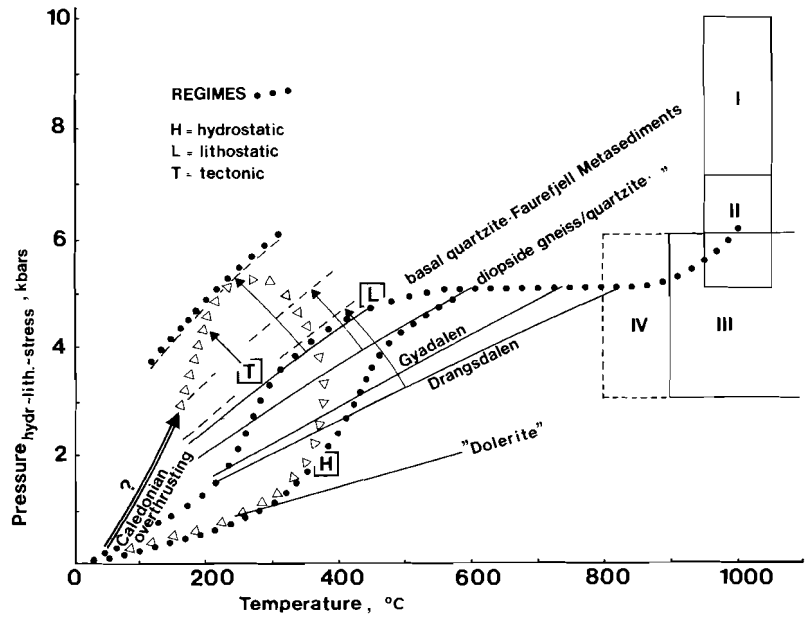

FIG. 74 Tentative P-T trajectory of the Rogaland high-grade metamorphic-igneous complex at post-paroxysmal conditions. Solid lines are isochores corresponding to frequency maxima in the T_h-histograms of monophase carbonic inclusions. Broken lines are isochores corresponding to the highest local CO_2-equivalent density. The possible P-T effect of Caledonian overthrusting is indicated by triangles. Roman figures refer to P-T estimates of high-grade events. I= Botnavatn Igneous Complex; II= Quartz Monzonitic Phase ,Bj.-Sk. Lopolith (Rietmeijer, 1979). III= Hermans *et al.*(1976). IV= Maijer *et al.*(1980).

A large-scale Caledonian overthusting would impose an additional P-T loop. The effect of such a loop on the properties of the inclusions is difficult to predict but it could produce high-density re-equilibrations during the early stages of overthrusting. The outline of the Caledonian loop (depicted in fig. 74) is in part determined by the 1.23 g/cc isochore for pure CO_2 and the maximum temperature of 300-350°C in the main part of the Rogaland area during retromorphism.

It is, however, considered unlikely that the Caledonian overthrusting has brought about a general re-equilibration of the inclusions. For instance, it is not known if the overthrusting has been operative in all parts of Rogaland where high-density inclusions are found. Furthermore, this, it remains difficult to explain the occurrence of low-density inclusions in quartz close to a dolerite dike (Precambrian age) if this Caledonian phase were generally active.

The details of the re-equilibration process are not completely understood. For instance, it is not known to what extent tectonic stress is active in this respect. The presence of high-density fluid inclusions (both carbonic and aqueous) in strongly deformed rocks (cf. figs 45 and 59-2), the existence of flattened, high-density N_2-rich inclusions (figs 50 and 57) and the stress-induced(?) migration of inclusions (figs 44-46) all suggest that an externally applied stress influences the inclusions and may "trigger" the re-equilibration towards a higher density. At least some kind of "overpressure" must be responsible for the extremely high densities, found in a number of carbonic and N_2-rich inclusions. Otherwise, the isobaric cooling would have continued down to about 250°C, which is difficult to reconcile with the fact that the extremely high densities are not a general feature of all carbonic and N_2-rich inclusions.

The isochores of the aqueous inclusions (fig. 67) indicate that these inclusions cannot have been generated at temperatures > 600°C if an isobaric cooling path is assumed. This is, of course, not unexpected because the P_{H_2O} is known to be low at temperatures down to 800-600°C (Rietmeijer, 1979) while the formation of secondary amphiboles, indicating a local high P_{H_2O}, starts when the temperature has dropped to about 600°C. Furthermore, the position of the isochores is in agreement with independently determined

P-T estimates on retromorphic mineral assemblages.

Phase theoretical studies on retromorphic mineral assemblages in Faurefjell metasediments (Teske, 1977a) indicate a temperature of 450-550°C at P_{H_2O} = 2-3 kbars and $X_{CO_2}^{H_2O-CO_2}$=0.1. The uncertainty in the temperature, however, is high because the pertinent reaction curves (decarbonation) in a T-X_{CO_2} plane are not accurately known at low X_{CO_2} . A Faurefjell quartz body that (re)crystallized at retrograde greenschist-facies conditions exclusively contains primary aqueous inclusions with a CO_2-content lower than 1-2 mole % CO_2 (no CO_2-hydrate has been detected). This observation reduces Teske's estimates of the temperature to maximum values.

Pressure-temperature estimates, based on experimental data, derived from low-grade metamorphic assemblages comprising pumpellyite, prehnite, and stilpnomelane indicate 300-350°C at a P_{H_2O} of about 2 kbars (Spits, 1979).

At first view the hypothesis of re-equilibration down to relatively low temperatures and pressures seems incompatible with the isochores of the aqueous inclusions and - even more pronounced - with the isochores for monophase carbonic inclusions in rocks close to a dolerite dike. Such differences, however, could be explained by assuming that in the low-temperature field (temperatures below 500-550°C) various pressure regimes have been operative:

a *lithostatic* regime, governed by the pressure that is exerted by a column of the overlying rock mass.

a *hydrostatic* regime, in principal governed by the H_2O-pressure ($P_{H_2O} < P_{lith.}$) which may be active only temporarily.

a *tectonic* regime, originating from anisotropic stresses, which create a locally and temporarily active overpressure (cf. Caron, 1977). This "tectonic overpressure" could amount up to 4 kbars (Rutland, 1965).

A number of thermo-optical phenomena are possibly related to interaction of these regimes. For example, cluster-like arrangements of carbonic, mixed H_2O-CO_2 inclusions could result from (partial) decrepitation of pre-existing dense inclusions (reflecting a lithostatic-tectonic regime) at low ambient pressures, in the sense of Kreulen (1977), Crawford *et al.*, 1979b, Hollister *et al.*, 1979, and Norris & Henley (1976). Subsequent interaction with internally or externally supplied aqueous fluid (hydrostatic regime) thus may give rise to unmixed H_2O-CO_2 and perhaps also H_2O-N_2 fluids.

A similar process may have been operative in those trails where monophase carbonic, mixed H_2O-CO_2, two- or multiphase aqueous inclusions (± salt), and carbonate flakes all occur in the same array. These observations suggest that secondary carbonate (a common alteration product in Rogaland rocks) may be produced by interacting CO_2-rich fluid(s) and Ca-rich aqueous solutions (possibly originating from decomposition of mafic and plagioclase-rich rocks).

A widely distributed hydrostatic regime may be developed as the result of large-scale extension fractures set up during uplift, at temperatures < 500°C. Most, if not all of the ENE-WSW running valleys in the Rogaland/Vest-Agder region probably represent the morphological expression of major feeder channels for hydrothermal fluids, which have produced retromorphism. A hydrostatic-like regime, with relatively low pressures, must have been active in rocks close to dolerite dikes intruded in this fracture system. This may be inferred from the relatively low densities of the monophase carbonic inclusions in these rocks.

It may be expected that, in general, inclusions in rocks that are exposed in the valleys have suffered more from the hydrostatic regime than inclusions in rocks far away. Such approach could perhaps in part explain the density differences between carbonic inclusions from Drangsdalen/Gyadalen and from Asheim. At a microscopic scale a similar observation on carbonic inclusions close to occurrences of aqueous inclusions shows that these are generally less dense than the carbonic inclusions in arrangements devoid of aqueous inclusion.

The late-stage history of the high-grade metamorphic-plutonic complex of Rogaland/Vest-Agder has probably been oversimplified thus far. Pertinent to that particular period is a contribution by Van den Haute (1977).

> Van den Haute (1977) reports fission track ages of apatite in the Rogaland intrusive masses. These ages range from 222 to 258 Ma (Zechstein) and are interpreted as the result of annealing in the 100°C temperature region. He argues that that, given the area was already peneplanized before Cambrian times, this temperature is an accompanying effect of a burial of the complex under a cover of (Cambro-Silurian) sediments. He does not rule out the possibility of the Caledonian orogeny as a cause for the supply of overlying rock. This implies that the fission track ages could be due to late-stage tempera-

ture effects of the Caledonian orogeny.

The occurrence of secondary minerals such as prehnite, pumpellyite, stilpnomelane and, in particular, green biotite has been ascribed to Caledonian metamorphism (Verschure *et al.*, 1980).

The high-temperature low-pressure part of the Caledonian loop (fig. 74) possibly produced secondary minerals such as prehnite, pumpellyite, stilpnomelane and, particularly, green biotite (cf. Verschure *et al.*, 1980). Its effect on the inclusions is difficult to evaluate because in principal it could produce decrepitation phenomena similar to those developed in a previous phase. Possibly, the preferential occurrence of "superheated" inclusions with satellite inclusions, observed in rocks from northern sampling sites reflects such a Caledonian "reheating".

II.7 CONCLUSIONS

1. In the high-grade metamorphic and related rocks from S.W. Norway, CO_2-rich (carbonic) and H_2O-rich (aqueous) fluid inclusions are the main types. Mixed H_2O-CO_2 inclusions are less abundant. All types are present in variable quantities and ratios at various scales (ranging from a single grain to an outcrop). At a regional scale, carbonic inclusions are perhaps more abundant in the granulite-facies rocks (W-part of Rogaland) than in the amphibolite-facies rocks in the east and north-east. In rocks close to a dolerite dike, large numbers of carbonic inclusions (low-density CO_2) have been found.

2. In Drangsdalen, the proportion of carbonic inclusions in enderbitic rocks is generally higher than in the charnockitic (or granitic) rocks. At the scale of a handspecimen, however, no distinct differences have been found in fluid inclusion properties between quartz-biotite-bearing zones (high P_{H_2O}?) and zones composed of anhydrous minerals only (low P_{H_2O}?).

3. In connection with Rb-Sr whole rock age determinations, it is suggested that those outcrops where aqueous inclusions are relatively abundant do not produce a reliable isochron. Outcrops where carbonic inclusions are the predominant type or CO_2-H_2O ratios are approximately constant, however, have produced well-defined isochrons.

4. Primary inclusions have only been recognized in quartz bodies of the Faurefjell metasediments. Carbonic and mixed H_2O-CO_2 inclusions (low degree of filling) in dispersed arrangements occur in folded quartz lenses within marble. Primary aqueous inclusions have been found in a large body of quartz, at least in part recrystallized at greenschist-facies conditions.

5. Aqueous inclusions typically occur in crystallographically non-rational, ill-defined trails, which may locally transect a grain boundary. Carbonic inclusions, probably predating the aqueous inclusions, are frequently encountered in subbasally oriented trails, confined to a single grain. It is still a matter of debate whether the subbasal trails are due to brittle or to ductile deformation. Mixed H_2O-CO_2 inclusions with variable phase ratios are not uncommon in cluster-like configurations or

trails that are otherwise composed of monophase carbonic inclusions

6. Transposition of fluid inclusion trails indicates that aqueous as well as carbonic inclusions are able to migrate, probably as the result of an externally anisotropic stress field.

7. Microthermometry of aqueous inclusions reveals a wide range in first and final melting temperatures of ice. Most first melting temperatures are well below the H_2O-NaCl-KCl eutectic, with a minimum of -80.2°C, indicating the presence of additional cations, probably Ca^{2+} and Mg^{2+}.
Final melting temperatures between 0° and -59°C indicate up to 30 eq.wt% $CaCl_2$.

8. N_2-rich fluid inclusions have been found in quartz-rich rocks that occur in the vicinity of or adjacent to mafic (preferably amphibole- or clinopyroxene-bearing) rocks; they have also been recognized in a number of pegmatites. The N_2-rich fluids have probably been trapped in an "early-secondary" stage, following the entrapment of carbonic inclusions but probably prior to to the introduction of aqueous fluids in a relatively late stage. Nitrogen could be a primary free (residual) phase in lower crust environments but an origin by decomposition of NH_4-bearing micas (prograde metamorphism) is also possible.

9. Microthermometry and gaschromatography indicate that N_2 is the main contaminant of the carbonic phase. Local exceptions occur in graphite-bearing rocks where relatively high amounts of CH_4 are found.

10. Homogenization temperatures of carbonic and N_2-rich inclusions (mainly liquid phase) display a wide range but most histograms that are based on a sufficiently large number of data show a distinct peak at relatively low temperatures. For carbonic inclusions a lowest homogenization temperature of -76.9°C and for N_2-rich inclusions a minimum of -180.5°C have been recorded. Low temperatures of homogenization have been found for carbonic inclusions in retromorphosed or deformed rocks.
The large range reflects compositional effects (in terms of CO_2-N_2) and true density variations. The CO_2-equivalent densities of the monophase carbonic inclusions range from about 0.70 to 1.23 g/cc (most common value about 0.95 g/cc). Densities of the N_2-rich inclusions range from 0.45 to 0.74 g/cc (commonly about 0.58 g/cc).
Compared with their equivalents in the median zone of a trail, more or

less isolated carbonic inclusions have somewhat higher densities.

11. In conjunction with petrologically determined P-T estimates, the fluid inclusion data suggest a post-entrapment re-equilibration of (pre-existing) inclusions towards higher densities. This re-equilibration is probably caused by isobaric cooling down to about 500^{o}. A Caledonian effect as the main cause for the high densities is considered unlikely. Tectonic activity probably aids in the re-equilibration.

12. The currently accepted assumption that *high-density* carbonic inclusions most closely approach a synmetamorphic granulite-facies fluid, is not valid in the Rogaland area.

13. The thermo-optical properties of aqueous and mixed H_2O-CO_2 inclusions with variable phase ratios point to conditions of entrapment at about $300^{o}C$ and pressures of 1-2 kbars. The H_2O-CO_2 inclusions possibly result from interaction of pre-existing CO_2 with a relatively late-stage aqueous phase, probably in the unmixing region in a salt-bearing H_2O-CO_2 system. This interaction may also have given rise to the formation of secondary carbonate.

14. In the low-temperature field, various pressure regimes may have been active. A lithostatic regime (governed by the load pressure) is regionally operative and is reflected in the densities of most carbonic and N - rich inclusions. A tectonic regime, resulting from anisotropic stresses and operative only at a limited scale for short periods of time, may give rise to "overpressures", exceeding the lithostatic pressure by several kbars (possibly up to 3.5 kb). This regime may re-equilibrate inclusions towards extremely high densities. A hydrostatic regime is in principal represented by the aqueous inclusions and by most mixed H_2O-CO_2 inclusions. This regime is characterized by a relatively low pressure. It may be set up during uplift of the rock complex. Perhaps the low-density carbonic inclusions that occur abundantly in rocks close to a dolerite dike also reflect a hydrostatic-like regime.

REFERENCES

ALBAREDE, F. (1976). Thermal models of post-tectonic decompression as exemplified by the Haut-Allier granulites (Massif Central, France) - Bull.Soc.géol.Fr. 18, 1023-1032.

AL-KHATIB, R. & TOURET, J. (1973). Fluides carboniques dans les roches du facies granulite du Sud de la Norvège. Utilisation semi-quantitative de la surplatine à écrasement - Bul.Soc.géol.Fr. 15, 321-325.

ANTUN, P. (1956). Géologie et pétrologie des dolérites de la région de Egersund - Ph.D. thesis, Université de Liège, 142 pp.

ARAI, Y., KAMINISHI, G.-I., & SAITO, S. (1971). The experimental determination of the P-V-T-X relations for the carbon dioxide- nitrogen and carbon dioxide- methane systems - J.Chem.Eng.Japan 4, 113-122.

AVE'LALLEMENT, H.G. & CARTER, N.L. (1971). Pressure dependence of quartz deformation lamellae orientation - Am.J.Sci. 270, 218-235

BARKER, C. & TORKELSON, B.E. (1975). Gas adsorption on crushed quartz and basalt - Geochim.Cosmochim.Acta 39, 212-218.

BENEDICT, M. (1937). Pressure, volume, temperature properties of nitrogen at high density. I. Results obtained with a weight piezometer - Am.Chem. Soc. 59, 2224-2233.

BERGLUND, L. & TOURET, J. (1976). Garnet-biotite gneiss in "Système du Graphite" (Madagascar): Petrology and fluid inclusions - Lithos 9, 139-148.

BILAL, A. (1976). Les inclusions fluides dans les enclaves des basaltes de Bournac - Massif Central Français. Implications sur les structures de la croûte continentale - "Thèse troisième cycle". Laboratoire de Géologie Structurale, Université de Nancy 1.

BILAL, A. & TOURET, J. (1976). Les inclusions fluides des enclaves catazonales de Bournac (Massif Central) - Bull.Soc.fr.Minér.Crist. 99, 134-139.

BRONS, J.-H. (1975). Berekende evenwichts-temperatuur en -druk relaties uit de geanalyseerde Fe-Mg verhouding in de drie fasen orthopyroxeen, granaat en cordieriet uit Rogaland, Z.W. Noorwegen - Internal report, Dept of Petrology, Rijksuniversiteit Utrecht, 53 pp.

BURNHAM, C.W., HOLLOWAY, J.R. & DAVIS, N.F. (1969). Thermodynamic properties of water to 1,000°C and 10,000 bars - Geol.Soc.Am. Spec.Paper 132, 96 pp.

CARSTENS, H. (1969). Arrays of dislocations associated with healed fractures in natural quartz - N.G.U. Nr. 258 (Årbok 1968), 368-369.

CHRISTIANSEN, L.J., FREDENSLUND, A. & GARDNER, N. (1974). Gas-liquid equilibria of the CO_2-CO_2 and CO_2-CH_4-CO systems - Advan. Cryog. Eng. 19 309-319.

CRAWFORD, M.L., FILER, J. & WOOD, C. (1979a). Saline fluid inclusions associated with retrograde metamorphism - Bull.Minéral. 102, 562-568.

CRAWFORD, M.L., KRAUS, D.W. & HOLLISTER, L.S. (1979b). Petrologic and fluid inclusion study of calc-silicate rocks, Prince Rupert, British Columbia - Am.J.Sci. 279, 1135-1159.

DAVIS, J.A., RODEWALD, N. & KURATA, F. (1962). Solid-liquid-vapor phase behavior of the methane-carbon dioxide system - A.I.Ch.E. Journal 8, 537-539.

DEKKER, A.G.C. (1978). Amphiboles and their host rocks in the high-grade metamorphic Precambrian of Rogaland, S.W. Norway - Geologica Ultraiectina 17, 277 pp.

DHAMELINCOURT, P., BENY, J.-M., DUBESSY, J. & POTY, B. (1979). Analyse d'inclusions fluides à la microsonde MOLE à effet Raman - Bull.Minéral. 102, 600-610.

DODDS, W.S., STUTZMAN, L.F. & SOLLAMI, B.J. (1956). Carbon dioxide solubility in water - Chem. and Eng.Data Series 1, 92-95.

DONNELLY, H.G. & KATZ, D.L. (1954). Phase equilibria in the carbon dioxide-methane system - Ind.Eng.Chem. 46, 511-517.

FISHER, J.R. (1976). The volumetric properties of H_2O- a graphical portrayal - J.Research U.S.Geol.Survey 4, 189-193.

FRANCK, E.U. & TODHEIDE, K. (1959). Thermische Eigenschaften überkritischen Mischungen von Kohlendioxyd und Wasser bis zu 750°C und 2000 Atm. - Z.f.Phys.Chem., N.F. 22, 232-245.

FRONDEL, C. (1962). Dana's system of Mineralogy, 7th ed. Volume III. Silica minerals - John Wiley & Sons Inc., New York, 334 pp.

GARY, M. McAFEE Jr., R. & WOLF, C.L. (eds. 1974). Glossary of geology - Am.Geol.Inst.Washington D.C., 805+(A)52 pp.

GREENWOOD, H.J. (1969). The compressibility of gaseous mixtures of carbon dioxide and water between 0 and 500 bars and 450° and 800° Centigrade - Am.J.Sci. 267-A, 191-208.

GRIGGS, D.T. (1967). Hydrolytic weakening of quartz and other silicates - Geophys.Jour. 14, 19-31.

GUILHAUMOU, N., DHAMELINCOURT, P., TOURAY, J.-C. & BARBILLAT, J. (1978). Analyse à la microsonde à effet Raman d'inclusions gazeuses du système N_2-CO_2 - C.r.Acad.Sci.D 287, 1317-1319.

HANEY, R.E.D. & BLISS, H. (1944). Compressibilities of nitrogen- carbon dioxide mixtures - Ind.Eng.Chem. 36, 985-989.

HARTMAN, P. (1979). Zum Verständnis des Mineralwachstums - Fortschr. Miner. 57, 127-171.

HEIER, K.S. (1956). The geology of the Ørsdalen district, Rogaland, S.W. Norway - Norsk geol.Tidsskr. 50, 45-88.

HERMANS, G.A.E.M., HAKSTEGE, A.L., JANSEN, J.B.H. & POORTER, R.P.E. (1976). Sapphirine occurrence near Vikesa in Rogaland, Southwestern Norway - Norsk Geol.Tidsskr. 56, 397-412.

HERMANS, G.A.E.M., TOBI, A.C., POORTER, R.P.E. & MAIJER, C. (1975). The high-grade metamorphic precambrian of the Sirdal-Ørsdal area, Rogaland/ Vest-Agder, Southwest Norway - Norges Geol.Unders. 318, 51-74.

HIRSCHFELDER, J.O., CURTISS, C.F., & BIRD, R.B. (1964). Molecular theory of gases and liquids - J. Wiley & Sons, Inc. New York, 1219 pp.

HOBBS, B.E., MEANS, W.D. & WILLIAMS, P.F. (1976). An outline of structural

geology - John Wiley & Sons,Inc. New York, London, Sydney, Toronto, 571 pp.

HOBBS, P.V. (1974). Ice physics - Clarendon Press, Oxford, 837 pp.

HOEFS, J. & TOURET, J. (1975). Fluid inclusions and carbon isotope study from Bamble granulites (South Norway) - Contrib.Mineral.Petrol. 52, 165-174.

HOLLISTER, L.S. & BURRUSS, R.C. (1976). Phase equilibria in fluid inclusions from the Khtada Lake metamorphic complex - Geochim.Cosmochim.Acta 40, 163-175.

HOLLISTER, L.S., BURRUSS, R.C., HENRY, D.L. & HENDEL, E.-M. (1979). Physical conditions during uplift of metamorphic terranes as recorded by fluid inclusions - Bull.Minéral. 102, 555-561.

HOLLOWAY, J.R. (1977). Fugacity and activity of molecular species in supercritical fluids - *In:* D.G. Fraser (ed.) Thermodynamics in Geology, 161-181.

JUZA, J., KMONICEK, V., & SIFNER, O. (1965). Measurements of the specific volume of carbon dioxide in the range of 700 to 4000 b and 50 to 475°C - Physica 31, 1735-1744.

ITIHARA, Y. & HONMA, H. (1979). Ammonium in biotite from metamorphic and granitic rocks of Japan - Geochim.Cosmochim.Acta 43, 503-509.

JACQUES DE DIXMUDE, S. (1978). Géothermométrie comparée de roches du facies granulite du Rogaland (Norvège méridionale) - Bull.Minéral. 101, 57-65.

KARS, H., SAUTER, P.,VELLINGA, M. & WEGELIN, A. (1977). Explanatory notes on the Geological Map of a part of the Øvre Sirdal Sheet, 1:50,000 (NGO 1312-1) - Internal report, Dept of Petrology, Rijksuniversiteit Utrecht.

KENNEDY, G.C. & HOLSER, W.T. (1966). Pressure-volume-temperature and phase relations of water and carbon dioxide - *In:* S.P. Clark (ed.) Handbook of physical constants. Geol.Soc.Am.Mem.97, 371-383.

KERRICH, R. (1976). Some effects of tectonic recrystallization on fluid inclusions in vein quarts - Contib.Mineral.Petrol. 59, 195-202.

KHITAROV, N.I. & MALININ, C.D. (1956). Experimental characteristics of a part of the system H_2O-CO_2 - Geochemistry (1956), 246-256.

KLATT, E. (1979). Die Flüssigkeitseinschlüsse in den Granuliten Nordlapplands und ihren Rahmengesteinen (Abstr.) - Fortschr.Mineral. 57, 62-63.

KONNERUP-MADSEN, J. (1977). Composition and microthermometry of fluid inclusions in the Kleivan granite, South Norway - Am.J.Sci.277, 673-696.

KONNERUP-MADSEN, J. (1979). Fluid inclusions in quartz from deep-seated granitic intrusions, South Norway - Lithos 12, 13-23.

KREULEN, R. (1977). CO_2-rich fluids during regional metamorphism on Naxos, a study on fluid inclusions and stable isotopes - Ph.D. thesis, Rijksuniversiteit Utrecht, 85 pp.

KREULEN, R. (1980). CO_2-rich fluids during regional metamorphism on Naxos (Greece); carbon isotopes and fluid inclusions - Am.J.Sci. in press.

LAEMMLEIN, G. (1929). Sekundäre Flüssigkeitseinschlüsse in Mineralien - Z.Krist. 71, 237-256.

LANDOLT-BORNSTEIN (eds, 1960). Zahlenwerte und Funktionen. II Band: Eigenschaften der Materie in ihren Aggregatzuständen. 2. Teil: Gleichgewichte ausser Schmelzgleichgewichten, 431-433.

LEMMLEIN, G. (1929). cf. Laemmlein, G. (1929).

LEMMLEIN, G.G. (1956). Formation of fluid inclusions in minerals and their use in geological thermometry - Geochemistry 1956, 630-642.

LEMMLEYN, G.G. and KLIYA, M.O. (1960). Distinctive features of the healing of a crack in a crystal under conditions of declining temperature - Int.Geol.Rev. 2, 125-128.

LEROY, J. (1979). Contribution à l'étallonage de la pression interne des inclusions lors de leur décrépitation - Bull.Minéral. 102, 584-593.

LOKERMAN, A.A. (1962). The possibility of study of the interrelation of dikes and mineralization from inclusions in minerals - L'vov Geol. Obshch.Mineralog. Sbornik, 16, 312-317 (in Russian).

MAIJER, C., JANSEN, J.B.H., HEBEDA, E.H., VERSCHURE, R.H. & ANDRIESSEN, P.A.M. (1980). Osumilite, a 970 Ma old high-temperature index mineral of the granulite facies metamorphism in Rogaland, S.W. Norway - in prep.

MAIJER, C., JANSEN, J.B.H., WEVERS, J. & POORTER, R.P.E. (1977). Osumilite, a mineral new to Norway - Norsk Geol.Tidsskr. 57, 187-188.

MALBRUNOT, P. & VODAR, B. (1973). Experimental pVT data and thermodynamic properties of nitrogen up to 1000°C and 5000 bar - Physica 66, 351-363.

MALININ, S.D. (1974). Thermodynamics of the H_2O-CO_2 system - Geochem.Int. 11, 1060-1085.

MARSHALL, D.R., SAITO, S. & KOBAYASHI, R. (1964). Hydrates at high pressures: Part I. Methane-water, argon-water, and nitrogen-water systems - A.I.Ch.E.Journal 10, 202-205.

MEHNERT, K.R. (1968). Migmatites - and the origin of granitic rocks - Elsevier Publishing Company, Amsterdam, 393 pp.

MORROY, H. (1974). Verslag van een geologisch-petrologisch veldwerk in het gebied tussen Oltedalsvatnet en Byrkjelandsvatnet, Gjesdal kommune, Rogaland, SW Noorwegen - Internal report, Dept of Petrology, Rijksuniversiteit Utrecht, 22 pp.

MULLIS, J. (1976). Das Wachstumsmilieu der Quarzkristalle im Val d'Illiez (Wallis, Schweiz) - Schweiz.mineral.petr.Mitt. 56, 219-268.

MULLIS, J. (1979). The system methane-water as a geologic thermometer and barometer from the external parts of the Central Alps - Bull.Minéral. 102, 526-536.

MULLIS, J., POTY, B. & LEROY, J. (1973). Nouvelles observations sur les inclusions fluides à méthane des quartz du Val d'Illiez, Valais (Suisse) - C.r.Acad.Sci.Paris D 277, 813-816.

MURCK, B.W., BURRUSS, R.C. & HOLLISTER, L.S. (1978). Phase equilibria in fluid inclusions in ultramafic xenoliths - Am.Mineral. 63, 40-46.

NORRIS, R.J. & HENLEY, R.W. (1976). Dewatering of a metamorphic pile - Geology 4, 333-336.

PARKINSON, W.J. & DE NEVERS, N. (1969). Partial molal volume of carbon dioxide water solutions - Ind.Eng.Chem.Fund. 8, 709-713.

PASTEELS, P. DEMAIFFE, D. & MICHOT, J. (1979). U-Pb and Rb-Sr geochronology of the eastern part of the south Rogaland igneous complex, southern Norway - Lithos 12, 199-208.

PATERSON, M.S. (1978). Experimental rock deformation - the brittle field - Springer Verlag, Berlin, Heidelberg, New York, 254 pp.

PERCHUK, L.L. (1976). Gas-mineral equilibria and a possible geochemical model of the earth's interior - Phys.Earth Planet.Inter. 13, 232-239.

PESUIT, D.R. (1978). Binary interaction constants for mixtures with a wide range in component properties - Ind.Eng.Chem.Fund. 17, 235-242.

POORTER, R.P.E. (1972). Palaeomagnetism of the Rogaland Precambrian (Southwestern Norway) - Phys.Earth Plan.Inter. 5, 167-176.

POTTER II, R.W. (1977). Pressure corrections for fluid inclusions homogenization temperatures based on the volumetric properties of the system NaCl-H_2O - Jour.Res.U.S.Geol.Survey 5, 603-607.

POTY, B., LEROY, J. & JACHIMOWICZ, L. (1976). Un nouveau appareil pour le mesure des températures sous le microscope: l'installation de microthermométrie Chaixmeca - Bull.Soc.fr.Minér.Crist. 99, 182-186.

RIETMEIJER, F.J.M. (1979). Pyroxenes from iron-rich igneous rocks in Rogaland, S.W. Norway - Geologica Ultraiectina 21, 341 pp.

ROBERTSON, S.L. & BABB Jr., S.E. (1969). Isotherms of nitrogen to 400°C and 10000 bar - J.Chem.Phys. 50, 4560-4564.

ROEDDER, E. (1965). Liquid CO_2 inclusions in olivine-bearing nodules and phenocrysts from basalts - Am.Mineral. 50, 1746-1782.

ROEDDER, E. (1967a). Metastable superheated ice in liquid-water inclusions under high negative pressure - Science 155, 1413-1417.

ROEDDER, E. (1967b). Fluid inclusions as samples of ore fluids - *In:* H.L. Barnes (ed.). Hydrothermal ore formation, 515-574. Holt, Rinehart, & Winston, New York.

ROEDDER, E. (1971). Metastability in fluid inclusions - Soc.Mining Geol. Japan, spec. issue 3, 327-334.

ROEDDER, E. (1972). Composition of fluid inclusions - *In:* M. Fleischer (techn.ed.) Data of geochemistry, 6th ed. Chap. JJ, U.S.Geol.Survey Prof.Paper 440-JJ.

ROEDDER, E. (1977). Fluid inclusion evidence on the genesis of ores in sedimentary and volcanic rocks - *In:* K.H. Wolff (ed.) Handbook of stratabound and stratiform ore deposits, 2, 67-110.

ROEDDER, E. & SKINNER, B.J. (1968). Experimental evidence that fluid inclusions do not leak - Ec.Geol. 63, 715-730.

RUTLAND, R.W.R. (1965). Tectonic overpressures - *In:* W.S. Pitcher & G.W. Flinn (eds.) Controls of metamorphism, 119-139.

RYZHENKO, B.N. & MALININ, S.D. (1971). The fugacity rule for the systems

CO_2-H_2O, CO_2-CH_4, CO_2-N_2 and CO_2-H_2 - Geochem. Int. 1971, 562-574 (transl. from Geokhimiya No. 8, 899-913 (1971).

SANTIS, R. DE, BREEDVELD, G.J.F. & PRAUSNITZ, J.M. (1974). Thermodynamic properties of aqueous gas mixtures at advanced pressures - Ind.Eng.Chem. Process Des.Dev. 13, 374-377.

SAUTER, P.C.C. (1980). Mineral relations in siliceous dolomites from the high-grade metamorphic Precambrian of Rogaland, S.W. Norway - In prep.

SCHRIJVER, K. (1973). Bimetasomatic plagioclase-pyroxene reaction zones in granulite facies - N.Jb.Miner.Abh. 119, 1-19.

SCHUILING, R.D. & KREULEN, R. (1979). Are thermal domes heated by CO_2-rich fluids from the mantle? - Earth.Planet.Sci.Letters 43, 298-302.

SHETTEL, D.L.,Jr. (1973). Solubility of quartz in H_2O-CO_2 fluids at 5 kb and 500-900° C (abstr.) - Trans.Am.Geophys.Union 54, 480 pp.

SHMONOV, V.M. & SHMULOVICH, K.I. (1974). Molal volumes and equation of state of CO_2 at temperatures from 100 to 1000°C and pressures from 2000 to 10,000 bars - Dokl.Akad.Nauk SSR 217, 935-938.

SIMMONS, G. & RICHTER, D. (1976). Microcracks in rocks - *In*: R.G.J. Strens (ed.) The physics and chemistry of minerals and rocks, 105-137.

SPITS, P. (1979). Het voorkomen van de mineralen pumpellyiet, prehniet en stilpnomelaan in Rogaland - Internal report, Dept of Petrology, Rijksuniversiteit Utrecht, 53 pp.

STALDER, H.A. & TOURAY, J.C. (1970). Fensterquarze mit Methan-Einschlüssen aus dem westlichen Teil der schweizerischen Kalkalpen - Schweiz. mineral.petr.Mitt. 50, 109-130.

STECHER, O. (1977). Phasediagrams of geological fluids - "Thèse troisième cycle", Dépt. Sciences de la Terre, Université de Paris VII.

STRECKEISEN, A. (1976). To each plutonic rock its proper name - Earth-Science Reviews 12, 1-33

SWANENBERG, H.E.C. (1979). Phase equilibria in carbonic systems, and their application to freezing studies of fluid inclusions - Contrib. Mineral.Petrol. 68, 303-306.

TAKENOUCHI, S. & KENNEDY, G. (1964). The binary system H_2O-CO_2 at high temperatures and pressures - Am.J.Sci. 262, 1055-1074.

TAKENOUCHI, S. & KENNEDY, G. (1965). Dissociation pressures of the phase $CO_2.5\frac{3}{4}H_2O$ - J.Geol. 73, 383-390.

TESKE, J. (1977a). Geochemisch en petrologisch onderzoek aan de Marmers in Rogaland - Internal report, Dept of Petrology, Rijksuniversiteit Utrecht, 42 pp.

TESKE, J. (1977b). Petrografisch veldwerk-verslag in het gebied Ålgård-Oltedal Rogaland, S.W. Noorwegen - Internal report, Dept of Petrology, Rijksuniversiteit Utrecht, 73 pp.

TODHEIDE, K. (1963). Das Zweiphasengebiet und die kritische Kurve im System Kohlendioxyd-Wasser bis zu Drucken von 3500 bar - Ph.D. thesis, Georg-August Universität Göttingen, 54 pp.

TOURAY, J.C. (1969). Hydrocarbures liquides et gazeux en inclusions dans

les minéraux - Bull.Centre Rech.Pau, SNPA, 3, 429-441.

TOURAY, J.-C. & JAUZEIN, A. (1967). Inclusions à méthane dans les quartz des "terres noires" de la Drôme - C.r.Acad.Sci.Paris D 264, 1957-1960.

TOURAY, J.-C. & SAGON, J.-P. (1967). Inclusions à méthane dans les quartz des marnes de la région de Mauléon (Basses-Pyrénées) - C.r.Acad.Sci. Paris D 265, 1269-1272.

TOURET, J. (1970). Le facies granulite, métamorphisme en milieu carbonique - C.r.Acad.Sci. Paris D 271, 2228-2231.

TOURET, J. (1971). Le facies granulite en Norvège méridionale. II. Les inclusions fluides - Lithos 4, 423-436.

TOURET, J. (1972). Le facies granulite en Norvège méridionale et les inclusions fluides: paragneiss et quartzites - Scis. de la Terre, XVI, 179-193.

TOURET, J. (1974a). Facies granulite et fluides carboniques - Cent.Soc. Géol.Belg./Géologie des domaines cristallins, Liège 1974, 267-287.

TOURET, J. (1974b). Fluid inclusions in high grade metamorphic rocks - NATO Advanced Study Institute: "Volatiles in metamorphism" Nancy,1974.

TOURET, J. & BOTTINGA, Y. (1979). Equation d'état pour le CO_2; application aux inclusions carboniques - Bull.Minéral. 102, 577-583.

TSIKLIS, D.S. & POLYAKOV, E.V. (1968). Measuring the compressibility of gases by the displacement method. Nitrogen compressibility at pressures up to 10,000 atm and temperatures to 400° - Dokl.Akad.Nauk, Soviet Physics 12, 901-904.

TUTTLE, O.F. (1949). Structural petrology of planes of liquid inclusions - J.Geol. 57, 331-356.

VAGARFTIK, N.B. (1972). Tables of thermophysical properties of gases and liquids - Izd.Nauka, Moscow, 720 pp (in Russian).

VAN DEN HAUTE, P. (1977). Apatite fission track dating of Precambrian intrusive rocks from the southern Rogaland (South-western Norway) - Bull.Soc.belge Géol. 86, 97-110.

VEDDER, W. (1965). Ammonium in muscovite - Geochim.Cosmochim.Acta 29, 221-228.

VERHOOGEN, J., TURNER, F.J., WEISS, L.E., WAHRHAFTIG, C. & FYFE, W.S. (1970). The earth - an introduction to physical geology - Holt, Rinehart & Winston, Inc. New York, 748 pp.

VERSCHURE, R.H., ANDRIESSEN, P.A.M., BOELRIJK, N.A.I.M., HEBEDA, E.H., PRIEM, H.N.A. & VERDURMEN, E.A.Th. (1979). Coexisting primary biotite of sveconorwegian age and secondary biotite of caledonian age in sveconorwegian basement rocks close to the caledonian front in S.W. Norway - Abstr. of papers ECOG VI, Lillehammer.

VERSTEEVE, A.J. (1975). Isotope geochronology in the high-grade metamorphic Precambrian of Southwestern Norway - Norges Geol.Unders. 318, 1-50.

WEAST, R.D. ed. (1975). Handbook of chemistry and physics - 56th ed. CRC Press Inc.

WEGELIN, A. (1979). Veldwerk in het gebied Ålgård-Gjesdal-Nedrabø - Internal report, Dept of Petrology, Rijksuniversiteit Utrecht, 98 pp.

WIEBE, R.A. (1979). Anorthosite dikes, southern Nain Complex, Labrador - Am.J.Sci. 279, 394-410.

WIEBE, R. & GADDY, V.L. (1941). Vapor phase composition of carbon dioxide-water mixtures at various temperatures and at pressures up to 700 atmospheres - J.Am.Chem.Soc. 63, pp. 475-477.

WIELENS, J.B.W. (1979). Morphology and U-Pb ages of zircons from the high-grade metamorphic Precambrian in the Sirdal-Ørsdal area, S.W. Norway - Verhand. nr. 4, ZWO Laboratorium voor isotopengeologie, Amsterdam, 94 pp.

WILKINS, R.W.T. & BARKAS, J.P. (1978). Fluid inclusions, deformation and recrystallization in granite tectonites - Contrib.Mineral.Petrol. 65, 293-299.

WISE, D.U. (1964). Microjointing in basement, Middle Rocky Mountains of Montana and Wyoming - Geol.Soc.Am.Bull.75, 287-306.

WLOTZKA, F. (1961). Untersuchungen zur Geochemie des Stickstoffs - Geochim.Cosmochim.Acta 24, 106-154.

YPMA, P.J.M. (1963). Rejuvenation of ore deposits, as exemplified by the Belledonne metalliferous province - Ph.D. thesis Leiden, 212 pp.

ZAGORUCHENKO, V.A. & ZHURAVLEV, A.M. (1969). Thermophysical properties of gaseous and liquid methane - Izd.Stadartov, Moscow, 243 pp.

APPENDIX

This appendix is essentially an annotated list of sample localities and -descriptions. The descriptions comprise sample code, locality, NGO map sheet 1:50.000 + coordinates (between parentheses), outcrop no. (for Drangsdalen rocks only), formation or field occurrence, rock name (Streckeisen, 1967) and some significant petrologic details. The fluid inclusion ratio, unless stated otherwise, refers to the volumetric proportion of monophase inclusions (carbonic or N_2-rich), biphase inclusions (composed of H_2O and a carbonic or N_2-rich phase), and aqueous inclusions (monophase and biphase). An asterisk (*) denotes that at least part of the inclusions is of the N_2-rich type. These optical estimates are based an the mean value of N determinations in the field of view of a 25x objective.

SAMPLING SITES, AS MENTIONED IN FIG. 28:

1. ASHEIM (Faurefjell metasediments, basal quartzite): 76HS250, 251, (275), 276; (quartz pods/diopside rock): 76HS273*, 274*.
2. AUSTRUMDALSVATNET (Garnetiferous migmatites): 76HS306, 307, 311, 312.
3. DRANGSDALEN (Charnockitic migmatites): See Table 8.
4. GYADALEN (Garnetiferous migmatites): 76HS264, 265, 266.
   ("East": Charnockitic migmatites): 75HS088*, 095, 096, 097, 102*, 104, 106, 107 (samples 102*104-106 related to dolerite dike)
   ("West": Charnockitic migmatites): 75HS109, 110, 111.
5. IVESDAL (Garnetiferous migmatites): 76HS255.
6. LOPOLITH OF BJERKREIM-SOKNDAL (+ immediate surroundings): 75HS232, 244*, 76HS256, 258, 272, 278, 279, 280, 281, 282, 283*.
7. NEDRABØ (Faurefjell metasediments, quartz-diopside gneisses): 75HS196, 197, 198, 199, 200, 201, 202, 203.
8. RUSDALSVATNET (rocks in the vicinity of a dolerite dike): 75HS233, 243.
9. SELDAL (Faurefjell metasediments): 75HS204, 205, 206, 207, 208.
10. STØLSFJELLET (Faurefjell metasediments): 76HS296, 297, 298, 299, 300, 301.
11. STORE MYRVATNET (Granitic migmatites): 76HS302, 304, 305.
12. TJØRHOM (Granitic migmatites): 76HS286, 287*, 288*, 290, 291, 295.
13. VIKESDAL (Garnetiferous migmatites): 76HS253.
14. ØRSDALEN (Charnockitic migmatites): 76HS308*, 309, 310.
15. ÅRDALEN (Charnockitic migmatites): 76HS267, 268, 271*.

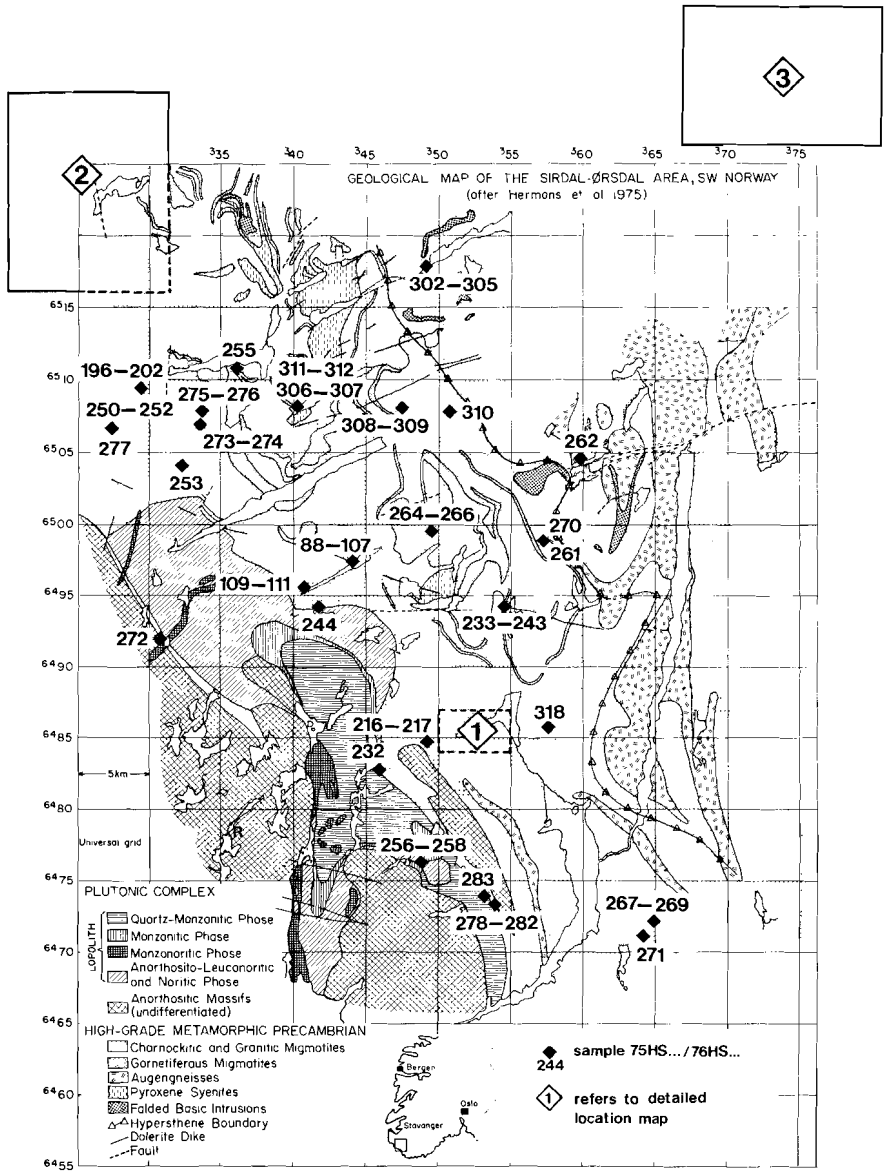

FIG. 75 Index map showing sample locations in the Rogaland/Vest-Agder region. Insets 1, 2, and 3 are enlarged in figs 76, 30, and 31 respectively. Geology simplified after Hermans *et al.* (1975).

Outcrop	Sample
1	75HS115
	75HS118
	75HS121
	75HS123
	75HS129
	75HS133
2	75HS136
	75HS046
	75HS141
	75HS137
	75HS049
	76HS324
	75HS052
	75HS139
3	75HS142
4	75HS144
5	75HS145*
	76HS325
	75HS147
6	75HS149
	75HS055*
	75HS150
	75HS056
	75HS057
7	75HS058
	75HS006
	75HS114
	75HS003
	75HS113
	75HS001
	75HS154
8	75HS059
	75HS014
	75HS015
	75HS155
9	75HS016
	75HS061
	75HS062
	75HS162
	75HS160
	75HS164
	75HS163
	75HS064
	75HS065
	75HS165
10	75HS166
	75HS170
	75HS167
	75HS067
11	75HS174
	75HS175
	75HS176
	75HS177
	75HS077
	75HS179
	75HS180
	75HS181
12	75HS183
	75HS184*
	75HS185
	76HS313
	75HS186
	75HS187
	75HS188
	75HS189
	75HS075
	75HS190
	75HS191*
	75HS248*
	75HS073
13	75HS193
	76HS331
	75HS195
14	75HS216
	75HS217

TABLE 8 Rock samples collected in Drangsdalen. Sequence from S to N or from E to W. Location of outcrops is indicated in fig. 75.

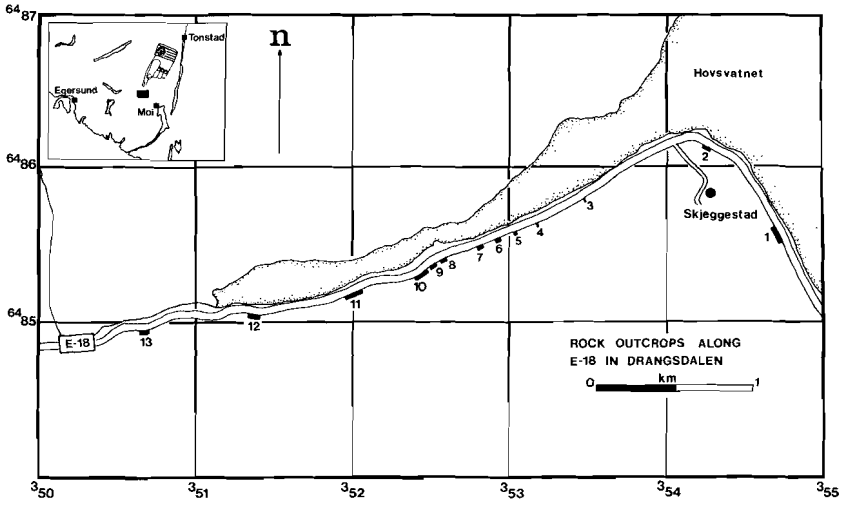

FIG. 76 Index map (inset 1 in figs 28 and 75) showing the location of principal outcrops along E-18 in Drangsdalen. Outcrop no. 14 (coordinates 3490-64845) has not been indicated. A list of samples is presented in Table 8.

LIST OF SAMPLES

75HS001 - Drangsdalen (Sokndal 3528-64855). Outcrop 7. Banded and folded "Early Migmatite" composed of coarse-grained alkalifeldspar syenite, fine-grained biotite norite and leucoenderbite (the latter possibly granulated). No biotite-quartz contact. Fluid inclusions: 84/09/07 (N=10).

75HS003 - Drangsdalen (Sokndal 3528-64855). Outcrop 7. Banded and folded "Early Migmatite". Fine-grained biotite leuconorite in contact with coarse-grained leucoenderbite. Plagioclase= 46An. No biotite-quartz contact. Fluid inclusions: 45/27/28 (N=50).

75HS006 - Drangsdalen (Sokndal 3528-64855). Outcrop 7. A 25 cm wide band in a sequence discordant to the general structural direction of the "Early Migmatite" (probably "Late Migmatite"). Enderbite and leucotonalite. Plagioclase= 45An. No biotite-quartz contact. Fluid inclusions: 65/16/19 (N=50).

75HS014 - Drangsdalen (Sokndal 3525-64855). Outcrop 9. Sequence of leucocratic rocks with varying grain sizes. Biotite leucocharnockite. Plagioclase: 33An. Biotite-quartz contact. Fluid inclusions: 28/20/52 (N=20).

75HS015 - Drangsdalen (Sokndal 3525-64854). Outcrop 9. Sequence of leucocratic rocks with varying grain sizes. Leucotonalite and biotite leuco-charnoenderbite. Plagioclase= 35An. Biotite-quartz contact in leuco-charnoenderbite. Relatively high degree of alteration in the coarse-grained part. Fluid inclusions in biotite-bearing part: 03/12/85 (N=25). Fluid inclusions in orthopyroxene-bearing part: 03/01/96 (N=25).

75HS016 - Drangsdalen (Sokndal 3525-64854). Outcrop 10. Somewhat discordant, coarse-grained band (garnet-bearing leucoenderbite) in relatively fine-grained charnockite. No biotite-quartz contact. Fluid inclusions: 48/19/33 (N=50).

75HS046 - Drangsdalen (Sokndal 3542-64861). Outcrop 2. Banded charnockitic migmatite (Late Migmatite?) composed of slightly foliated coarse-grained leucocharnoenderbite and fine-grained monzonite. Plagioclase: 46-42An. Fluid inclusions: 09/21/70 (N=50).

75HS049 - Skjeggestad (Sokndal 3542-64861). Outcrop 2. A 50-75 cm wide, folded, ilmenite-magnetite leucoenderbite, discordant in a noritic body. Plagioclase= 38An. Secondary biotite overgrowth on opaques. Fluid inclusions: 09/21/70 (N=50)

75HS052 - Skjeggestad (Sokndal 3542-64861). Outcrop 2. A small zone (about 1 cm) within a noritic body characterized by relatively coarse grained plagioclase and pyroxene. The parent rock is a biotite-amphibole leuconorite (plag= 73An) whereas the coarse-grained band , devoid of hydrous minerals, is composed of plagioclase (52An), orthopyroxene, and clinopyroxene.

75HS055*- Drangsdalen (Sokndal 3529-64856). Outcrop 6. Sequence of poorly foliated mesocratic rocks with concordantly intercalated quartz-rich bands. Quartz-leuconorite and quartz enderbite. Plagioclase= 46An. Secondary biotite overgrowths on opaques. Fluid inclusions: 51*/05*/44 (N=50)

75HS056 - Drangsdalen (Sokndal 3529-64856). Outcrop 6. Coarse-grained leucocratic component of "Early Migmatite". Biotite-alkalifeldspar charnockite (plagioclase=39An). Biotite-quartz contact. Fluid inclusions: 38/19/43 (N= 50).

75HS057 - Drangsdalen (Sokndal 3529-64856). Outcrop 6. Banded charnockitic migmatite. Fine-grained norite with coarse-grained quartz. Plagioclase= 52An. Relatively large amount of apatite. Monazite is present. No biotite-quartz contact. Fluid inclusions: 28/15/57 (N=50).

75HS058 - Drangsdalen (Sokndal 3828-64855). Outcrop 7. Banded charnockitic migmatite. Biotite norite (plag= 52An) with associated leucoenderbite (plag= 41An). The contactzone is biotite-deficient. No biotite-quartz contact. Fluid inclusions: 97/02/01 (N=20).

75HS059 - Drangsdalen (Sokndal 3526-64855). Outcrop 8. Coarse-grained biotite-charnockite (plag= 31An) in an otherwise foliated enderbitic rock mass. Biotite-quartz contact is doubtful. Fluid inclusions: 07/18/75 (N=50).

75HS061 - Drangsdalen (Sokndal 3526-64855). Outcrop 8. A quartz-rich pod in a coarse-grained part of "Early Migmatite". Quartz-rich leucocharnockite or -granite. Fluid inclusions: 54/11/35 (N=40).

75HS062 - Drangsdalen (Sokndal 3526-64855). Outcrop 8. A quartz-rich pod in a coarse-grained part of "Early Migmatite". Quartz-rich charnockite. Fluid inclusions: 51/19/30 (N=30).

75HS064 - Drangsdalen (Sokndal 3525-64854). Outcrop 8. Pegmatoid intercalation in a medium-grained charnockite. Quartz in the leucogranite contains abundant opaque/silicate inclusions. Retrograde metamorphism. Rather large zircon crystals. Secondary biotite overgrowths on opaques. Fluid inclusions: 03/23/74 (N=50).

75HS065 - Drangsdalen (Sokndal 3525-64854). Outcrop 8. Coarse-grained leucoenderbitic intercalation (plag=31An) in medium-grained leucocratic rocks. Fluid inclusions: CO_2/H_2O= 42/58 (N=8).

75HS067 - Drangsdalen (Sokndal 3525-64854). Outcrop 8. A 30 cm wide fine grained melanocratic band in medium-coarse-grained leucocratic rocks. At the boundary between the biotite norite (plag=46An) and the leucoenderbite (plag =41An) a biotite-depleted zone of leuconoritic composition (plag=46An) is present. Relatively high degree of alteration in the coarse-grained band as opposed to the fine-grained biotite norite. No biotite-quartz. Fluid inclusions: 60/07/33 (N=30).

75HS073 - Drangsdalen (Sokndal 3514-64851). Outcrop 12. Wedge-shaped leucocratic band in banded charnockitic migmatites. High degree of alteration precludes a correct determination of the rock. Fluid inclusions: 69/12/19 (N= 25).

75HS075 - Drangsdalen (Sokndal 3514-64851). Outcrop 12. Banded charnockitic migmatite composed of coarse-grained quartz enderbite and finer grained charnockite (plag=30An). K-feldspar is largely microcline. Concentrations of opaques and monazite at the boundary between the enderbite and the charnockite. Fluid inclusions: 70/02/28 (N=20).

75HS077 - Drangsdalen (Sokndal 3519-64852). Outcrop 11. So called "Early Migmatite" comprising dis- and concordant coarse grained quartz-feldspar components. Biotite-bearing quartzmonzonite with concentrations of apatite and monazite. Biotite-quartz contact. K-feldspar is largely microcline. Fluid inclusions: 85/01/14 (N=25).

75HS088* - Gyadalen "East" (Ørsdalsvatnet 3445-64978). Banded charnockitic migmatites. Coarse-grained leucodiorite and fine-grained norite with large clinopyroxene crystals at the boundary. Fluid inclusions: 30*/44*/26 (N=25).

75HS095 - Gyadalen "East" (Ørsdalsvatnet 3445-64978). Banded charnockitic migmatites in the vicinity of a 2.5 m wide biotite amphibolite body. Vaguely banded fine-grained leuconorite and coarse-grained leucodiorite. Fluid inclusions: 53/28/19 (N=20).

75HS096 - Gyadalen "East" (Ørsdalsvatnet 3445-64978). Banded charnockitic migmatites. Lens-shaped leucocratic component. Foliated and vaguely banded quartz-leucoenderbite. Fluid inclusions: 35/24/41 (N=20).

75HS097 - Gyadalen "East" (Ørsdalsvatnet 3445-64978). Banded charnockitic migmatites. Medium-grained leucocharnockite with coarse-grained quartz-rich seams. Fluid inclusions: 40/42 /18 (N=40).

75HS102* - Gyadalen "East" (Ørsdalsvatnet 3445-64978). Banded charnockitic migmatite. Country rock at about 20 cm distance from a 1.2 m wide dolerite. Opaque-rich charnockite with coarse-grained quartz. Local concentrations of large apatite crystals. Fluid inclusions: 32*/48*/10 (N=30).

75HS104 - Gyadalen "East" (Ørsdalsvatnet 3445-64978). Banded charnockitic migmatites. Contactzone between a 1.2 m wide dolerite dike (probably Egersund system) and the country rock. Extensive hydrothermal alteration (serpentine, carbonate) has overprinted a pre-existing leuconorite. Large opaques at the contact. Fluid inclusions: 73/18/09 (N=13).

75HS106 - Gyadalen "East" (Ørsdalsvatnet 3445-64978). Banded charnockitic migmatites. Country rock at about 2.5 m distance from a 1.2 m wide dolerite dike. Inequigranular garnet-bearing leucocharnockite. Plagioclase 27An. Many small birefingent solid particles included in quartz. Fluid inclusions: 37/45/18 (N=30).

75HS107 - Gyadalen "East" (Ørsdalsvatnet 3445-64978). Banded charnockitic migmatites. Contactzone between a 3.5 m wide dolerite dike (probably Egersund system) and the country rock. Dolerite contains plagioclase laths and pyroxene (phenocrysts) in a very fine grained matrix of plagioclase, opaques, and (altered) pyroxene. Extensive alteration (serpentine, leucoxene, and, in particular, carbonate) is superimposed on a quartz leucoenderbite. Fluid inclusions: 45/45/10 (N=10).

75HS109 - Gyadalen "West" (Ørsdalsvatnet 3410-64956). Banded charnockitic migmatites. Fine-grained norite in contact with coarse-grained leucoenderbite. Fluid inclusions: 40/23/37 (N=25).

75HS110 - Gyadalen "West" (Ørsdalsvatnet 3410-64956). Banded charnocktic migmatites. Leuconorite and leucoenderbite (inequigranular) with quartz vein. Large crystals of orthopyroxene at the contact between the mesocratic and the leucocratic part. Fluid inclusions: 35/18/47 (N=40)

75HS111 - Gyadalen "West" (Ørsdalsvatnet 3410-64956). Banded charnockitic migmatite. Fine to medium-grained charnockitic and coarse-grained alkalifeldspar-charnockite (inequigranular). Fluid inclusions: 35/27/38 (N=25).

75HS113 - Drangsdalen (Sokndal 3528-64855). Outcrop 7. A quartz-rich lens-shaped body of 10 cm length, enclosed in "Early Migmatite". The lens is a leucoenderbite whereas the parent rock is a biotite norite. Plagioclase 51An. Both biotite-quartz contact as well as antipathetic relation between biotite and quartz has been established. Carbonate flakes. Fluid inclusions: 24/51/25 (N=35).

75HS114 - Drangsdalen (Sokndal 3528-64855). Outcrop 7. A discordant pegmatoid component in fine-grained "Early Migmatite". This component is a coarse-grained leucocharnockite (plag=41An) whereas the parent rock is a fine-grained leucoenderbite (plag=43An). Concentrations of opaque, zircon, and monazite in the contact zone. No biotite-quartz contact. Fluid inclusions: 77/06/17 (N=50).

75HS115 - Skjeggestad (Sokndal 3547-64855). Outcrop 1. Pegmatite body south of Skjeggestad. Alkalifeldspar charnockite. Plagioclase= 22, 27An. Fluid inclusions: 23/11/66 (N=25).

75HS118 - Skjeggestad (Sokndal 3547-64855). Outcrop 1. Pegmatite body south of Skjeggestad. Alkalifeldspar charnockite with graphic texture. Fluid inclusions: 14/16/70 (N=20).

75HS121 - Skjeggestad (Sokndal 3547-64855). Outcrop 1. Coarse-grained pegmatite adjacent to a series of banded rocks. Large amounts of magnetite/ilmenite at the contact. Retromorphosed charnoenderbite (carbonate, serpentine, green amphibole). Fluid inclusions: 49/10/41 (N=25).

75HS123 - Skjeggestad (Sokndal 3547-64855). Outcrop 1. Pegmatite body south of Skjeggestad. Leucogranite. Fluid inclusions: 13/22/65 (N=30).

75HS129 - Skjeggestad (Sokndal 3547-64856). Outcrop 1. Pegmatoid body intercalated in migmatite. Anorthosite (?). Rock shows distinct cumulus structures and intercumulus clinopyroxene and quartz. Plagioclase 30An. Large apatite crystals. Biotite-quartz contact. Fluid inclusions: 50/03/47 (N=18).

75HS133 - Skjeggestad (Sokndal 3547-64856). Outcrop 1. Probably banded charnockitic migmatite. Alternating fine-and coarse-grained rocks. Leucogranite with extremely coarse perthites. Plagioclase= 12An. Secondary alteration. Fluid inclusions: 05/19/76 (N=20).

75HS136 - Skjeggestad (Sokndal 3543-64861). Outcrop 2. A 50-75 cm wide magnetite-bearing leucocratic band, probably discordant in a noritic body. Composition ranges from leucoenderbite to quartz enderbite. Plagioclase 40An. Locally large zircons. Opaques form an important intergranular phase. Locally strong hydrothermal alteration. Fluid inclusions: 33/11/56 (N=25).

75HS139 - Skjeggestad (Sokndal 354264861). Outcrop 2. Coarse-grained biotite-bearing intercalation in "Early Migmatite". Biotite-bearing leuco enderbite. Biotite-quartz contact. Fluid inclusions: 69/09/22 (N=25).

75HS141 - Skjeggestad (Sokndal 3542-64861). Outcrop 2. A relatively narrow zone (order of cm's) within a biotite norite. Strongly retromorphosed and deformed leuconorite. No biotite-quartz. A few large apatite crystals (up to 2 mm). Relatively large amount of carbonate. Fluid inclusions: 90/06/04 (N=25).

75HS142 - Drangsdalen (Sokndal 3535-64858). Outcrop 3. Early Migmatite (?). Vaguely banded, fine-grained mesocratic leuconorite or enderbitic parent rock with coarse-grained intercalations of leucocharnockite. Fluid inclusions (in leucocharnockite): 01/01/99 (N=10).

75HS144 - Drangsdalen (Sokndal 3532-64857). Outcrop 4. Early Migmatite. Vaguely banded sequence of leuconoritic- enderbitic rocks. Fluid inclusions: 87/03/10 (N=45).

75HS145 - Drangsdalen (Sokndal 3531-64856). Outcrop 5. Fine-grained biotite norites and associated, folded quartz-feldspar bands (leucoenderbites) that are a few cm wide. Plagioclase=45An. Rather strong hydrothermal alteration. Fluid inclusions: 79/02/19 (N=25).

75HS147 - Drangsdalen (Sokndal 3531-64856). Outcrop 5. Probably Early Migmatite. Fine grained charnockite. Fluid inclusions: 11/07/82 (N=22).

75HS149 - Drangsdalen (Sokndal 3529-64855). Outcrop 6. Rather fine-grained, poorly foliated charnoenderbite. Fluid inclusions: 52/07/41 (N=20).

75HS150 - Drangsdalen (Sokndal 3529-64855). Outcrop 6. Fine-grained biotite leuconorite and associated biotite-bearing charnockite. No biotite-quartz contact. Fluid inclusions/ 87/08/05 (N=20).

75HS154 - Drangsdalen (Sokndal 3528-64855). Outcrop 7. Intricately folded (?) Early Migmatite with quartz-feldspar bands (probably discordant) and biotite-rich pod. The band is an alkalifeldspar syenite and the pod is a biotite norite. Monazite and opaques are concentrated along the contact area. A macroscopically greyish-purplish zone in the parent rock is a quartz-free biotite-bearing leuconorite. Fluid inclusions: 77/17/07 (N=40).

75HS155 - Drangsdalen (Sokndal 3525-64854). Outcrop 8. Typical Early Migmatite with dis- and concordant pegmatoid component. Well-foliated, fine-to medium-grained leucogranite. No contact between primary biotite and quartz. Fluid inclusions: 39/25/36 (N=50).

75HS160 - Drangsdalen (Sokndal 3526-64855). Outcrop 9. A 10 cm wide, slightly discordant coarse-grained biotite-bearing alkalifeldspar charnockite within a vaguely foliated medium-grained biotite-free leucoenderbite. The discordant band shows biotite-quartz contact in thin seams (tension gashes?). Plagioclase =35An. Fluid inclusions (discordant band): 43/19/38 (N=50). Fluid inclusions (parent rock): 44/09/47 (N=50).

75HS162 - Drangsdalen (Sokndal 3526-64855). Outcrop 9. A 10 cm wide, 5 m long, coarse-grained leucocratic biotite-bearing band in Early Migmatite. Biotite-quartz contact in rock with compositional variation from alkalifeldspar charnockite to charnoenderbite. Fluid inclusions: 28/23/49 (N=50).

75HS163 - Drangsdalen (Sokndal 3525-64854). Outcrop 9. A medium-grained leucocratic rock mass. Banding is caused by alternating grain size and amount of quartz. Mesocratic bands are present as well. Parent rock is a leuco-charnoenderbite whereas the band is a biotite enderbite. Plagioclase=40An. Apart from symplectites there is no biotite-quartz contact. Fluid inclusions: 20/26/54 (N=50).

75HS164 - Drangsdalen (Sokndal 3525-64854). Outcrop 9. Medium-grained leucoenderbites and mesocratic biotite leuconorites. Plagioclase 37An. No contact between biotite and quartz. Fluid inclusions: 21/14/65 (N=20).

75HS165 - Drangsdalen (Sokndal 3525-64854). Outcrop 9. Contactzone between Early Migmatite parent rock and a coarse-grained, pegmatoid quartz-feldspar rock (ranging from leuco-charnoenderbite to leucocharnockite). Plagioclase=27An. Fluid inclusions: 27/05/68 (N=30).

75HS166 - Drangsdalen (Sokndal 3525-64853). Outcrop 10. Bands of fine-grained biotite norite (thickness up to 10 cm) in fine- to medium-grained foliated quartz-feldspar rock. The leucocratic rock near the contact is a leucoenderbite, locally containing monazite. The biotite norite is relatively rich in quartz. Plagioclase 41An. Biotite-quartz contact. Fluid inclusions: 65/05/30 (N=20).

75HS167 - Drangsdalen (Sokndal 3525-64853). Outcrop 10. Contactzone between fine-grained mesocratic rock (biotite leuconorite) and parent rock (quartz-leuco-enderbite). Plagioclase=46An. Fluid inclusions: 75/06/19 (N=25).

75HS170 - Drangsdalen (Sokndal 3525-64853). Outcrop 10. Slightly discordant coarse-grained. leucocratic biotite charnoenderbite in Early Migmatite parent rock that is orthopyroxene-bearing and devoid of biotite. Plagioclase=32An. Biotite-quartz contact. Fluid inclusions: 65/13/22 (N=20).

75HS174 - Drangsdalen (Sokndal 3520-64852). Outcrop 11. More or less concordantly intercalated leucocharnockite in medium-grained parent rock. Plagioclase=27An. Fluid inclusions: 06/06/88 (N=20).

75HS175 - Drangsdalen (Sokndal 3520-64852). Outcrop 11. Coarse-grained part of Early Migmatite. Leucocharnockite. Plagioclase=35An. Fluid inclusions: 31/13/56 (N=30).

75HS176 - Drangsdalen (Sokndal 3520-64852). Outcrop 11. Part of Early Migmatite. Fine-grained,biotite-bearing parent rock in contact with medium-grained,foliated biotite-bearing leucocharnockite. Plagioclase=31An. Biotite-quartz contact. Fluid inclusions: 71/00/29 (N=50).

75HS177 - Drangsdalen (Sokndal 3520-64852). Outcrop 11. Medium grained rock mass containing coarse-grained pegmatoid components with locally large orthopyroxene crystals. Biotite-bearing parts, however, are also present. In the biotite-bearing leuco-charnoenderbite biotite-quartz contacts have been observed. Plagioclase=32An. Degree of alteration in the orthopyroxene-bearing part is considerably higher than in the biotite-bearing part. Fluid inclusions (biotite zone): 84/00/16 (N=50). Fluid inclusions (orthopyroxene zone): 78/00/22 (N=50).

75HS179 - Drangsdalen (Sokndal 3520-64852). Outcrop 11. Discordant, biotite-feldspar-rich band (about 10 cm wide) in Early Migmatite. Biotite schist with feldspar augen. Plagioclase=32An. Biotite-quartz contact. Fluid inclusions: 53/11/36 (N=10).

75HS180 - Drangsdalen (Sokndal 3520-64852). Outcrop 11. Early Migmatite. Medium- to coarse-grained parent rock ranging in composition from charnockite to charnoenderbite. Rather strong alteration. Fluid inclusions: 47/14/39 (N=50).

75HS181 - Drangsdalen (Sokndal 3520-64852). Outcrop 11. A subhorizontal system of coarse-grained feldspar-rich bands in (discordant) contact with Early Migmatite. The parent rock is a charnockite wehereas the band is syenitic to monzonitic in terms of quartz and feldspars. At the contact, concentrations of monazite, zircon, magnetite, and clinopyroxene are found. Plagioclase=27An (parent rock), 31An (band). Fluid inclusions parent rock: 24/12/64 (N=20); fluid inclusions band: 50/05/45 (N=25). Cf. Wielens (1979).

75HS183 - Drangsdalen (Sokndal 3514-64851). Outcrop 12. Well-banded migmatitic (Late Migmatite?) rocks with agmatic structures. Fine-grained, amphibole-bearing leuconorite alternating with medium- to coarse-grained, foliated, leucocratic enderbite. Plagioclase=44An. No biotite-quartz. Fluid inclusions: 62/07/31 (N=35).

75HS184* - Drangsdalen (Sokndal 3514-64851). Outcrop 12. Coarse-grained garnet-serpentine bearing enderbite, located about 40 cm above a mesocratic intercalation in Early Migmatite. Plagioclase=30An. Fluid inclusions: 23*/17*/60 (N=50).

75HS185 - Drangsdalen (Sokndal 3514-64851). Outcrop 12. A biotite-rich band cross-cutting a vaguely banded sequence. Parent rock is an alkalifeldspar charnockite; the band is composed of augen that contain plagioclase, myrmekite, quartz, and some biotite, surrounded by a biotite-rich zone with minor amounts of orthopyroxene and plagioclase. Near the contact with a coarse-grained quartz band a thick rim of orthopyroxene has developed. No biotite-quartz contact. Fluid inclusions: 31/21/48 (N=50).

75HS186 - Drangsdalen (Sokndal 3514-64851). Outcrop 12. Near the contactzone with a biotite-rich band a noritic band with leucocratic lenses is found. Enderbite. Plagioclase=37An. Fluid inclusions: 43/05/52 (N=15).

75HS187 - Drangsdalen (Sokndal 3514-64851). Outcrop 12. A noritic band (same as in 75HS186), 25 cm below the contact. Amphibole-bearing leuconorite, containing a pocket of quartz-leucoenderbite. Contact between amphibole and quartz; no biotite-quartz contact. Plagioclase=46An. Fluid inclusions: 73/07/20 (N=20).

75HS188 - Drangsdalen (Sokndal 3514-64851). Outcrop 12. A noritic band (same as in 75HS186), 60 cm below the contact. Amphibole-bearing (leuco)norite with (folded) quartz lens. No biotite-quartz contact. Fluid inclusions: 85/04/11 (N=25).

75HS189 - Drangsdalen (Sokndal 3513-64851). Outcrop 12. A leucocratic, subhorizontal band, discordant with respect to the general structural direction. Medium-grained leucoenderbite. Fluid inclusions: 10/05/85 (N=50).

75HS190 - Drangsdalen (Sokndal 3513-64851). Outcrop 12. A banded sequence of mesocratic and leucocratic rocks dissected by coarse-grained quartz-feldspar bands. The mesocratic rock is a fine-grained amphibole-bearing (leuco)norite which, near the contact with the quartz-feldspar rock, develops an amphibole-depleted zone. No biotite-quartz contact. Plagioclase=46-52An.

75HS191* - Drangsdalen (Sokndal 3513-64851). Outcrop 12. Banded sequence of mesocratic and leucocratic rocks. At the intersection of discordant leucocratic rocks and leucocratic rocks of the concordant system. Leucoenderbite with quartz band. High degree of retromorphosis. Quartz partly recrystallized. Plagioclase=36An. No biotite-quartz contact. Fluid inclusions: 23*/43*/34 (N=50).

75HS193 - Drangsdalen (Sokndal 3507-64849). Outcrop 13. Discordant, coarse-grained magnetite-bearing enderbite in a medium grained foliated rock mass. Quartz shows numerous deformation lamellae, well visible in subbasal sections (fig.39). Plagioclase=27-28An. No biotite-quartz contact. Fluid inclusions: 79/04/17 (N=50).

75HS195 - Drangsdalen (Sokndal 3507-64849). Outcrop 13. Subhorizontal, 5 cm wide, coarse-grained band, discordantly intercalated in a rather massive, medium-to coarse-grained retromorphosed quartz-feldspar rock. The band is a leucogranite. Plagioclase=31An. Fluid inclusions: 33/26/41 (N=20).

75HS196 - Nedrabø (Bjerkreim 3295-65098). Faurefjell Metasediments. Coarse-grained leucoenderbite; retromorphic activity. Fluid inclusions: 66/16/18 (N=35).

75HS197 - Nedrabø (Bjerkreim 3296-65096). Faurefjell Metasediments. Discordant quartz-rich vein composed of retromorphosed, medium-grained alkalifeldspar-charnockite with coarse-grained quartz-rich levels. Fluid inclusions: 34/18/48 (N=25).

75HS198 - Nedrabø (Bjerkreim 3295-65096). Faurefjell Metasediments. Fine-grained quartzite. Fluid inclusions: 76/10/14 (N=20).

75HS199 - Nedrabø (Bjerkreim 3295-65093). Faurefjell Metasediments. Fine-grained greyish-green diopside rock with concordantly intercalated coarse-grained quartzite. Quartz crystals are strongly deformed (mosaic texture, undulatory extinction). Extensive hydrothermal alteration along the boundary. Titanite and carbonate are not uncommon. Fluid inclusions coarse grained part: 91/5/4 (N=25); fluid inclusions fine grained part: 97/2/1 (N=25).

75HS200 - Nedrabø (Bjerkreim 3295-65093). Faurefjell Metasediments. Alternating medium- and fine-grained diopside quartzite and alkalifeldspar granite. The larger crystals of quartz display undulatory extinction and mosaic texture; smaller crystals are deformed only to a moderate degree. Titanite and apatite are present. Fluid inclusions: 96/2/2 (N=30). A trail with CO_2-rich inclusions has been found in apatite.

75HS201 - Nedrabø (Bjerkreim 3295-65093). Faurefjell Metasediments. Alkalifeldspar-granite with large crystals of (rutilized) quartz, locally showing a high degree of plastic deformation. Fluid inclusions: 92/3/5 (N=20).

75HS202 - Nedrabø (Bjerkreim 3296-65092). Faurefjell Metasediments. Quartzitic bands in contact with finer grained biotite-bearing quartz-feldspar rock. A pyroxene-rich rim is present. Quartz (rutilized) sizes up to 10 mm and is moderately to strongly deformed. Fluid inclusions: 70/14/16 (N=30).

75HS203 - Nedrabø (Bjerkreim 3296-65092). Faurefjell Metasediments. Phlogopite-diopside rock.

75HS204 - Seldal (Høle 3266-65259). Faurefjell Metasediments. Marble (calcite) + pyroxenite (hedenbergite) + retromorphosed diopside rock (diopside, zoisite, and epidote). Prehnite, close to contact with pyroxenite.

75HS205 - Seldal (Høle 3267-65258). Faurefjell Metasediments. Diopside granite, altered to a high degree (secondary carbonate, epidote, colorless mica, orthite). Quartz is tectonized to a high degree (mosaic texture). Fluid inclusions: 86/1/13 (N=25).

75HS206 - Seldal (Høle 3267-65259). Faurefjell Metasediments. Diopside rock with both primary and secondary carbonate.

75HS207 - Seldal (Høle 3267-65259). Faurefjell Metasediments. Contact zone between diopside marble and quartzite. Coarse-grained quartz (up to 20 mm) containing solid inclusions of diopside, carbonate, and tremolite (replacing diopside). Low to moderate degree of deformation. Fluid inclusions: 55/39/6 (N=25).

75HS208 - Seldal (Høle 3267-65259). Faurefjell Metasediments. Contact zone between marble and quartzite. Diopside-phlogopite-forsterite marble. Both calcite and dolomite are present. Dolomite occurs as unmixed phases and as individual crystals. Rims of dolomite around phlogopite and rims of diopside around forsterite.

75HS209 - Heltanuten (Høle 3279-65255). Faurefjell Metasediments. A 1 m wide band of fine-grained quartz-rich diopside- alkalifeldspar granite. Tremolite locally replaces diopside. Quartz is slightly rutilized, sizes up to 5 mm and displays a low degree of deformation. Fluid inclusions: 29/38/20/13 (N=15).

75HS210 - Heltanuten (Høle 3279-65255). Faurefjell Metasediments. Medium-grained foliated leucogranite. Quartz displays moderate degree of deformation. K-feldspar largely developed as microcline. Fluid inclusions: 8/11/74/7 (N=20).

75HS211 - Heltanuten (Høle 3279-65255). Faurefjell Metasediments. Macroscopically bluish-grey colored fine-to coarse-grained quartzite. Quartz crystals (rutilized) size up to 20 mm. Moderate to high degree of deformation and extensive hydrothermal alteration (colorless mica, clino-zoisite, epidote). Fluid inclusions: 8/4/68/20 (N=20).

75HS212 - Heltanuten (Høle 3278-65255). Faurefjell Metasediments. Contact zone between marble and quartzite. Fine-grained diopside rock containing carbonate and titanite. Extensive hydrothermal alteration.

75HS213 - Heltanuten (Høle 3278-65255). Faurefjell Metasediments. Contact zone between marble and quartzite. Diopside rock and diopside-bearing quartzite. Quartz is relatively fine grained and contains abundant yellowish-greenish inclusions with low birefringence and moderate refractive index (apatite?). Fluid inclusions: 78/5/17 (N=4).

75HS216 - Drangsdalen (Sokndal 3490-64845). Outcrop 14. Strongly foliated and extensively retromorphosed quartz-feldspar rock. Fluid inclusions: 6/6/88 (N=10).

75HS217 - Drangsdalen (Sokndal 3490-64845). Outcrop 14. A coarse-grained pegmatite with graphic texture and opaque-chlorite-rich central part, within a strongly foliated and extensively retromorphosed rock mass. Leucogranite. Fluid inclusions: 20/10/70 (N=20).

75HS232 - Eikeland (Sokndal 3458-64826). Contact zone between the lopolith of Bjerkreim-Sokndal and the Charnockitic Migmatites. Leucogranitic band in leuconorite Locally, strings of carbonate. Fluid inclusions: 28/30/42 (N=50).

75HS233 - Rusdalsvatnet (Ørsdalsvatnet 3544-64942). Banded Charnockitic Migmatite. Contact zone between a dolerite dike (thickness probably about 5 m) and the country rock. The dolerite is equal to the one described under 75HS107. The country rock is a biotite-bearing charnockite. Fluid inclusions: 69/18/13 (N=20).

75HS243 - Rusdalsvatnet (Ørsdalsvatnet 3544-64942). Banded Charnockitic Migmatite. The same, 15 cm wide, leucocratic band as 75HS233, at 13 m distance from the contact with a dolerite dike. Extensively retromorphosed charnockite showing a very high degree of deformation. Locally, mylonitic textures are developed; recrystallization has taken place. Fluid inclusions: 89/10/1 (N=5).

75HS244*- Teksevatnet (Ørsdalsvatnet 3405-64940). Contact area between the Lopolith of Bjerkreim-Sokndal and the Charnockitic Migmatites. Pegmatite. (Biotite) leucogranite. Fluid inclusions: 16*/9*/75 (N=25).

75HS248*- Drangsdalen (Sokndal 3513-64851). Outcrop 12. Banded Charnockitic Migmatite close to amphibolitic and/or noritic body. Concordant quartz vein with fine-grained clinopyroxene-bearing norite. Extensive alteration along the contact. Fluid inclusions: 13*/10*/77 (N=25).

76HS250 - Asheim (Bjerkreim 3336-65075). Faurefjell Metasediments. Basal quartzite. Coarse-grained bluish-grey quartzite. Quartz contains rutile. In contact with diopside rock. Fluid inclusions: 55/4/41 (N=35).

76HS251 - Asheim (Bjerkreim 3336-65075). Faurefjell Metasediments. Basal quartzite. Coarse-grained quartzite at about 4.5 m below the contact with diopside rock. Fluid inclusions: 0/0/100 (N=20).

76HS252 - Asheim (Bjerkreim 3335-65075). Banded Charnockitic Migmatite. Concordantly intercalated quartzitic band. Fluid inclusions: 96/3/1.

76HS253 - Vikesdal (Bjerkreim 3326-65042). Garnetiferous Migmatite. Coarse-grained quartz-feldspar rock with dark streaks containing cordierite, osumilite, orthopyroxene and garnet. Fluid inclusions: 58/6/36. See also Maijer et al.(1977).

76HS255 - Ivesdal (Bjerkreim 3356-65108). Garnetiferous Migmatite. Quartz-enderbite close to sapphirine-bearing rocks. Fluid inclusions: 40/38/22 (N=20). See also Hermans et al.(1976).

76HS256 - Mydland (Sokndal 3487-64762). Tunnel outcrop. Lopolith of Bjerkreim-Sokndal. Coarse-grained pegmatite in phase A. Amphibole granite. Contact between amphibole (brownish-green) and quartz. Fluid inclusions: 74/9/17 (N=20).

76HS258 - Mydland (Sokndal 3487-64762). Outcrop W. of tunnel. Lopolith of Bjerkreim-Sokndal. A 1 m wide pegmatite intercalation in phase A. Coarse-grained biotite granite. Fluid inclusions: 61/23/16 (N=20).

76HS261 - Kvitingen (Ørsdalsvatn 3569-64989). A 2 m wide strongly retromorphosed pegmatite body enclosed within foliated, massive Charnockitic Migmatite. Coarse grained quartz + epidote, minor amounts of allanite. Probably leucogranitic composition. Fluid inclusions: 4/1/95 (N=25).

76HS262*- Bjørnestadvatn (Ørsdalsvatnet 3959-65045). A 15 cm wide discordant leucogranitic band in Folded Basic Intrusion. Leucogranite (band) in contact with biotite-quartz leuconorite (parent rock). Contact between biotite and quartz. No rim of orthopyroxene at the contact. Fluid inclusions: 19*/11*/69 (N=25).

76HS264 - Gyadalen (Ørsdalsvatnet 3490-64993). Garnetiferous Migmatite. A 1-1.5 m wide coarse-grained garnet-cordierite granofels, concordantly intercalated in fine-grained spinel-bearing parent rock. Contact between biotite and quartz. Fluid inclusions: 9/6/85 (N=25).

76HS265 - Gyadalen (Ørsdalsvatnet 3490-64993). Garnetiferous Migmatite. Fine-grained spinel-quartz granofels. Fluid inclusions: 46/8/46 (N=25).

76HS266 - Gyadalen (Ørsdalsvatnet 3490-64993). Garnetiferous Migmatite. Coarse-grained 'pod' in fine-grained spinel-quartz granofels. Opaque-rich cordierite-bearing granofels. Fluid inclusions: 75/1/24 (N=20).

76HS267 - Årdalen (Flekkefjord 3653-64725). Charnockitic Migmatite. Banded sequence. Fine-grained norite and associated leucotonalite. Fluid inclusions: 36/15/49 (N=40).

76HS268 - Årdalen (Flekkefjord 3653-64725). Charnockitic Migmatite. Banded sequence. Leuconorite in contact with coarse-grained quartz band. Concentration of orthopyroxene at the contact. High degree of alteration in coarse-grained part. Fluid inclusions: 2/10/88 (N=30).

76HS269 - Årdalen (Flekkefjord 3653-64725). Charnockitic Migmatite. Banded sequence. Leuconorite in contact with retromorphosed leuco-enderbite. Fluid inclusions: 9/6/85 (N=35).

76HS270 - Kvitingen (Flekkefjord 3569-64990). Charnockitic Migmatite. Pegmatoid rock with bluish-grey colored quartz. Fluid inclusions: 17/27/56 (N=25).

76HS271* - Årdalen (Flekkefjord 3649-64719). Charnockitic Migmatite. Mesocratic lenses enclosed in medium-coarse-grained leucocratic massive rock. Fine-grained leuconorite in contact with coarse-grained quartz-rich tonalite. Concentrations of clinopyroxene at the contact. Fluid inclusions: 19*/13*/68 (N=35).

76HS272 - Brynesland (Bjerkreim 3310-64914). Anorthosite of Egersund-Ogna. Intercalation of strongly retromorphosed leucotonalite in anorthosite. Fluid inclusions: 50/33/17 (N=20).

76HS273* - Asheim (Bjerkreim 3335-65067). Faurefjell Metasediments. Folded quartz veins in contact with diopside rock. Fluid inclusions: 33*/8*/59 (N=40).

76HS274* - Asheim (Bjerkreim 3335-65067). Faurefjell Metasediments. Folded quartz vein at about 10 cm distance from the contact. Fluid inclusions: 8*/10*/82 (N=40).

76HS275 - Asheim (Bjerkreim 3338-65071). Faurefjell Metasediments. Mesocratic phlogopite-diopside rock with enclosed 4 cm wide fine-medium-grained rock composed of diopside, calcite, biotite, muscovite and K-feldspar.

76HS276 - Asheim (Bjerkreim 3338-65071). Faurefjell Metasediments. Basal quartzite (?) Hypersthene-cordierite quartzite in contact with sample 76HS275. Fluid inclusions: 47/3/50 (N=35).

76HS277 - Snøsvatnet (Bjerkreim 3279-65071). Charnockitic Migmatite. A 20 m thick quartz-rich level in leucocranitic rocks. Quartzite. Fluid inclusions: 94/2/4 (N=25).

76HS278 - Årsvolltjørna (Sokndal 3538-64735). Garsaknatt Anorthosite. Quartz lens in anorthosite, close to the contact with banded Charnockitic Migmatite. Fluid inclusions: 30/8/61 (N=25).

76HS279 - Årsvolltjørna (Sokndal 3538-64735). Banded Charnockitic Migmatite. Sequence of relatively fine-grained biotite-norites and quartz-rich enderbites. A biotite-depleted zone with relatively large orthopyroxenes occurs in the mesocratic rock near the contact with the leucocratic rock. Fluid inclusions: 33/8/59 (N=35).

76HS280 - Årsvolltjørna (Sokndal 3538-64735). Contact zone between the Garsaknatt Anorthosite and banded Charnockitic Migmatite. A 50 cm wide lens-shaped quartz vein. Contact with host rock (leucoenderbite). Fluid inclusions: 6/32/62 (N=25).

76HS281 - Årsvolltjørna (Sokndal 3538-64735). Contact zone between Garsaknatt Anorthosite and banded Charnockitic Migmatite. A 50 cm wide lens shaped quartz vein (same as 76HS280) in contact with leucoenderbite. Fluid inclusions: 20/30/50 (N=25).

76HS282 - Årsvolltjørna (Sokndal 3538-64735). Contact zone between Garsaknatt Anorthosite and banded Charnockitic Migmatite. A 50 cm wide lens-shaped quartz vein (same as 76HS280); the central part. Fluid inclusions: 42/10/48 (N=30).

76HS283* - Årsvolltjørna (Bjerkreim 3532-64740). Lopolith of Bjerkreim-Sokndal; phase C. A lens-shaped body of quartz enclosed in foliated leucocratic - mesocratic rocks. Quartzite in contact with biotite-norite. Clinopyroxene concentrated along the contact. Fluid inclusions: 34*/20*/46 (N=25).

76HS286 - Tjørhom area, Beinesvatnet (Øvre Sirdal 3755-65318). Banded Granitic Migmatite. Quartz-rich pegmatitic pod (dimensions about 40 cm) in migmatite. Erratic sample (although clearly from the pod). Fluid inclusions: 29/55/16 (N=20).

76HS287* - Tjørhom area, Halseheii (Øvre Sirdal 3678-65307). Granitic Migmatite. Banded sequence. Coarse-grained quartz vein in contact with amphibolite but separated from it by a relatively thick rim of orthopyroxene crystals. Fluid inclusions: 49*/14*/37 (N=25).

76HS288* - Tjørhom area, Halseheii (Øvre Sirdal 3678-65307). Granitic Migmatite. Banded sequence. Quartzite in contact with biotite-amphibole bearing enderbite, close to (biotite) amphibolite. Biotite in contact with quartz. Fluid inclusions: 55*/9*/36 (N=35).

76HS290 - Tjørhom area, Sandtjørna (Øvre Sirdal 3824-65285). Granitic Migmatite. Massive leucogranite. Fluid inclusions: 1/0/99 (N=17).

76HS291 - Tjørhom area, Sandvatnet (Øvre Sirdal 3742-65299). Granitic Migmatite. Amphibole-biotite enderbite in contact with leucogranite. Biotite and amphibole are concentrated at the boundary, both are in contact with quartz. No concentration of orthopyroxene at the boundary. Fluid inclusions: 37/31/32 (N=25).

76HS295 - Tjørhom area, Sinnes-Kvaevemoen (Øvre Sirdal 3798-65345). Granitic Migmatite. Tonalite with concentrations of biotite and/or brownish green amphibole; both minerals in contact with quartz. Fluid inclusions: 1/0/99 (N=20).

76HS296 - Stølsfjellet (Høle 3255-65273). Charnockitic Migmatite. A 20 cm wide discordant quartz vein at about 2.5 m distance from Faurefjell Metasediments (marbles), in contact with alkalifeldspargranite. Fluid inclusions: 39/6/55 (N=30).

76HS297 - Stølsfjellet (Høle 3255-65273). Faurefjell Metasediments. Coarse-grained, relatively dark-gray quartzite in diopside rock. Serpentine is quite common. Fluid inclusions: 21/6/73 (N=25). Opaque inclusions (carbonaceous?) constitute ca. 5% of the total.

76HS298 - Stølsfjellet (Høle 3255-65273). Faurefjell Metasediments. A 20 cm wide boudin of dark gray coarse-grained quartz enclosed in marble and separated from it by a diopside-tremolite rim. Fluid inclusions: 31/56/13 (N=20).

76HS299 - Stølsfjellet (Høle 3255-65273). Faurefjell Metasediments. Phlogopite-forsterite marble at approximately 1 m distance from sample 76HS298.

76HS300 - Stølsfjellet (Høle 3255-65273). Faurefjell Metasediments. Extensive body of quartz (thickness probably well over 6 m) overlying marbles. Greenish-gray quartzite, sampled at 1 m above a talc-rich horizon which occurs between the quartz body and the marbles. Fluid inclusions: 0/0/100 (N=10).

76HS301 - Stølsfjellet (Høle 3255-65273). Faurefjell Metasediments. Quartzite (same body of quartz as in 76HS300) sampled at 4 m above talc-rich horizon. Fluid inclusions: 0/0/100 (N=30).

76HS302 - Store Myrvatnet (Frafjord 3492-65179). Massive Granitic Migmatite. Medium-grained slightly foliated pyrite-bearing amphibole granite. Contact between amphibole and quartz. Fluid inclusions: 28/22/50 (N=25).

76HS304 - Store Myrvatnet (Frafjord 3492-65179). Pegmatite within foliated amphibole granite. Central part (present sample) is quartz-rich. Fluid inclusions: 4/5/91 (N=30).

76HS305 - Store Myrvatnet (Frafjord 3495-65179). Banded Granitic Migmatite. Biotite-garnet tonalite and biotite granite. Contact between biotite and quartz. Fluid inclusions: 0/0/100 (N=25).

76HS306 - Austrumdalsvatnet (Ørsdalsvatnet 3400-65082). Garnetiferous Migmatite. Quartz-rich lens enclosed in garnet-cordierite bearing rock. Graphite-bearing leucogranite. Fluid inclusions: 29/13/58 (N=25).

76HS307 - Austrumdalsvatnet (Ørsdalsvatnet 3400-65082). Garnetiferous Migmatite. Alternation of foliated garnet-cordierite granofels, coarse-grained leucogranite and coarse-grained garnet-biotite granofels. Fluid inclusions (leucogranite): 60/8/32 (N=20).

76HS308** - Ørsdalen (Ørsdalsvatnet 3476-65072). Charnockitic Migmatite. Banded sequence of rocks close to a 3 m wide body of amphibolite. Fine-grained amphibole norite in contact with foliated coarse-grained quartz-rich rock. Fluid inclusions: 73**/5**/22 (N=15).

76HS309 - Ørsdalen (Ørsdalsvatnet 3476-65072). Charnockitic Migmatite. Poorly foliated medium-coarse-grained quartz-rich rock at 5 m distance from a 3 m wide body of amphibolite. Fluid inclusions: 1/1/98 (N=20).

76HS310 - Ørsdalen (Ørsdalsvatnet 3512-65076). Banded Charnockitic Migmatite. Mine tailings, showing fine-grained biotite-amphibole norite with associated coarse-grained leuco-charnoenderbite. Concentrations of clinopyroxene at the boundary. Contact between quartz and amphibole (greenish-brown) but no contact between quartz and biotite. Fluid inclusions: 24/7/69 (N=55).

76HS311 - Austrumdalsvatnet (Ørsdalsvatnet 3400-65802). Contact area between Garnetiferous Migmatite and Charnockitic Migmatite. Partly discordant, coarse-grained leucocratic granodiorite (graphite-bearing) within Garnetiferous migmatite. Fluid inclusions: 7/2/91 (N=20).

76HS312 - Austrumdalsvatnet (Ørsdalsvatnet 3400-65092). Contact area between Garnetiferous Migmatite and Charnockitic Migmatite. Partly discordant coarse-grained leucocratic granodiorite. No graphite present. Fluid inclusions: 37/5/58 (N=25).

76HS313 - Drangsdalen (Sokndal 3514-64851). Outcrop 12. A 25 cm wide discordant band. Biotite-charnockite; contact between biotite and quartz. Fluid inclusions: 69/10/21 (N=20).

76HS318 - Hauklandsvatnet (Sokndal 3575-64857). Banded Charnockitic Migmatite. Fine-medium-grained noritic rock with quartz-bearing pockets rich in clino- and ortho-pyroxene. Fluid inclusions: 61 /8 /31 (N=49).

76HS324[1] Drangsdalen (Sokndal 3542-64861). Outcrop 2. A 50-75 cm wide (folded) ilmenite-magnetite leuco-enderbite intercalated in a leuconorite. Fluid inclusions: 00/11/89 (N=12). 1) sample not equal to sample studied for orientation of fluid inclusion planes.

76HS325 - Drangdalen (Sokndal 3531-64856). Outcrop 5. Biotite-leuconorite with leuco-enderbite. Fluid inclusions: 91/3/6 (N=20).

76HS331 - Drangsdalen (Sokndal 3507-64849). Outcrop 13. Amphibole granite. Contact between amphibole and quartz. Fluid inclusions: 18/64/18 (N=20).

CURRICULUM VITÆ

Toegevoegd op verzoek van het College van Decanen der Rijksuniversiteit te Utrecht.

De schrijver van dit proefschrift behaalde in 1967 het getuigschrift H.B.S.-B aan de Christelijke Hogere Burgerschool (thans Koningin Wilhelmina College) te Culemborg. Na een aanvankelijke start met Natuur- en Sterrekunde werd in november van hetzelfde jaar begonnen met de studie Geologie aan de Rijksuniversiteit te Utrecht. Het kandidaatsexamen G3 legde hij af in 1970; het doktoraalexamen met hoofdvak petrologie en bijvakken toegepaste- en structurele geologie en ertskunde werd behaald in 1974.

Van januari 1976 tot juli 1976 en van mei 1979 tot maart 1980 was de schrijver verbonden als wetenschappelijk medewerker/assistent aan de Rijksuniversiteit Utrecht. Van september 1976 tot maart 1978 werd hij door middel van een stipendium van de Niels Stensen Stichting in staat gesteld het onderzoek aan vloeistofinsluitsels voort te zetten. Een part-time dienstbetrekking als wetenschappelijk medewerker bij Billiton Research, B.V. te Arnhem werd vervuld van maart 1978 tot november 1978.